Virginia Commonwealth University
VCU Scholars Compass

Theses and Dissertations | Graduate School

2017

Development of General Purpose Liquid Chromatography Simulator for the Exploration of Novel Liquid Chromatographic Strategies

Lena N. Jeong
Virginia Commonwealth University

Follow this and additional works at: https://scholarscompass.vcu.edu/etd

Part of the Analytical Chemistry Commons

© Lena N. Jeong

Downloaded from
https://scholarscompass.vcu.edu/etd/5079

This Dissertation is brought to you for free and open access by the Graduate School at VCU Scholars Compass. It has been accepted for inclusion in Theses and Dissertations by an authorized administrator of VCU Scholars Compass. For more information, please contact libcompass@vcu.edu.

Development of General Purpose Liquid Chromatography Simulator for the Exploration of Novel Liquid Chromatographic Strategies

A dissertation submitted in partial fulfillment of the requirements for the degree of Doctor of Philosophy in Chemistry at Virginia Commonwealth University

By

Lena N. Jeong
Bachelor of Science in Chemistry, University of Virginia, 2010

Director: Sarah C. Rutan
Professor, Department of Chemistry

Virginia Commonwealth University
Richmond, VA
September 2017

Acknowledgements

I would have not been able to complete this journey without the help I received from great people in my life. First and foremost, I would like to thank my advisor Dr. Sarah Rutan, for making it possible for me to pursue this journey. She has molded me into the scientist I have become today. I have learned so much from Matlab programming/debugging to fundamental theories behind liquid chromatography. She has been the most supportive, patient, and understanding advisor I could have asked for. She has pushed me and challenged me to the limits that I never imagined I could reach. I will forever be grateful to her. Also many thanks to our collaborators in Minnesota, Dr. Dwight Stoll (Gustavus Adolphus College) and Dr. Peter Carr (University of Minnesota). It has been an honor to have worked with two great names in separation science. I am grateful that I was able to spend these few years with my lab-mate and a great friend, Dr. Daniel Cook. We endured through this program together from cumulative exams to seminar preparations. We had great scientific discussions and I look forward to many more in the future. Thanks to Dr. Maryanne Collinson, our collaborator for stationary phase gradient project, but more notably the person who made an exception to accept me into the program after admissions deadline. I thank her for taking a chance in me and trusting that I would live up to the expectation of this program. Newest member to stationary phase gradient group, my great friend Anna Forzano, I thank her for her genuine interest in my work and for listening to me vent. Former undergraduate, Steven Forte, was the best undergraduate research assistant any graduate student could have asked for.

My parents, Dr. Jaesoon Jeong and Hyeyoung Kim, have provided endless support and encouragement despite the miles between us. They have always made education a priority and sacrificed so much to make my American dream come true. I would also like to thank my little brother, Minsung Jeong, for his emotional support through the years of us being here alone. I remember the day he taught me how to find the peak maximum in Matlab. I have come very far. As he starts his MBA program this fall, still working full-time, I plan to be there to support him. My husband, my love and my inspiration, Dr. Frank Schmidtmann, has always believed in my abilities and provided financial and emotional support. Lastly, my greatest accomplishment, our beautiful daughter, Lyra, I thank her for being my muse, the reason for everything I do. I look forward to the day she pursues her dreams, whatever it may be, I will be there to fully support her through it.

Table of Contents

Acknowledgements ii

List of Tables viii

List of Figures ix

List of Abbreviations xvi

List of Symbols xvi

Preface xxi

Abstract xxiii

1. Overview of Objectives 1

2. Introduction 4

2.1. Liquid Chromatography 4

2.2. Two-Dimensional Liquid Chromatography (2D-LC) 9

2.3. Simulators 12

3. Theory 15

3.1. Craig distribution model 15

3.2. Linear solvent strength (LSS) theory 17

3.2.1. Retention time prediction 17

3.2.2. Peak width prediction 20

3.3. Non-LSST gradient retention model (Neue and Kuss) 23

3.4. Sample/eluent solvent mismatch theory 24

3.4.1. Peak width prediction 24

4. Development of Simulation Program 26

4.1. Introduction 26

4.2. Simulation of simple mobile phase gradient conditions 27

4.2.1. Isocratic experiments 27

4.2.2. Gradient experiments 28

4.2.3. Simulation codes 29

4.2.4. Prediction of alkylbenzene retention under gradient elution conditions using Neue-Kuss parameters determined from isocratic retention data 30

4.2.5. Prediction of amphetamine retention under gradient elution conditions using LSS parameters determined from gradient retention data 32

4.3. Solvent mismatch under isocratic condition 34

4.3.1. Experimental 34

4.3.2. Prediction of alkylbenzene retention with sample/eluent solvent mismatch under isocratic conditions 34

4.4. Incorporation of experimental injection profiles and solvent mismatch under gradient condition 38

4.4.1. Retention time and peak width 44

4.4.2. Effect of dilution 48

4.5. Effect of temperature 50

4.6. Conclusion 52

5. Convolution 55

5.1. Introduction 55

5.2. Closed form theory 56

5.2.1. Retention time calculation 56

5.2.2. Peak width calculation 57

5.3. Conditions studied 58

5.4. Closed form retention predictions 59

5.5. Convolution strategy 61

5.5.1. Feasibility testing 64

5.5.2. Automated convolution approach 67

5.6. Conclusion 70

6. Stationary Phase Gradients 71

6.1. Introduction 71

6.2. Stationary phase gradient theory 73

6.3. Validation of retention time and peak width for linear stationary phase gradients 76

6.4. Phase-optimized liquid chromatography (POPLC) 77

6.4.1. Experimental 77

6.4.2. Simulation codes 78

6.4.3. Determination of Neue-Kuss parameters 79

6.4.4. Stationary phase gradient simulations 80

6.4.5. Comparison of simulation to experimental data 85

6.5. In-house built continuous amine stationary phase gradients 89

6.5.1. Experimental LC conditions 91

6.5.2. LC data analysis 92

6.5.3. LC characterization 93

6.5.4. Comparison of simulation to experimental data 100

6.6. Conclusion 103

7. Summary and Conclusions 105

7.1. Reflections on Chapter 4.....105

7.2. Reflections on Chapter 5.....107

7.3. Reflections on Chapter 6.....108

7.4. Future Work 109

List of References 111

Appendix A.....124

Appendix B 127

Appendix C 134

Appendix D.....166

Vita.....177

List of Tables

Table 4.1. Neue-Kuss parameters for the alkylbenzenes 28

Table 4.2. LSS parameters for the amphetamine 30

Table 4.3. Experimental and simulated retention data for AB1-5 separated under gradient elution conditions 31

Table 4.4. Comparison of retention time and peak width prediction of simulation, LSS and experiments for amphetamines 33

Table 4.5. Neue-Kuss parameters for the solutes used in this work 44

Table 4.6. Comparison of simulated and experimental retention times and peak widths at 100 % loop filling. 47

Table 4.7. Diffusion coefficients for solutes used in simulations 51

Table 5.1. Closed form equations for retention time calculations under solvent mismatch condition 57

Table 5.2. Closed form equations for calculation of bandwidth before gradient 58

Table 5.3. Comparison of average computation time when using experimental injection profiles 69

Table 6.1. Combined linear solvent-strength parameters for the amphetamine for C_{18} and phenyl based columns from fits to equation 6.6 80

Table 6.2. Experimental and simulated retention data for amphetamines separated under isocratic elution conditions 86

Table 6.3. Experimental and simulated retention data for amphetamines separated under gradient elution conditions 88

Table 6.4. Experimental and simulated retention data for weak acids separated under gradient stationary phase and isocratic mobile phase elution conditions 101

List of Figures

Figure 2.1. The impact of selectivity, efficiency and retention on resolution (R_s). Fixed values: α = 1.05, N = 5000, and k = 5. Figure recreated from [2,3]. 6

Figure 2.2. Van Deemter plot. The minimum plate height (H_{min}) and optimum linear velocity (u_{opt}) is indicated by the dashed line. 7

Figure 2.3. Typical setup for LC x LC with a 10-port/2-position valve and two sample loops: loop 1 (orange) and loop 2 (green). The dilution pump is optional along with the possible addition of second diode array detector (DAD) between the first dimension column outlet and the sampling valve. Figure recreated from [12]. 9

Figure 2.4. Comparison of degree of separation correlation: (A) strong correlation; (B) moderate correlation; and (C) no correlation. Figure recreated from [19]. 11

Figure 3.1. Propagation of the analyte through a time-distance grid in the Craig distribution model. Adapted from [58]..... 16

Figure 3.2. LSS plot: linear dependence of ln k on ϕ..... 17

Figure 3.3. Simulation of an analyte with high initial retention factor under conditions where there is a significant gradient delay, t_D. The total column length = C1 + C2. During the gradient delay time, the analyte experiences isocratic condition (C1), whereas a changing solvent strength is experienced when the mobile phase gradient catches up with the analyte (C2). Simulation conditions: Δz = 0.01 cm; Δt = 0.06 s; ϕ_o = 0.02; $\Delta\phi$ = 0.8; k_w = 100; S = 100; t_G = 5 min; t_D = 3.5 min; L = 5 cm. Under these conditions, the gradient catches up with the analyte peak after 3.76 min, at a distance 2.59 cm down the column. The profile at 2 cm occurs at 2.9 min and the profile at 3.9 cm occurs at 4.1 min. 21

Figure 3.4. NK plot: non-linear dependence of ln k on ϕ 23

Figure 4.1. Structures and abbreviations for five amphetamines..... 29

Figure 4.2. Experimental (bottom) and simulated (top) chromatograms collected for gradient separations of alkylbenzenes AB1-5. The solvent gradient was 50-90% ACN from 0-2.25 min, and injection volume was 1 µL. The measured gradient delay time of 0.055 min was used in the simulation..... 31

Figure 4.3. Experimental (bottom) and simulated (top) chromatograms collected for gradient separations amphetamines. The solvent gradient was 5-35% ACN from 0-18 min. The measured gradient delay time of 0.795 min was used in the simulation. The heights of simulated peaks are scaled to the heights of the experimental peaks. The gaps in the baseline of the experimental chromatograms are due to the fact that the compounds were injected in different samples. 33

Figure 4.4. Experimental (black) and simulated (red) chromatograms collected for isocratic separations of alkylbenzenes AB1 (first peak), AB3, and AB5 (last peak). The eluent was 70% ACN, and injection volume was 100 µL. Sample solvents were 50 (A), 70 (B), or 90 (C) % ACN. 36

Figure 4.5. Comparison of experimental (black, open symbols) and simulated (red, closed symbols) retention times for sample/eluent solvent mismatch. Retention times for (A) methylbenzene (k = 1.67) and (B) pentylbenzene (k = 7.81) injected from either 50% (circles) or 90% (squares) ACN samples into an eluent containing 70% ACN. The percent difference between the experimental and simulated retention times was within 2.2% for AB1 and within 1.0% for AB5. 36

Figure 4.6. Percent increase in peak width for pentylbenzene (AB5) as a function of injection volume. Samples are in (A) 50% and (B) 90% (v/v) ACN for an eluent containing 70% (v/v) ACN. Black open circles are experimental, red open squares are for simulation and blue open diamonds are for theory (equations 3.22-3.25). 38

Figure 4.7. Experimentally measured injection profiles obtained from sample loops of different sizes, at different filling levels: (A) 0.4 µL; (B) 13.5 µL; (C) 20 µL; (D) 40 µL; (E) 60 µL; and (F) 80 µL. Filling levels were 25 (green), 50 (blue), 75 (red), and 100 (**black**) %, except for the 0.4 µL loop, which was filled to 200 %. Other conditions: Mobile phase, 50/50 ACN/water; injected sample was 10 µg/mL uracil in mobile phase; flow rate, 2.5 mL/min. 39

Figure 4.8. Graphic showing piecewise construction of solvent profiles (at column inlet) used in this work (here, for the specific case of 100% filling of a 40 µL loop). The red trace shows a simple linear solvent gradient over a gradient time t_G. The green and blue traces show rectangular or experimental injection profiles preceding the solvent gradient, respectively. The sample solvent is 20 % greater in organic composition relative to the initial mobile phase composition. 40

Figure 4.9. Structures and abbreviations for compounds used for the study discussed in section 4.4..... 42

Figure 4.10. Comparison of the simulated chromatograms obtained for DiEtF using a rectangular (red) or experimental (**black**) injection profile. Conditions: Loop volume was 40 µL, with 100 % loop filling; injection of sample in 50/50 ACN/water. Other conditions: column, 30 mm x 2.1 mm i.d. Zorbax SB-C18, 3.5 µm; flow rate 2.5 mL/min; temperature, 40 ºC; gradient elution from 30-65-30-30 % ACN from 0-0.25-0.26-0.50 min. 45

Figure 4.11. Comparison of experimental (A-C) and simulated (D-F) separations of (1) diethylformamide, (2) methylparaben, (3) propylparaben, and (5) butyrophenone. Loop volume was 40 µL, with 100 % loop filling. Panels A and D correspond to injections of sample in 10/90

ACN/water; B and E, 30/70 ACN/water; C and F, 50/50 ACN/water. Other conditions are as in Fig. 4.10. Experimental signals are due to absorption of UV light at 210 nm. The scale of the signal axis for the simulated chromatograms is arbitrary. 46

Figure 4.12. Peak height (A) and resolution (B) from simulation results vs. nominal loop volume (100% filling) for peaks 4 and 5 at different $\Delta\phi_{sample}$ levels. The peak height is taken as the average height of peaks 4 and 5. All other conditions are as in Figure 4.9. 49

Figure 4.13. Simulation of peaks 4 and 5 for (A) nominal loop volume of 40 µL (100% filling) at $\Delta\phi_{sample}$ = +0.1 (B) nominal loop volume of 80 µL (100 % filling) at $\Delta\phi_{sample}$ = -0.1. All other conditions are same as Figure 4.10. 50

Figure 4.14. Experimental (A) and simulated (rectangular injection) (B) chromatograms collected for gradient separations of hydroxyphenones and parabens at 70 ºC. Conditions: capillary C_{18} column packed in-house (78 mm x 0.15 mm ID, 1.7 µm d_p), injection volume of 1500 nL, mobile phase gradient 95:5 to 55:45 10 mM H_3PO_4:ACN over 16 min at flow rate of 3.00 µL/min. Experimental data reproduced from [20], with permission. 52

Figure 5.1. Structures and abbreviations for compounds used in the convolution study 59

Figure 5.2. Comparison of retention prediction by closed form to full simulation using rectangular injection profiles (A) retention time and (B) peak width. These correspond to cases where the sample solvent is the same as the solvent composition at the start of the gradient. 60

Figure 5.3. Comparison of retention prediction by closed form to full simulation using rectangular injection profiles (A) retention time and (B) peak width for all 1008 conditions. 61

Figure 5.4. Convolution of a Gaussian function with an exponential decay function to produce an exponentially modified Gaussian function 62

Figure 5.5. Convolution method applied to LC. (A) Two column segments for convolution approach: a full simulation is performed for first segment C1 and the known closed form solution for second segment C2 is used to make a Gausssian peak (B) Stepwise schematic of the convolution approach. 63

Figure 5.6. Relationship between $z_{1,f}$ (A), $z_{2,f}$ (B), and $z_{2,m}$ (C). Sample solvent band (blue), analyte band (red), and mobile phase gradient (green). 64

Figure 5.7. Comparison of (A) convolution to (B) full simulation in prediction of PEA retention on 5 cm C_{18} column under 2 % - 5 % ACN gradient over 3 minutes 66

Figure 5.8. Comparison of retention prediction by convolution to full simulation (A) retention time and (B) peak width using rectangular injection profiles. Only the 854 conditions where convolution is useful are plotted. 68

Figure 5.9. Comparison of retention prediction by convolution to full simulation (A) retention time and (B) peak width using experimental injection profiles. Only the 854 conditions where convolution is useful are plotted. 69

Figure 6.1. Structures and abbreviations for ten amphetamines 78

Figure 6.2. Relative concentration of phenyl (dashed curves) and C_{18} (solid curves) functional groups for simulated phenyl/C_{18} gradients: (A) linear gradient, (B) step gradient, and (C) exponential gradient. Resulting simulated chromatogram with isocratic mobile phase composition (ϕ = 0.1) of each stationary phase gradient (D), (E), (F), respectively. Amphetamine elution order is as listed in Table 1. 82

Figure 6.3. Simulation of four amphetamines: 4. EP, 5. PSE, 7. MDA and 8. Mamp on 11 different stationary phases with isocratic mobile phase composition (ϕ = 0.1) with varying C_{18}/phenyl composition. The gradient columns were simulated to have exponential profiles. 83

Figure 6.4. Predicted separation of ten amphetamines by varying stationary phase composition and ϕ. (A) Resolution map with optimum separation condition marked with a red square, (B) simulation using the optimum separation conditions 70 % phenyl gradient column and ϕ = 0.1. The peak numbers correspond to the amphetamines shown in Figure 6.1. Resolution of the critical pair is marked with an arrow. 84

Figure 6.5. Comparison of experimental (blue) and simulated (orange) separations of (A) PE, PEA, and MDA; (B) EP and Mamp; (C) PSE and MDMA; and (D) PPA, Amp, and Moxy. Isocratic separation condition at ϕ = 0.2. Experimental signals relative intensity. The scale of the signal axis for the simulated chromatograms is arbitrary. 86

Figure 6.6. Comparison of experimental (blue) and simulated (orange) separations of (A) PE, PEA, and MDA; (B) EP and Mamp; (C) PSE and MDMA; and (D) PPA, Amp, and Moxy. Gradient separation condition: ϕ_o = 0.1 to ϕ_f = 0.15 over t_G = 10 min. Experimental signals are relative intensity. The scale of the signal axis for the simulated chromatograms is arbitrary. 89

Figure 6.7. Structures and pKa's of analyzed compounds [132] 93

Figure 6.8. Stacked chromatograms of uracil (red) and cytosine (blue) standards on (A) unmodified, (B) gradient, and (C) uniformly modified monolithic columns. The chromatograms are normalized to represent a 5.8 cm column in each case. 94

Figure 6.9. Retention factors for uracil and cytosine on unmodified (n = 5), gradient (n = 11), and uniformly modified monolithic columns (n = 5). 95

Figure 6.10. Van Deemter plots of uracil (blue circles) and cytosine (red squares) on unmodified, gradient and uniformly modified monolithic columns. 97

Figure 6.11. Stacked chromatograms resolved by MCR-ALS of 3-ABA (red), BA (black), 2-APy (blue) and 4-AP (green), on unmodified, gradient, and uniformly modified monolithic columns. The chromatograms are scaled to represent a 5.8 cm column in each case. 98

Figure 6.12. Retention factor for BA, 3-ABA, 4-AP and 2-APy on unmodified (n=5), gradient (n=10), and uniform (n=3). 100

Figure 6.13. Resolution of critical pair for gradient columns with varying composition of amine calculated at 10 % increment of amine concentration at 90:10 ACN:ammonium acetate buffer (10 mM; pH 3.64).....101

List of Abbreviations

^{1}D	first dimension
1D	one-dimensional
^{2}D	second dimension
2D	two-dimensional
1D-LC	one-dimensional liquid chromatography
2D-LC	two-dimensional liquid chromatography
C1	first section of the column (convolution)
C2	second section of the column (convolution)
DAD	diode array detector
HILIC	hydrophilic interaction liquid chromatography
LC	liquid chromatography
LCxLC	comprehensive two-dimensional liquid chromatography
LSS	linear solvent strength
NK	Neue-Kuss
NPLC	normal phase liquid chromatography
POPLC	phase optimized liquid chromatography
RPLC	reversed phase liquid chromatography
SOSLC	stationary phase optimized selectivity liquid chromatography

UPLC	ultra-high pressure liquid chromatography
XPS	x-ray photoelectron spectroscopy

List of Symbols

A	eddy dispersion (cm)
a	slope of the linear stationary phase gradient
B	longitudinal diffusion (cm^2/min)
b	intrinsic gradient steepness ($t_m \Delta\phi S/t_G$)
b^*	intrinsic gradient steepness ($t_{m,grad} \Delta\phi S/t_G$)
$b^\dagger$	intrinsic gradient steepness for NK model
C	resistance to mass transfer (min)
$D_{m,T}$	diffusion coefficient at a given temperature (cm^2/s)
D_z	effective axial dispersion coefficient (cm^2/s)
F	flow rate (mL/min)
$f_{coverage}$	fractional coverage of the two dimensional separation space
G_{bR}	gradient compression factor
H	height equivalent of theoretical plate; Δz (cm)
k	retention factor
k^*	retention factor at column midpoint
k_o	initial retention factor
k_e	retention factor at elution
k_{mp}	retention factor in the mobile phase

k_{ss}	retention factor in the sample solvent
k_w	retention factor in purely aqueous mobile phase
$k_{w,T}$	temperature dependent retention factor in purely aqueous mobile phase
L	column length (cm)
L_{sim}	simulation column length (cm) (C1, convolution)
m_d	detected mass
$m_{L,t}$	total mass at time t at the column exit
$m_{z,t}$	mass at position z and time t
m_s	mass of solute in the stationary phase
m_m	mass of solute in the mobile phase
N	plate number
n_c	peak capacity
n_s	moles of analyte in the stationary phase
n_m	moles of analyte in the mobile phase
N_{SYS}	plate number (Foley-Dorsey expression)
R_s	resolution
S	slope of the ln k vs. ϕ plot
S^*	slope of ln k vs ϕ plot at elution (Neue-Kuss model)
S_1	slope of the ln k vs. ϕ plot (Neue-Kuss model)
$S_{1,T}$	temperature dependent slope of the ln k vs. ϕ plot (Neue-Kuss model)
S_2	curvature of the ln k vs. ϕ plot (Neue-Kuss model)
$S_{t,injection}$	signal of injected solute from injection loop (mAU)
T	temperature (Kelvin)

t_D	dwell time (min)
$t_{D,loop}$	time required to travel the length of the sample loop (min)
$t_{D,pump}$	gradient delay time (min)
t_G	gradient time (min)
t_{inj}	injection time (min)
t_M	void time (min)
t_R	retention time (min)
$t_{R,cf}$	retention time calculated by closed form equations (min)
t_s	sampling time (min)
t_{sim}	simulation time (min) (convolution)
Δt	time increment (min)
u_a	analyte velocity (cm/min)
u_e	analyte velocity at elution (cm/min)
u_m	mobile phase velocity (cm/min)
u_{mp}	solute velocity in mobile phase (cm/min)
u_{opt}	optimal mobile phase velocity (cm/min)
u_{ss}	solute velocity in the sample solvent (cm/min)
V_{inj}	injected volume (mL)
V_{loop}	experimentally determined sample loop volume (mL)
V_M	void volume (mL)
V_R	retention volume (mL)
V_{stat}	stationary phase volume (mL)
ΔV_{sim}	sampling interval in volume units (mL)

w_{10}	peak width at 10 % height (min)
w_{50}	peak width at half height (min)
$w_{4.4}$	peak width at 4.4 % height (min)
$z_{1,f}$	analyte bandwidth after injection has been completed (cm)
$z_{2,m}$	the position at which the midpoint of the analyte band lines up with the tail end of the sample solvent band (cm)
$z_{2,f}$	the position at which the front end of the analyte band lines up with the tail end of the sample solvent band (cm)
z_{inj}	sample solvent injection bandwidth (cm)
Δz	distance increment; plate height (cm)

Greek Symbols

α	selectivity
$<\beta>$	broadening correction factor
η_T	viscosity at given mobile phase composition and temperature (cP)
μ	solute mobility; fraction of solute in mobile phase; normalized solute velocity
μ_R	solute mobility at elution
${}^1\sigma$	first dimension peak width before sampling (min)
σ_b	bandwidth of the injected band (cm)
σ_{cf}	peak width calculated by closed form (min)
σ_{col}	peak width caused by the column (min)
σ_D	band broadening during the elution while in the dwell volume (cm)
σ_{grad}	gradient peak width (min)

σ_{sample}	band broadening during elution while in the sample solvent (cm)
$\Delta\sigma_{inj}$	peak width of the injected sample (min)
$\Delta\sigma$	extra column broadening due to non-ideal injection (min)
$\Delta\sigma_{iso}$	gradient focused isocratic peak width (min)
$\Delta\sigma_{tot}$	total peak width (min)
ϕ	organic solvent composition
ϕ^*	organic solvent composition at the column midpoint
ϕ_o	initial organic solvent composition
ϕ_e	organic solvent composition at elution
ϕ_f	final organic solvent composition
$\phi_{t,gradient}$	mobile phase gradient as a function of time
$\phi_{t,injection}$	injected solvent composition as a function of time
$\phi_{V,injection}$	injected solvent composition as a function of volume
$\Delta\phi$	change in organic solvent composition over gradient
$\Delta\phi_{sample}$	the composition difference between the sample solvent and the initial mobile phase
ω	solute immobility; fraction of solute in stationary phase
ω_o	solute immobility at the start of the gradient

Preface

This dissertation is a result of several great collaborations. Here I briefly describe roles each individual fulfilled in the projects presented in the following chapters.

The studies presented in Chapter 4 were in collaboration with the Stoll group. A version of sections 4.2 and 4.3 has been published in *J. Chromatogr. A.* I was responsible for developing a simulation program independently from the Stoll group and cross checking our simulation results to validate our codes. S.G. Forte was responsible for gathering chromatographic data for amphetamines. All alkylbenzene experiments were performed by the Stoll group. A portion of Chapter 4, specifically section 4.4, was adapted from manuscript recently published in *J. Chromatogr. A.* The experimental work was performed by the Stoll group. I was responsible for incorporating experimental injection profiles to our simulation code for validation of all simulation results obtained from Stoll group's simulation program. I was involved in writing the explanation of how we made the experimental injection profile incorporation possible along with reviewing and editing the manuscript.

The convolution study presented in Chapter 5 was in collaboration with Dr. Dwight Stoll and Dr. Peter Carr. The idea was proposed by Dr. Peter Carr. I was responsible for implementing the approach by developing convolution program and comparing its performance against full simulation. Dr. Carr and Dr. Stoll also provided valuable theoretical insights to the approach

which made it possible for us to compose closed form expressions for approximate retention prediction under non-ideal solvent mismatch conditions.

The studies presented in Chapter 6 were carried out in collaboration with the Collinson group. I was responsible for developing and validating simulation program by comparing the simulated results to the experimental data. A portion of Chapter 6, specifically section 6.5, was published in *Anal. Chem.* V.C. Dewookar synthesized monolithic columns and performed chromatography. K.M. Ashraf acquired XPS data. D.W. Cook and I were responsible for chromatographic data analysis.

It goes without saying that my advisor Dr. Sarah Rutan was an essential part of all above mentioned projects. She provided guidance, developed and debugged several codes, and provided endless amount of support in manuscript preparation and editing. Finally, this work was funded by three NSF grants and the Altria graduate student fellowship (Fall 2016 and Spring 2017).

Abstract

DEVELOPMENT OF GENERAL PURPOSE LIQUID CHROMATOGRAPHY SIMULATOR FOR THE EXPLORATION OF NOVEL LIQUID CHROMATOGRAPHIC STRATEGIES

By Lena N. Jeong

A dissertation submitted in partial fulfillment of the requirements of the degree of Doctor of Philosophy at Virginia Commonwealth University

Virginia Commonwealth University, 2017

Director: Sarah C. Rutan, Professor, Department of Chemistry

The method development process in liquid chromatography (LC) involves optimization of a variety of method parameters including stationary phase chemistry, column temperature, initial and final mobile phase compositions, and gradient time when gradient mobile phases are used. Here, a general simulation program to predict the results (i.e., retention time, peak width and peak shape) of LC separations, with the ability to study various complex chromatographic conditions is described. The simulation program is based on the Craig distribution model where the column is divided into discrete distance (Δz) and time (Δt) segments in a grid and is based on parameterization with either the linear solvent strength or Neue-Kuss models for chromatographic retention. This

algorithm is relatively simple to understand and produces results that agree well with closed form theory when available. The set of simulation programs allows for the use of any eluent composition profile (linear and nonlinear), any column temperature, any stationary phase composition (constant or non-constant), and any composition and shape of the injected sample profile. The latter addition to our program is particularly useful in characterizing the solvent mismatch effect in comprehensive two-dimensional liquid chromatography (2D-LC), in which there is a mismatch between the first dimension (^{1}D) effluent and second dimension (^{2}D) initial mobile phase composition. This solvent mismatch causes peak distortion and broadening. The use of simulations can provide a better understanding of this phenomenon and a guide for the method development for 2D-LC. Another development that is proposed to have a great impact on the enhancement of 2D-LC methods is the use of continuous stationary phase gradients. When using rapid mobile phase gradients in the second dimension separation with diode array detection (DAD), refractive index changes cause large backgrounds such as an injection ridge (from solvent mismatch) and sloping baselines which can be problematic for achieving accurate quantitation. Use of a stationary phase gradient may enable the use of an isocratic mobile phase in the ^{2}D, thus minimizing these background signals. Finally, our simulator can be used as an educational tool. Unlike commercially available simulators, our program can capture the evolution of the chromatogram in the form of movies and/or snapshots of the analyte distribution over time and/or distance to facilitate a better understanding of the separation process under complicated circumstances. We plan to make this simulation program publically available to all chromatographers and educators to aid in more efficient method development and chromatographic training.

Chapter 1: Overview and Objectives

Liquid chromatography (LC) is an important part of analytical science and a very powerful separation technique. It is a versatile technique which allows for variations in experimental conditions to achieve fine-tuned separation of mixture of interest. The process of finding the best separation conditions involves optimization of variety of separation parameters such as solvent composition, column type, and temperature. The optimization process by conventional trial-and-error approach in LC method development can be time consuming. The conventional trial-and-error approach in LC method development usually results in significant experimental time and resources. Naturally chromatographers have sought out fast and accurate retention prediction which has been a driving force for innovations in computer simulators (based on theoretical studies of band propagation). Currently available simulators, although useful, are expensive and lack flexibility. Here we describe the development of a general simulation program which is simple to understand with several added capabilities not offered by commercially available simulators.

There were three reasons for pursuing the development of our own LC simulation program: (1) to save time and money involved in conventional method development; (2) to produce more reliable and accurate results with the flexibility to handle a variety of different separation conditions; and (3) to offer an easy to use simulation tool free of charge for the purpose of education and research. In the next five chapters we will explore the theoretical basis for liquid

chromatography, the development and extension of our simulation program, and further acceleration of retention prediction process. Chapter 2 explains the basics of LC and introduces two-dimensional liquid chromatography (2D-LC). Chapter 3 describes all theoretical equations used as the bases for the development of the simulation program.

The work presented here was motivated by four major goals which are discussed in detail in the following chapters. First, we wanted to support conventional LC method development with a simulation program with more flexibility and accuracy compared to what is offered by existing simulators. The simulation algorithm is based on the Craig distribution model where the column is divided into discrete distance and time segments. Equilibration occurs at each position and time, and the concentration at the end of the column is recorded. Chapter 4 discusses the creation of the simulation program and each extension made to improve its flexibility. Although 2D-LC offers increased separation power, its lower detection sensitivity compared to one-dimensional LC has been a limitation. This is believed to be due to difficulties in controlling the conditions that the analytes experience when they are transferred from the first to the second dimension. Upon successful simulation of conventional mobile phase gradients and validation of the simulation program against a well-known theory (Linear Solvent Strength), our second goal was to extend the simulation program capability to accurately predict the effect of common conditions used in 2D-LC method development.

The third goal of this work was to accelerate the simulation process along with full automation. Our simulation program is shown to provide accurate retention prediction with ability to monitor the band propagation, which can be captured as snapshots or movies. Although it is faster than a trial-and-error approach in method development, the exhaustive search for the most optimal separation condition is limited by the need to calculate the retention factor stepwise at

every position and time. Chapter 5 presents a convolution approach applied to chromatographic retention prediction to speed up this process. Under the convolution approach, full simulation is required for a shorter length of the column and retention on the remainder of the column is predicted by closed form calculation. A six-fold speed increase with utilization of convolution approach compared to full simulation for 854 conditions clearly illustrate its potential for exhaustive search for optimal separation condition.

Our fourth and final goal was to further extend the capabilities of the simulation program to support the development of continuous stationary phase gradients. The simulator can provide a better understanding of the effects of the placement of different functionalities on column selectivity. Chapter 6 describes additional adaptation of the simulator to include retention prediction on a non-uniform stationary phase column under isocratic and gradient elution conditions. This extension in the simulation program was validated by comparing retention prediction of ten amphetamines to experimental data acquired on a commercially available discontinuous stationary phase system. In collaboration with the Collinson lab, we successfully synthesized continuous amine gradient columns, which resulted in a change in selectivity compared to bare silica and uniform amine columns. Comparison of simulation retention prediction for probe compounds to the experimental data revealed possible neighboring ligand effect present in the continuous amine gradient column. We believe that the following chapters will clearly show the usefulness of our simulation program in LC method development and that it will prove to be a great educational tool.

Chapter 2: Introduction

2.1. Liquid Chromatography

Liquid chromatography (LC)* is a physical separation technique that utilizes two phases – a liquid mobile phase and a solid or liquid stationary phase. Separation is achieved based on the difference in the degree of interaction of each analyte to both phases through a partition or adsorption mechanism. The interactions can be based on polarity, electrical charge, and molecular size [1]. This dissertation focuses on LC separations based on polarity. Two different types of bonded phase LC separations are available where polarity of the stationary and mobile phases are changed to separate mixtures. The stationary phase is polar and the mobile phase is non-polar in normal phase liquid chromatography (NPLC), whereas the opposite is true for reversed phase liquid chromatography (RPLC). RPLC is the most widely used technique and therefore discussions in this work will focus on this mode of separation with the exception of hydrophilic interaction liquid chromatography (HILIC), which is discussed in section 6.5. HILIC is a form of normal phase chromatography when water is one of the components of the mobile phase. Stationary phases under RPLC conditions are hydrophobic in nature and are usually chemically bonded to the surface of a silica particle supports. Some of the most commonly used stationary phases are alkyl chains (C_{18}, C_8, C_4), phenyl, cyano and amino. The rate at which each analyte moves through the system

* High performance or high pressure liquid chromatography (HPLC) uses high-pressure to move mobile phase through the stationary phase and is simply referred to as LC throughout this dissertation.

depends on its interaction with each phase. If the analyte has no interaction with the mobile phase, then it will stick to the stationary phase and never elute. On the other hand, if there is no interaction with the stationary phase, the analyte will move through the column at the same rate as the mobile phase. The degree of the solute's affinity to the stationary phase is known as the retention factor (k) and is simply defined as the ratio of moles of analyte in the stationary phase (n_s) to moles of analyte in the mobile phase (n_m). Or, it can also be calculated from experimental data:

$$k = \frac{n_s}{n_m} = \frac{t_R - t_M}{t_M} \tag{2.1}$$

where t_R is the retention time of the analyte and t_M is the column dead time or retention time of an un-retained compound. The higher the k value, longer the retention and slower the elution.

The separation between two peaks can be quantified by the term known as resolution (R_s):

$$R_s = \frac{1}{4}\sqrt{N}\,\frac{(\alpha - 1)}{\alpha}\,\frac{k}{k+1} \tag{2.3}$$

There are three factors that contribute to resolution: retention (k), selectivity (α), and efficiency (N). Selectivity is directly related to the quality of chromatographic separation and is defined as the ratio of the retention factors of two analytes:

$$\alpha = \frac{k_2}{k_1} \tag{2.2}$$

Since $k_2 > k_1$, the selectivity is always greater than one by definition.

The column efficiency is directly related to resolution and inversely related to the plate height (H):

$$N = \frac{L}{H} \tag{2.4}$$

where L is the column length. In order to increase resolution or improve separation, we can increase N, which decreases the peak widths, or increase α by increasing the space between two peaks. As shown in Figure 2.1, α has the greatest impact on improving resolution. Usually it is

necessary to increase retention of analytes in order to increase selectivity. However, longer analysis time is not desirable and therefore, the preferred approach historically is to improve the column efficiency.

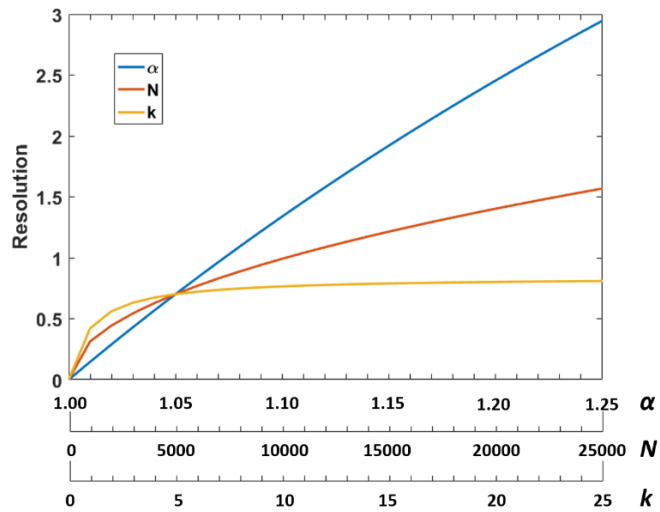

Figure 2.1. The impact of selectivity, efficiency and retention on resolution (R_s). Fixed values: α = 1.05, N = 5000, and k = 5. Figure recreated from [2,3].

The impact of column efficiency on separation performance can be represented by the peak capacity (n_c). It is defined as the maximum number of Gaussian peaks which can fit within the separation window with R_s = 1. At a resolution smaller than 1, analysis of peaks becomes difficult and is considered to be an inadequate separation.

The column efficiency can be enhanced by controlling three phenomena in chromatography. The van Deemter equation defines theoretical plate height, H, as a sum of these three factors:

$$H = A + \frac{B}{u_m} + Cu_m \tag{2.5}$$

The first term, A, is eddy dispersion and it explains the peak broadening caused by the different paths the analyte can take down the column length. Non-uniform packing of the particles in the column bed causes more dispersion. The second term, B, is the longitudinal diffusion along the column. This term is inversely related to the mobile phase velocity, u_m. In other words, the analyte has more time to diffuse, resulting in a broader peak at slower mobile phase velocities. The last term, C, is the resistance to mass transfer and its contribution is directly related to the mobile phase velocity. The faster the flow rate, less time for analyte to partition between the two phases. When we plot equation 2.5, we can find the optimum mobile phase velocity, u_{opt}, which results in minimum H value as shown in Figure 2.2. Although this is the mobile phase velocity that will provide the best efficiency, it often is slower than the desired analysis speed. Therefore, linear velocities faster than the optimal velocity are often used, with careful consideration of the effect of C term on the resulting separation.

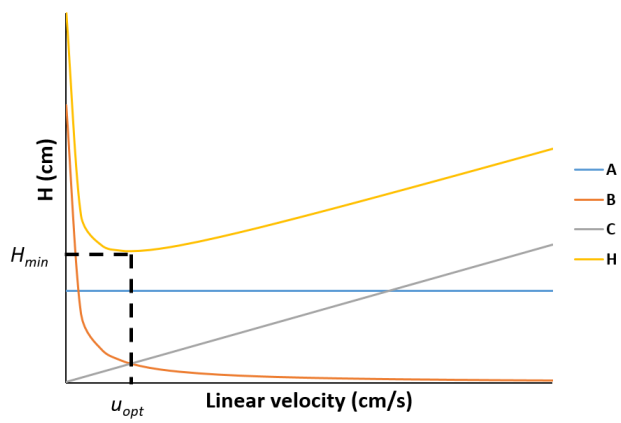

Figure 2.2. Van Deemter plot. The minimum plate height (H_{min}) and optimum linear velocity (u_{opt}) is indicated by the dashed line.

Each of these van Deemter terms can be minimized with careful selection of separation conditions and improvement in column technology, resulting in improve separation efficiency. Continuous

efforts have been made in the advancement of stationary phase particles and packing over the years. In the early 2000s small sub-2 μm particles were introduced along with ultra-high pressure liquid chromatography (UPLC) [4]. These small particles provide increased efficiency with an increase in surface area and a decrease in eddy dispersion (A term) due to tighter and more uniform packing. Also, flow rates above the optimal velocity do not cause much loss in efficiency due to a decreased C term allowing for faster analysis. However, increased flow rate inherently causes increase in back pressure. The progression of particles from sub-2 μm fully porous particles to a 2.7 μm superficially porous or core shell particles in 2007 has provided similar efficiencies along with much lower back pressure allowing for the use of traditional LC systems [5].

It is evident that the above-mentioned advancements in chromatographic technologies have provided higher peak capacities. However, improvement in column efficiency is not enough to solve separation issues for co-eluting compounds such as isomers with similar chemical properties. Under these conditions it is also necessary to change chromatographic selectivity to achieve further separation between two peaks. In practical sense this change in selectivity can be obtained by utilizing more than one stationary phase chemistry. Mixed mode columns provide two different mode of separation simultaneously on a single column (e.g., the combination of RPLC with ion chromatography [6]). Simply connecting multiple columns with different stationary phase chemistry also allows for changes in selectivity. However, the use of tubing for connection of columns introduces dead volume which leads to peak broadening. Although a commercially available serially coupled column system known as POPLC claims to eliminate dead volumes with a patented segment technology, experimental data prove otherwise [7]. This is also confirmed in our own study discussed in Chapter 6. An alternate approach is the use of multidimensional

separations. Under two-dimensional liquid chromatography (2D-LC), two 'orthogonal' columns are coupled to achieve separations with increased peak capacities.

2.2. Two-Dimensional Liquid Chromatography (2D-LC)

A highly complex mixture can result in an inadequate separation even with extended analysis times when using one-dimensional (1D) LC methods. Use of more than one separation mechanism simultaneously, as in two-dimensional liquid chromatography (2D-LC), can provide increased separation power [8,9]. The two dimensions of separation are coupled with sampling valve which collects and delivers a preset volume of effluent from the first dimension (^{1}D) to the second dimension (^{2}D). The sampling can either be done for only regions of interest from the ^{1}D as in a heart-cutting method or for the entirety of the ^{1}D effluent as in a comprehensive method [10,11]. Figure 2.3 shows the instrumental set-up for comprehensive 2D-LC (LC x LC).

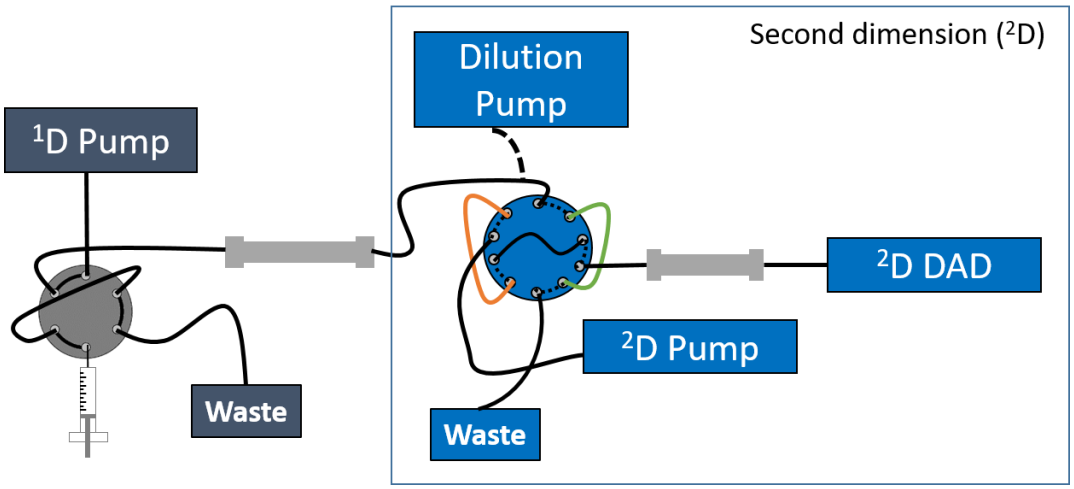

Figure 2.3. Typical setup for LC x LC with a 10-port/2-position valve and two sample loops: loop 1 (orange) and loop 2 (green). The dilution pump is optional along with the possible addition of second diode array detector (DAD) between the first dimension column outlet and the sampling valve. Figure recreated from [12].

The 2D-LC technique possesses increased peak capacity resulting in more potential for better resolution compared to 1D-LC. The theoretical total peak capacity in 2D-LC is equal to the product of the peak capacities in the first and second dimensions [8,13,14]:

$$n_{c,2D} = {}^{1}n_c \times {}^{2}n_c \tag{2.6}$$

However, the peak capacity obtained in reality is much lower than this theoretical value due to ^{1}D undersampling and correlated retention between the columns in the first and second dimensions. The sampling rate of first dimension effluent is determined by the rate of second dimension separation, which means at slower ^{2}D separation speeds, fewer data points are available to represent the ^{1}D peak. This leads to broadening of the peak and loss of peak capacity from the ^{1}D. This broadening effect has been studied extensively in the past [15–17]. An average ^{1}D peak broadening correction factor <β> determined from simulation studies [18] can be incorporated to correct for the loss of peak capacity due to ^{1}D undersampling:

$$<\beta> = \sqrt{1 + 0.21\left(\frac{t_s}{{}^{1}\sigma}\right)} \tag{2.7}$$

where t_s is the sampling time and ${}^{1}\sigma$ is the peak width before sampling.

The second contributing factor in the observed decrease in peak capacity is correlation of retention in the two dimensions. In order to utilize the largest amount of the separation space that is available, the retention mechanisms in two dimensions must be as different as possible. This is known as "orthogonality." Completely uncorrelated or orthogonal separations result in even distribution of peaks in the 2D separation space (Figure 2.4C), whereas completely correlated separations result the analytes appearing only along a diagonal line in the separation space (Figure 2.4A).

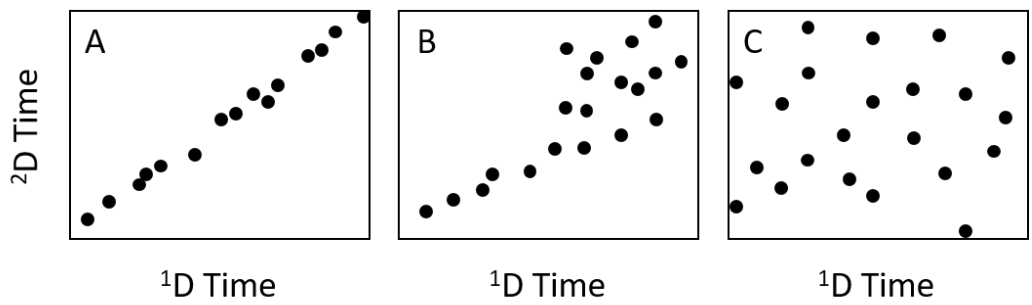

Figure 2.4. Comparison of the degree of separation correlation: (A) strong correlation; (B) moderate correlation; and (C) no correlation. Figure adapted from [19].

Under popular RP x RP separation conditions, it is impossible to achieve complete orthogonality and therefore the 2D separation space is only partially utilized (Figure 2.4B). This partial coverage is called the fractional coverage ($f_{coverage}$) and is directly related to the overall peak capacity.

$$n_{c,2D} = {}^{1}n_c \times {}^{2}n_c \times \frac{1}{<\beta>} \times f_{Coverage} \tag{2.8}$$

The low fractional coverage is usually caused by the similarity of retention in the two dimensions.

When using two different separation mechanisms it is important to consider mobile phase compatibility. The use of gradient elution in both dimensions usually results in a first dimension effluent in that has a high organic composition compared to the initial mobile phase conditions in the second dimension. This is referred to as solvent mismatch, and it results in peak distortion and broadening. A common practice to overcome this issue is to dilute first dimension effluent with weaker solvent (aqueous) to match the initial mobile phase composition in the second dimension. However, dilution results in a large injection volume, and therefore large injection band. It has been shown that dilution of the first dimension effluent to weaker composition than the initial mobile phase composition of second dimension can focus the injection band on column [8,11]. Another approach developed by Weber *et al.* is the use of temperature in place of solvent to

encourage focusing of analyte bands [20–22]. Although this approach has shown great promise, it is currently only applicable to capillary column formats. Another approach to eliminate the solvent mismatch issue in LC x LC is to use a stationary phase gradient that provides increased separation selectivity and therefore allowing for elimination of mobile phase gradient in the first dimension. It is clear that rapid and accurate retention prediction of a variety of different separation conditions by computer simulation is highly desirable, in order to effectively explore the effectiveness of these different solutions to the solvent mismatch problem.

2.3. Simulators

The method development process in LC involves the optimization of method parameters such as the stationary phase, column dimensions, initial and final mobile phase compositions, as well as gradient time when gradient elution is used [23]. Computer simulation can aid in the optimization of separation methods, which can save time and money as compared to trial-and-error approaches [23–31]. In the past, several different methods for solving the mass transport equations defining the evolution of chromatographic peaks have been used, including the Craig distribution model (based on the concept of theoretical plates) and mass balance equations (based on obtaining elution profiles through numerical integration) [32–40]. There are also several commercially available simulation software packages that use linear solvent strength (LSS) theory or linear free energy-type relationships such as DryLab (Molnar-Institute) [24,25,28,41], LC&GC Simulator (ACD/Labs) [31,42] and ChromSword Offline (Merck KGaA) [27,43]. The ChromSword offline program builds a physico-chemical retention model based on the structural formulae of the compounds, the type of column, and the type of organic solvent [27]. The simulation result achieved by this method of retention modeling becomes the initial starting point

for method optimization. Several method conditions can be varied once a few experimental data are entered. The ACD/Labs package uses either a database of experimental chromatograms or physico-chemical parameters such as log*P*, log*D*, and pK_a to model chromatograms and to predict optimal separation conditions. This simulator provides different models for separations such as HILIC and virtually any pH system can be simulated for method optimization [42]. The ACD/Labs also offers ChromGenius which predicts retention under standard analytical method conditions and allows for selection of best separation conditions [44]. DryLab predictions are based on LSS theory and are initiated solely by experimental data obtained from training separations [45,46]. Kaliszan *et al.* compared the performance of two of these programs and concluded that the structure-based predictions by ChromSword offline were less accurate compared to the retention measurement-based simulations of DryLab [28,47]. The limitations of these methods result from the lack of flexibility in modeling unusual gradient shapes and realistic injection profiles. As an example, these methods do not allow for the characterization of the effect of solvent mismatch between the sample solvent and the eluent.

A number of reports in the literature have described methods for chromatographic simulations using a variety of numerical methods to solve the mass transport equations [29,33–35,37,39,40,48–52]. These methods vary in terms of accuracy, speed and complexity. In the following chapters we present a general simulation program to predict the results of LC separations using a Craig-type simulation where the analyte propagates through a discretized space and time grid [29,32]. While this algorithm can be slow because of the necessity of calculating results at each point in time and space, it is relatively simple to understand and as we will show, produces results that agree well with closed form theory, when available. Our program incorporates pre-elution of weakly retained compounds before the gradient reaches the head of the column. In

addition, it can be easily adapted to any eluent composition profile (not just a linear profile) [53,54], any stationary phase composition (constant or non-constant) [55], and any composition and shape of the injected sample profile [56]. Therefore, these simulations can be particularly useful in characterizing the solvent mismatch effect in comprehensive two-dimensional liquid chromatography, where the sample solvent frequently differs in strength or polarity and causes peak distortion (broadening) [57–59] and for supporting the synthesis of novel continuous stationary phase gradient for liquid chromatography.

Chapter 3: Theory

This chapter has been adapted, with permission, from L.N. Jeong, R. Sajulga, S.G. Forte, D.R. Stoll, S.C. Rutan, *J. Chromatogr. A.* 1457 (2016) 41–49.

3.1. Craig distribution model

The Craig model explains the chromatographic process as a series of pseudo counter-current distributions between two immiscible liquids [32]. In an actual Craig counter-current extraction experiment, the sample mixture is introduced into liquids with different densities and undergoes equilibration between the two phases. The mobile phase is moved to the next tube while fresh mobile phase is introduced into the first tube. Equilibration occurs in each tube and the concentration of solute in the last tube is monitored. This concept can be applied to chromatography by dividing the column into discrete distance segments to represent tubes. This is one of the simplest, yet physically reasonable finite-difference strategies for the numerical solution of the differential equation shown by equation A1 (see Appendix). According to Czok and Guiochon, the Craig distribution model can be used to explain the continuous chromatographic process by replacing a column with segments of distance (Δz) and time (Δt) in a grid [32]. Here, we assume Δz is equal to the plate height (H) for the chromatographic system under study. As shown in Figure 3.1, at every time interval, part of the analyte mass from initial position, z-1,

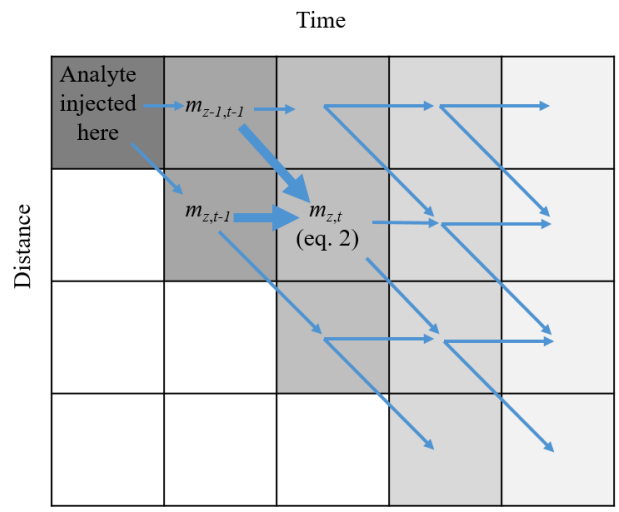

Figure 3.1. Propagation of the analyte through a time-distance grid in the Craig distribution model. Adapted from [60].

travels to the next cell downstream (z, t), while the remaining mass stays at the initial position, (z-1, t). The fraction of mass that travels to the next position in the column (z, t) is equal to μ, which is the peak velocity normalized to mobile phase velocity or simply the solute mobility, where k is the chromatographic retention factor (see equation 3.1).

$$\mu = \frac{1}{k+1} \tag{3.1}$$

Alternatively, one can view μ as the fraction of analyte in the mobile phase, while 1-μ represents the fraction remaining in the stationary phase, which is also called the analyte immobility, ω. The analyte mass is moved from one cell to the next, one step at a time. Therefore, the mass (m) at particular position (z) and at time (t) can be calculated using equation 3.2:

$$m_{z,t} = \omega m_{z,t-1} + \mu m_{z-1,t-1} \tag{3.2}$$

Finally, the last row of the grid (where z equals the column length, L) contains the numerical mass of analyte that has exited the column as a function of time – in other words, plotting the masses at

$z = L$ as a function of time gives the analyte elution profile, or the chromatogram, that we are most familiar with.

3.2. Linear solvent strength (LSS) theory

3.2.1. Retention time prediction.

According to the LSS model of Snyder *et al.*, the retention of an analyte separated under conditions where a linear mobile phase gradient is used can be predicted based on measurements of isocratic retention factor (k) as a function of solvent concentration (ϕ) [45].

$$\ln k = \ln k_w - S\phi \tag{3.3}$$

where S is the slope of a plot of isocratic ln k values versus ϕ, and k_w is the retention factor for the solute in a purely aqueous phase. A graphical representation of equation 3.3 is shown in Figure 3.2.

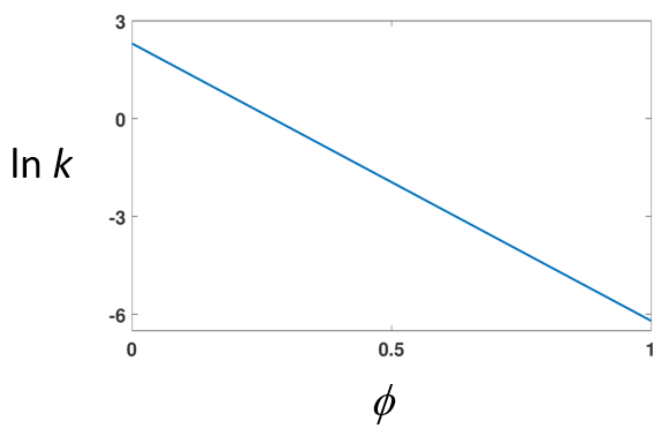

Figure 3.2. LSS plot: linear dependence of ln k on ϕ

The analyte retention time (t_R) under gradient elution conditions can be predicted using the LSS model, which includes a pre-elution phase that exists when there is a non-zero gradient delay time (t_D) [45,61,62]:

$$t_R = \left(\frac{t_m}{b}\right)\ln\left\{k_o b\left(1-\frac{t_D}{t_M k_o}\right)+1\right\}+t_M+t_D \tag{3.4}$$

Here, t_M is the void time, k_0 is the initial retention factor at the start of the gradient, calculated as $k_0 = k_w e^{-S\phi}$, and b is the intrinsic, dimensionless gradient steepness that can be expressed as

$$b = \frac{V_M \Delta\phi S}{t_G F} = \frac{t_M \Delta\phi S}{t_G} \tag{3.5}$$

If a linear gradient is simulated with the Craig model using the assumptions of LSS, the closed form expression given in equation 3.4 can be used to validate the retention times of the analyte obtained by the simulation code.

In order to ensure the mass balance conservation for the gradient chromatography simulations (where the retention factor k depends on both time and position), the mass profile equation must be derived from the time and distance dependent retention factor k (see Appendix A). The following equation (equation 3.6) differs from the equation given by Czok and Guiochon due to the fact that the analyte velocity is dependent on position inside the column. According to Blumberg [48], the velocity of the analyte, not just its dispersion, must be a function of position to ensure mass conservation of a gradient system. Therefore, the differential of analyte velocity must be taken over the position (see Appendix A).

$$m_{z,t} = m_{z,t-1}\omega_{z,t-1} + m_{z-1,t-1}\mu_{z-1,t-1} \tag{3.6}$$

A shortcoming of the Craig model is that it does not accurately account for peak broadening. However, as mentioned by Czok and Guiochon [32], this can be addressed empirically by

assuming that the extra peak broadening can be treated as a dispersion process where the extent of the dispersion is estimated using Fick's second law. The additional dispersion (D_z) each peak experiences depends on the local retention factor [32,46,63] . Fick's second law states the following:

$$\frac{\partial m}{\partial t} = D_z \frac{\partial^2 m}{\partial z^2} \tag{3.7}$$

Or, in other words, the analyte at position $m_{z,t}$ is redistributed to the previous, current, and next positions to simulate kinetic broadening of the analyte zone:

$$\frac{m_{z,t+1} - m_{z,t}}{\Delta t} = D_z \frac{m_{z+1,t} - 2m_{z,t} + m_{z-1,t}}{\Delta z^2} \tag{3.8}$$

The effective dispersion coefficient, D_z, is calculated at the local k value [32]:

$$D_z = \frac{1}{2(k_{z,t-1}+1)^2} \frac{\Delta z^2}{\Delta t} \tag{3.9}$$

Note that in the present work we have assumed that the Δz is constant along the column length. In gradient separations, the peak width (determined by the efficiency) is linked to the choice of Δz. The effect of the change of analyte velocity during the course of the mobile phase gradient is captured by equation 3.9 by adjusting the peak width according to the local retention factor. The more subtle effect on the plate height caused by changes in the analyte diffusion coefficient in the mobile phase, as the mobile phase composition varies, is not accounted for here.

In order to accurately assess the degree of band broadening the mass of solute present at position, z, and time, t, along the column is first determined using equation 3.6, and then equation 3.8 is used to add the additional broadening by adding the following differential mass to $m_{z,t}$:

$$m_{z,t+1} - m_{z,t} = D_z \frac{\Delta t}{\Delta z^2}\left(m_{z+1,t} - 2m_{z,t} + m_{z-1,t}\right) \tag{3.10}$$

This results in the final simulated chromatogram exhibiting a peak width corresponding to $H = \Delta z$. Finally, because the amount detected by the detector, m_d, is the analyte mass in the mobile phase, the simulated total mass profile ($m_{L,t}$) has to be corrected using the retention factor at the elution point, k_e (see Appendix A, equations A8 and A9). If this is not done, the area of the peak at the column outlet is dependent on retention factor, which is physically unreasonable.

$$m_d = \frac{m_{L,t}}{1 + k_e} \tag{3.11}$$

3.2.2. Peak width prediction

The widths of simulated peaks can be validated by considering the effect of a negative solvent strength gradient through the column on peak widths [45]. In the case of a significant gradient delay time, the analyte experiences an isocratic mobile phase during its travel through the first section of the column (C1 in Figure 3.3), followed by a solvent of changing composition as it travels through the rest of the column (C2). Therefore, one can view the broad peak from section C1 as a non-ideal sample injection into section C2.

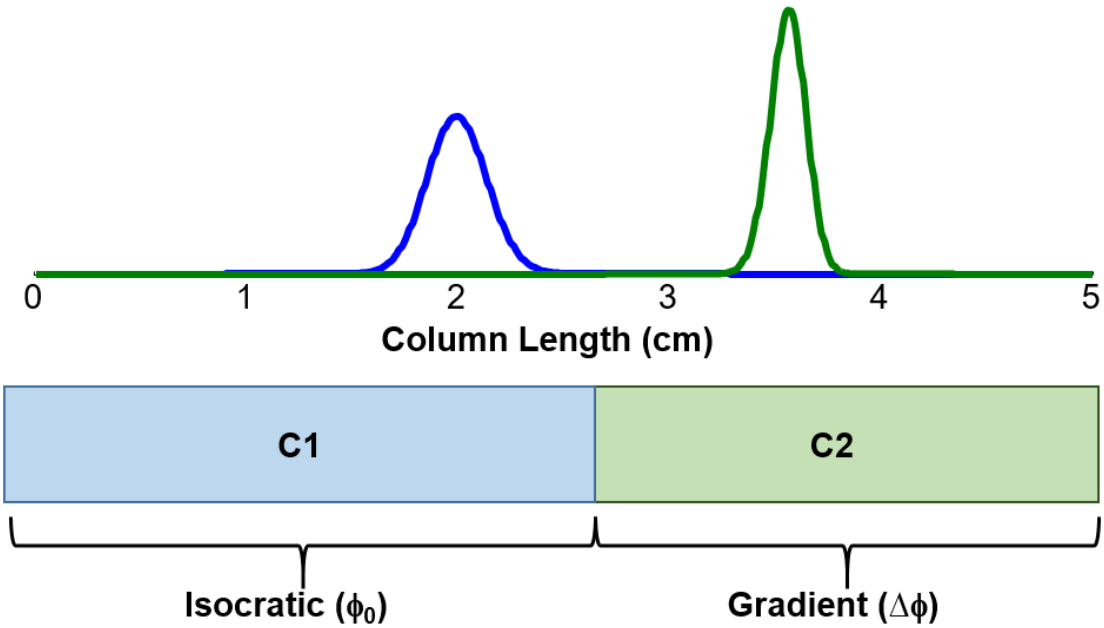

Figure 3.3. Simulation of an analyte with high initial retention factor under conditions where there is a significant gradient delay, t_D. The total column length = C1 + C2. During the gradient delay time, the analyte experiences isocratic condition (C1), whereas a changing solvent strength is experienced when the mobile phase gradient catches up with the analyte (C2). Simulation conditions: Δz = 0.01 cm; Δt = 0.06 s; ϕ_o = 0.02; $\Delta\phi$ = 0.8; k_w = 100; S = 100; t_G = 5 min; t_D = 3.5 min; L = 5 cm. Under these conditions, the gradient catches up with the analyte peak after 3.76 min, at a distance 2.59 cm down the column. The profile at 2 cm occurs at 2.9 min and the profile at 3.9 cm occurs at 4.1 min.

The total peak variance is the sum of the variance that develops in section C2 (σ^2_{grad}) and the variance developed during travel through C1 ($\Delta\sigma^2_{iso}$). The increase in solvent strength over time at all positions in the column under gradient conditions accelerates band migration, resulting in a substantial decrease in the peak retention times and widths [23,32]. In addition to that, the front of the band moves slower than its tail, resulting in relatively minor additional peak width reductions [32]. The gradient band compression factor describing this effect can be written as

$$G_{bR} = \frac{1}{1+b^*\omega_o}\sqrt{1+b^*\omega_o+\frac{1}{3}b^{*2}\omega_o^2} \tag{3.12}$$

where the fraction of solute in the stationary phase at the beginning of the gradient is indicated as ω_o (solute initial immobility). The fraction of solute in the mobile phase (solute mobility) as the band elutes (μ_R) can be expressed in terms of ω_0 and the dimensionless gradient steepness [63]:

$$\omega_o = \frac{k_o}{k_o + 1} \tag{3.13}$$

$$\mu_R = 1 - \frac{\omega_o}{1 + \omega_o b^*} \tag{3.14}$$

The peak width developed due to injecting a finite bandwidth (σ_b) onto the column can be calculated as [63]:

$$\Delta\sigma_{iso} = \frac{t_M \sigma_b}{L\mu_R(1 + b^* \omega_o)} \tag{3.15}$$

The dimensionless gradient slope, b^*, is only applicable over the section of the gradient that the analyte experiences. Therefore, the void time used in this equation must be a fractional t_M (*i.e.*, $t_{M,grad}$) for the gradient section only:

$$b^* = \frac{t_{M,grad} \Delta\phi S}{t_G} \tag{3.16}$$

$$\sigma_{grad} = \frac{G_{bR} t_{M,grad}}{\mu_R} \sqrt{\frac{\Delta z}{L_{grad}}} \tag{3.17}$$

The total peak variance on column when there is significant pre-elution caused by a finite t_D is finally calculated as

$$\sigma_{col}^2 = \Delta\sigma_{iso}^2 + \sigma_{grad}^2 \tag{3.18}$$

3.3. Non-LSST gradient retention model (Neue and Kuss)

An alternative description of the retention factor dependence on the mobile phase composition has been proposed by Neue and Kuss, which takes into account the fact that the variation of the logarithm of retention factor as a function of the solvent strength is actually nonlinear and has a curved relationship [64,65]:

$$k = k_w (1 + S_2\phi)^2 \exp\left[\frac{-S_1\phi}{1 + S_2\phi}\right] \tag{3.19}$$

where S_1 and S_2 are parameters describing the slope and the curvature of the ln k vs. ϕ plot, respectively. The graphical representation of equation 3.19 is shown in Figure 3.4.

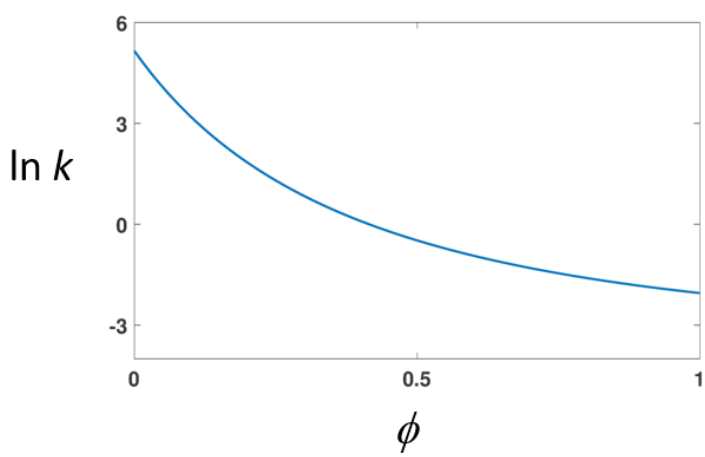

Figure 3.4. NK plot: non-linear dependence of ln k on ϕ

The parameters k_w, S_1 and S_2 can be extracted by fitting experimental retention factors from isocratic elution experiments to equation 3.19, and then retention times can be predicted using

$$t_R = \frac{t_G(\phi_e - \phi_o)}{\Delta\phi} + t_M + t_D \tag{3.20}$$

where the organic composition at elution (ϕ_e) can be expressed as [65,66]:

$$\phi_e = \frac{\phi_o + \frac{1+S_2\phi_o}{S_1}\ln\left(\frac{\Delta\phi k_w S_1}{t_G}\left(t_M - \frac{t_D}{k_o}\right)\exp\left(\frac{-S_1\phi_o}{1+S_2\phi_o}\right)+1\right)}{1-\frac{S_2(1+S_2\phi_o)}{S_1}\ln\left(\frac{\Delta\phi k_w S_1}{t_G}\left(t_M - \frac{t_D}{k_o}\right)\exp\left(\frac{-S_1\phi_o}{1+S_2\phi_o}\right)+1\right)} \tag{3.21}$$

(Note that this equation is given in the supporting material of reference [65] as equation S21.) The extracted Neue-Kuss parameters can also be used to calculate retention times and peak widths in simulations of mobile phase gradients with or without sample/eluent solvent mismatch conditions.

3.4. Sample/eluent solvent mismatch theory

3.4.1. Peak width prediction.

The width of peaks injected under conditions of sample volume overload with a mismatched sample solvent can be estimated using a similar analysis to that used to estimate the peak width under gradient conditions. The total peak width (σ_{tot}) can be described as the combination of peak width caused by the column (σ_{col}) and the broadening ($\Delta\sigma_{inj}$) caused by non-ideal sample injection.

$$\sigma_{tot}^2 = \sigma_{col}^2 + \Delta\sigma_{inj}^2 \tag{3.22}$$

There is a deviation in peak variance due to the injected sample when the composition of the sample solvent and mobile phase is different and the sample volume is large. This variance due to the injected sample/eluent solvent mismatch and sample volume overload can be estimated as follows [67]

$$\Delta\sigma_{inj}^2 = \left[\frac{k_{mp}+1}{k_{ss}+1}\right]^2\left[1+\frac{k_{mp}-k_{ss}}{k_{ss}+k_{ss}k_{mp}}\right]^2\left(\frac{V_{inj}^2}{12F^2}\right) \tag{3.23}$$

where k_{mp} and k_{ss} are the retention factors of the analyte in the mobile phase and the sample solvent, respectively, and V_{inj} and F are injection volume and flow rate, respectively. This equation is obtained by simplification of the expression given by Raglione *et al.* for a system comprised of an analytical column coupled to an accelerator column [67]. This equation can be simplified further to give

$$\Delta\sigma_{inj}^2 = \left(\frac{k_{mp}}{k_{ss}}\right)^2 \left(\frac{V_{inj}^2}{12F^2}\right) \tag{3.24}$$

which assumes a rectangular injection pulse. The contribution to the total peak variance due to dispersion inside the column is calculated from the expected plate number (N) and retention time (t_R)

$$\sigma_{col}^2 = \frac{t_R^2}{N} \tag{3.25}$$

It should be noted that when the injection peak width is larger than the column peak width, as in the case of sample/eluent solvent mismatch and injection volume overload conditions, the resulting peak is not Gaussian. Therefore, the retention time and peak variance cannot be reliably estimated from the max position and full width at half maximum, which are based on the assumption of a Gaussian peak shape. The correct retention time and peak variance must be calculated using the first and second central moment of the peak, respectively.

Chapter 4: Development of Simulation Program

This chapter has been adapted, with permission, from L.N. Jeong, R. Sajulga, S.G. Forte, D.R. Stoll, S.C. Rutan, *J. Chromatogr. A.* 1457 (2016) 41–49.

Section 4.4 has been adapted, with permission, from D.R. Stoll, R.W. Sajulga, B.N. Voigt, E.J. Larson, L.N. Jeong, S.C. Rutan, *J. Chromatogr. A,* in press.

4.1. Introduction

The goal of the work in this chapter was to design and implement a simple algorithm for simulation of liquid chromatographic separations that allows for characterization of the effect of (1) the mobile phase gradient; (2) injection solvent mismatch and injection solvent volume overload; (3) temperature; and (4) both experimental and rectangular injection profiles. The simulations yield full analyte profiles during solute migration and at elution, which enable a thorough physical understanding of the effects of method variables on chromatographic performance. The Craig counter-current distribution model (the plate model) is used as the basis for simulation. The algorithm, which is an adaptation of an approach originally described by Czok and Guiochon [60], is sufficiently flexible to allow the use of either linear (LSS [45]) or non-linear (NK [64]) models of solute retention. In this study, both types of models were used. The simulation program was validated first by comparison of simulated retention times and peak widths for five amphetamines to predictions obtained using LSS theory, and to results from experimental

separations of these compounds. Secondly, the program was evaluated for simulating the case where there is a compositional mismatch between the mobile phase at the column inlet and the injection solvent (*i.e.*, the sample matrix) under isocratic or gradient elution conditions with rectangular or experimental injection profiles.

4.2. Simulation of simple mobile phase gradient conditions

4.2.1. Isocratic experiments

Isocratic retention data were collected for the alkylbenzenes methylbenzene (AB1), ethylbenzene (AB2), propylbenzene (AB3), butylbenzene (AB4), and pentylbenzene (AB5) using a system composed of a binary pump, autosampler, column thermostat, and diode-array UV detector, all from the 1290 Infinity series from Agilent Technologies (Santa Clara, CA). The column used for this experiment was Zorbax Stablebond C_{18} (50 x 4.6 mm, 3.5µm, Agilent). This specific column and particle size was selected so that measured peak variances would be minimally affected by peak dispersion outside of the column. Retention times were measured at 40 °C in mobile phases between 10% and 90% (v/v) acetonitrile (ACN) in steps of 10% for solute/eluent pairs that gave retention factors less than 50. The column dead volume was measured using uracil in a mobile phase of 50/50 ACN/water, and the extra-column volume was determined under the same conditions, but with the column replaced with a zero dead volume union. The Neue-Kuss parameters were extracted from this data set by fitting to equation 3.19, and the resulting parameters are given in Table 4.1. These parameters were used to simulate both isocratic (see section 4.3.2) and gradient (see section 4.2.4) separations of the alkylbenzenes, and the retention

times and peak widths resulting from simulations of gradient separations of the alkylbenzenes were then compared to experimental results.

Table 4.1. Neue-Kuss parameters for the alkylbenzenes

Solute	S_1[a]	S_2[a]	k_w[a]	n[b]	s_R[c]	N[d]
AB1	18.59 (0.41)	1.044 (0.032)	1011 (48)	7	0.0290	7000
AB2	24.0 (2.6)	1.24 (0.15)	5300 (1800)	6	0.0765	6900
AB3	20.0 (2.6)	0.92 (0.15)	6200 (2700)	5	0.0526	6800
AB4	16.8 (3.6)	0.65 (0.22)	8000 (5400)	5	0.148	6650
AB5	14.7 (2.7)	0.49 (0.16)	9300 (5600)	4	0.0616	6500

[a]Standard errors of the parameters are given in parenthesis. [b]Number of points fit to equation 3.19. Composition values (ϕ) started at 0.9 and were reduced at 0.1 until the number of points shown was reached. [c]Standard error of the fit to k. [d]Efficiency value used for simulations.

4.2.2. Gradient experiments

Gradient elution separations of alkylbenzenes were carried out using the Agilent 1290 Infinity system and Stablebond C_{18} column described above in section 4.2.1. The flow rate was 2.0 mL/min, the column temperature was 40 °C, the injection volume was 1 µL, and a gradient from 50-90% ACN over 2.25 min was used for elution.

A group of five amphetamines was selected to characterize the performance of simulations of gradient elution separations. The structures, names, and abbreviations for these compounds are shown in Figure 4.1. The gradient data were collected on a system composed of binary pump, autosampler, column thermostat, and diode array detector (DAD) from the HP 1090 system (Agilent). The column was an Accucore Phenyl-Hexyl column (100 x 2.1 mm, 3 µm, Thermo Scientific), and the mobile phases were 10 mM potassium phosphate buffer at pH 2.5 and ACN.

The S and k_w values were estimated using nonlinear least squares regression using equations 3.4 and 3.5 and fitting to the different experimental gradient retention times as a function of the gradient times (t_G) and initial mobile phase compositions (ϕ_o). These S and k_w values were used to simulate the retention of amphetamines under various gradient conditions, and these parameters are given in Table 4.2. The retention times and peak widths resulting from simulations of gradient elution separations of these compounds were compared to both predictions based on LSS theory, and to experimental results.

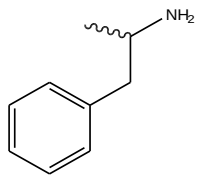

Amphetamine (Amp)

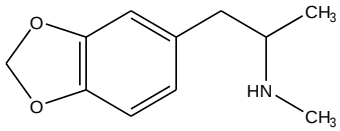

3,4-Methylenedioxymethamphetamine (MDMA)

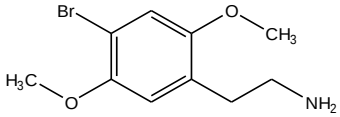

4-Bromo-2,5-methylenedioxyethylamphetamine (Bromo)

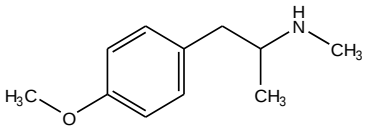

3,4-Methylenedioxyethylamphetamine (MDE)

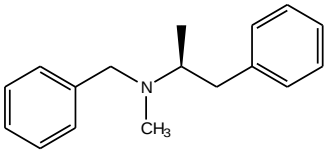

Benzphetamine (BP)

Figure 4.1. Structures and abbreviations for five amphetamines.

4.2.3. Simulation codes

All simulation codes were written in the Matlab program (Mathworks, Natick, MA) version R2013a. Non-linear regression to obtain the parameters necessary to implement

Table 4.2. LSS parameters for the amphetamines

Solute	S[a]	k_w[a]	n[b]	s_R (min)[c]
Amp	20.8 (2.4)	11.5 (1.3)	5	0.0801
MDMA	22.0 (3.8)	22.5 (5.2)	5	0.117
MDE	20.3 (4.0)	32.0 (9.2)	5	0.134
Bromo	16.6 (1.6)	68.2 (12)	5	0.0868
BP	16.0 (1.1)	167 (28)	5	0.0794

[a]Standard errors of the parameters are given in parenthesis. [b]Number of points fit to equations 3.4 and 3.5. Conditions were (1) ϕ_0 =0.02, t_G = 14 min; (2) ϕ_0 =0.02, t_G = 18 min; (3) ϕ_0 =0.02, t_G = 22 min; (4) ϕ_0 =0.05, t_G = 14 min; (5) ϕ_0 =0.05, t_G = 22 min; for all conditions ϕ_f =0.35; t_m = 0.5946 min; t_D = 0.795 min. [c]Standard error of the fit to t_R.

simulations was accomplished using the function lsqnonlin found in the Matlab Optimization Toolbox.

4.2.4. Prediction of alkylbenzene retention under gradient elution conditions using Neue-Kuss parameters determined from isocratic retention data

Simulation of gradient elution separations of alkylbenzenes were performed using the extracted Neue-Kuss parameters and plate numbers shown in Table 4.1, assuming a linear change in solvent composition with time. Figure 4.2 shows a qualitative comparison of experimental and simulated chromatograms collected for gradient separations of alkylbenzenes AB1-5 for a solvent gradient with a ϕ_o of 0.50 and a $\Delta\phi$ of 0.40 over a t_G of 2.25 min. Table 4.3 summarizes the comparison of experimental and simulated retention times and peak widths. Predicted retention times were accurate to within 1.5 %, and predicted peak widths were accurate to within 6.0 %. The simulated data compare well with the experimental data even though no correction of the simulated

results has been made to account for increases in retention time and peak dispersion caused by extra-column volume.

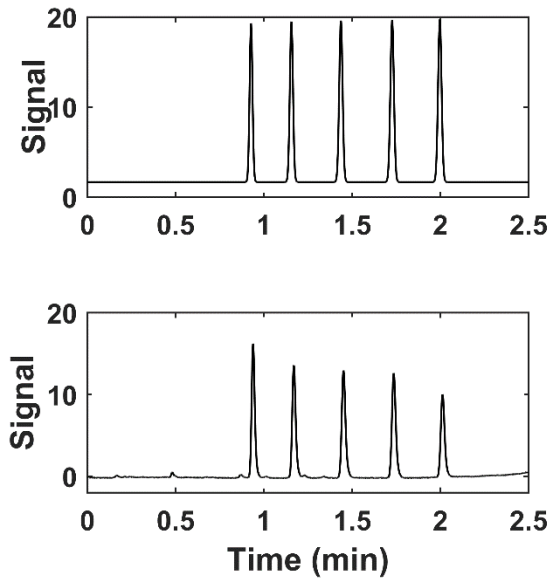

Figure 4.2. Experimental (bottom) and simulated (top) chromatograms collected for gradient separations of alkylbenzenes AB1-5. The solvent gradient was 50-90% ACN from 0-2.25 min, and injection volume was 1 µL. The measured gradient delay time of 0.055 min was used in the simulation.

Table 4.3. Experimental and simulated retention data for AB1-5 separated under gradient elution conditions[a]

	Retention Time (min)		**Peak Width ($w_{1/2}$, min)**	
Solute	**Experiment**	**% Difference (Simulation – Experiment)[b]**	**Experiment**	**% Difference (Simulation – Experiment)[b]**
AB1	0.939	-1.3	0.0198	-4.9
AB2	1.169	-1.2	0.0217	-4.9
AB3	1.451	-1.0	0.0233	-5.3
AB4	1.736	-0.5	0.0242	-5.7
AB5	2.012	-0.8	0.0244	-5.8

[a]The solvent gradient was 50-90% ACN from 0-2.25 min, and injection volume was 1 µL. The measured gradient delay time of 0.055 min and a rectangular injection profile were used for the simulations. [b] $\%\ \text{difference} = {(\text{sim} - \text{exp})}/{\text{exp}} * 100$

4.2.5. Prediction of amphetamine retention under gradient elution conditions using LSS parameters determined from gradient retention data

The Neue-Kuss parameters could not be extracted from the gradient experimental data for the amphetamine-class compounds since the system is ill-conditioned. This was because a limited experimental data set was available. This means that a wide range of Neue-Kuss parameters predicted experimental gradient retention times with very similar values. For gradients with shallower slopes, the linear model resulted in better predictions [65]. Therefore, the linear parameters S and k_w were extracted from the gradient data for the amphetamine-class compounds. The simulation results were then validated with LSS theory, as discussed below. The simulated results were also compared to the experimental data, and these comparisons are also shown in Figure 4.3 and Table 4.4. The retention time predictions agreed to within 2.5 %. The experimental peak width comparisons are also quite reasonable. This level of agreement indicates that the LSS model for these parameters is adequate for generating reasonable predictions for retention behavior.

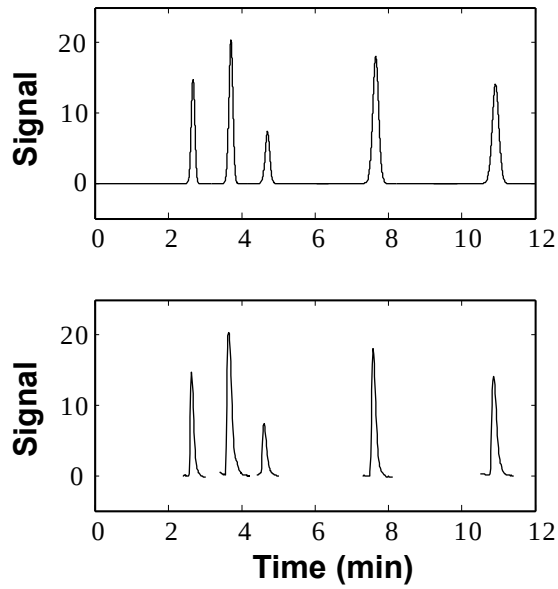

Figure 4.3. Experimental (bottom) and simulated (top) chromatograms collected for gradient separations amphetamines. The solvent gradient was 5-35% ACN from 0-18 min. The measured gradient delay time of 0.795 min was used in the simulation. The heights of simulated peaks are scaled to the heights of the experimental peaks. The gaps in the baseline of the experimental chromatograms are due to the fact that the compounds were injected in different samples.

Table 4.4. Comparison of retention time and peak width prediction of simulation, LSS and experiments for amphetamines[a]

	Retention Time (min)			**Peak Width ($w_{1/2}$, min)**		
Solute	**LSS[b]**	**% Difference (Simulation –LSS)[c]**	**% Difference (Simulation – Experiment)[d]**	**LSS & Simulation[e]**	**% Difference (Simulation – LSS)[c]**	**% Difference (Simulation – Experiment)[d]**
Amp	2.6741	-0.016	1.49	0.1089	-0.017	7.51
MDMA	3.7052	-0.018	1.96	0.1250	-0.011	-12.9
MDE	4.7021	-0.019	2.20	0.1430	-0.0074	21.2
Bromo	7.6523	-0.017	1.07	0.1882	-0.00036	46.5
BP	10.9164	-0.014	0.51	0.2091	-0.0050	41.0

[a]The solvent gradient was 5 – 40 % ACN from 0-18 min. The measured gradient delay time of 0.795 min and a rectangular injection profile were used for the simulations.
[b]Calculated using equations 3.4-3.5.

[c] $\% \text{ difference} = {(\text{sim} - \text{LSS})}/{\text{LSS}} * 100$

[d] $\% \text{ difference} = {(\text{sim} - \text{exp})}/{\text{exp}} * 100$

[e]Calculated using equations 3.12-3.18.

4.3. Solvent mismatch under isocratic conditions

4.3.1. Experimental

A second set of experimental data (retention times and peak widths) was collected for the alkylbenzenes under isocratic conditions, where the initial mobile phase and injection solvents were different (*i.e.*, 'solvent mismatch' conditions). In this case a system composed of a pump and autosampler from the HP1050 series (Agilent), and column thermostat and diode-array UV detector from the Agilent 1100 series was used. This particular system was chosen for this experiment because the autosampler is equipped with a syringe and sample loop that allows injections of up to 100 µL. The Neue-Kuss parameters extracted previously (see section 4.2.1) were used to simulate separations under sample/eluent solvent mismatch conditions, and the resulting retention times and peak widths were compared to experimental results.

4.3.2. Prediction of alkylbenzene retention with sample/eluent solvent mismatch under isocratic conditions

There is a great interest in the peak distortion caused by a difference in the solvent composition of the sample and the eluent used in an LC method [58,68–72]. This may result from low solubility of the analyte in water, or be a consequence of other method development decisions in two-dimensional liquid chromatography (2D-LC). This is particularly problematic when the eluent from the first dimension contains more organic solvent than the initial eluent composition in the second dimension of 2D-LC under reversed-phase conditions [71–75]. Sample volume overload can also produce problematic peak shapes [21,70,76].

In 2D-LC the first dimension (^{1}D) effluent can be diluted to be more similar to the starting solvent composition when gradient elution is used in the second dimension. However, there are practical limits to how much the ^{1}D effluent can or should be diluted [75]. Given the complexity associated with optimizing these conditions, it is of great interest to accurately simulate such large volume injection conditions to give a better understanding of analyte behavior under these conditions. Here, we investigate these effects under isocratic conditions, in which the retention times and peak widths are very sensitive to the volume and composition of the sample. Figures 4.4 - 4.6 show comparisons of results obtained from experiments, simulations, and predictions based on theory.

Figure 4.4 shows a qualitative comparison of experimental and simulated chromatograms obtained for isocratic separations at 70/30 ACN/water of alkylbenzenes AB1, AB3, and AB5 in samples with varying solvent composition. Simulations were based on rectangular injection profiles. The retention times, widths, and shapes of the simulated peaks are consistent with those observed in experiments. Figures 4.5A and 4.5B show comparisons of retention times extracted from the experimental or simulated chromatograms across the variable space studied (1-100 μL injection volume; 50 or 90% ACN sample solvent). We don't show results for retention times calculated from theory in this figure, because no satisfactory closed form theory for this effect has been proposed in the literature. Figure 4.5A shows data for methylbenzene (AB1, k =1.67) and 4.5B shows data for pentylbenzene (AB5, k = 7.81) when injected from samples containing either 50 or 90% ACN. These figures show that retention times shift later with increasing volume of sample containing less ACN compared to the mobile phase, and shift to earlier times when increasing volume of sample containing more ACN compared to the mobile phase is injected. This

observation is as expected since the analyte peak elutes faster at the higher concentration of organic solvent, and the simulations accurately capture this effect.

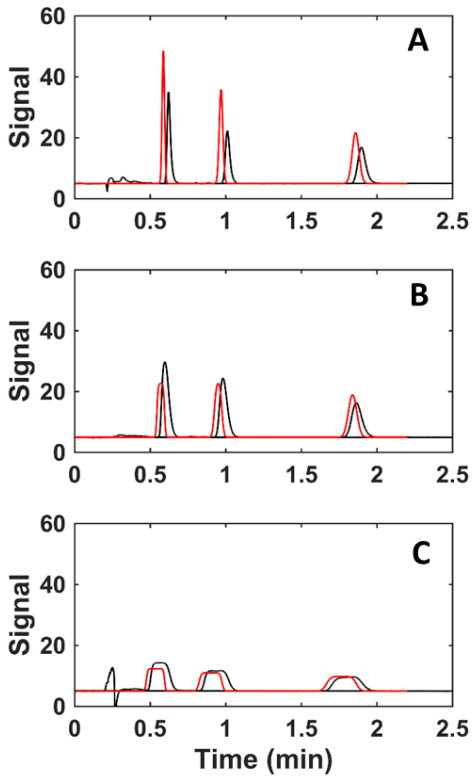

Figure 4.4. Experimental (black) and simulated (red) chromatograms collected for isocratic separations of alkylbenzenes AB1 (first peak), AB3, and AB5 (last peak). The eluent was 70% ACN, and injection volume was 100 µL. Sample solvents were 50 (A), 70 (B), or 90 (C) % ACN.

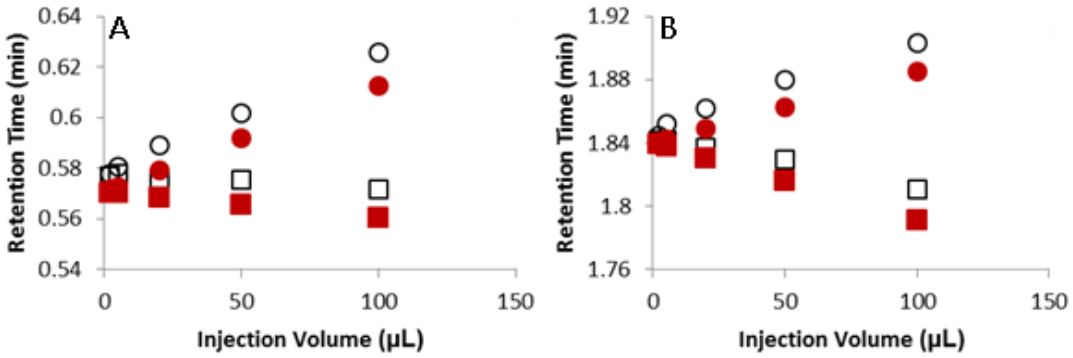

Figure 4.5. Comparison of experimental (black, open symbols) and simulated (red, closed symbols) retention times for sample/eluent solvent mismatch. Retention times for (A) methylbenzene (k = 1.67) and (B) pentylbenzene (k = 7.81) injected from either 50% (circles) or 90% (squares) ACN samples into an eluent containing 70% ACN. The percent difference between the experimental and simulated retention times was within 2.2% for AB1 and within 1.0% for AB5.

The peak shape is also distorted when the injection and eluent solvents are mismatched [71]. As mentioned before, this peak distortion is more pronounced when the injection solvent is stronger than the eluent solvent. The peak widths measured from simulations were validated by comparison with theoretical peak width calculations (equations 3.22 – 3.25). As shown in Figure 4.6B, as the sample injection volume increases, the peak tends to get broader due to the initial solute elution in the injection solvent before the peak is slowed down by weaker solvent. This peak broadening effect does not exist for samples with the weaker injection solvent due to the focusing achieved in the weaker mobile phase (Figure 4.6A). We attribute the slightly larger widths measured in experiments (Figure 4.6A) to peak tailing that is not accounted for in the simulations or predictions from theory, as well as the fact that the theory is only approximate. This is a subject of ongoing work that we will address in detail in the next section. Briefly, we now believe that most of the tailing observed in this case originates from the asymmetric profile of the injected sample as it exits the injection system and enters the column. The simulations carried out as described here have assumed that the sample enters the column as a perfectly rectangular pulse. Subsequent work will show that when an asymmetric profile that accurately reflects the way the sample actually enters column is used to introduce analyte mass into the simulated column the simulation produces tailed peaks that are more consistent with experimental results.

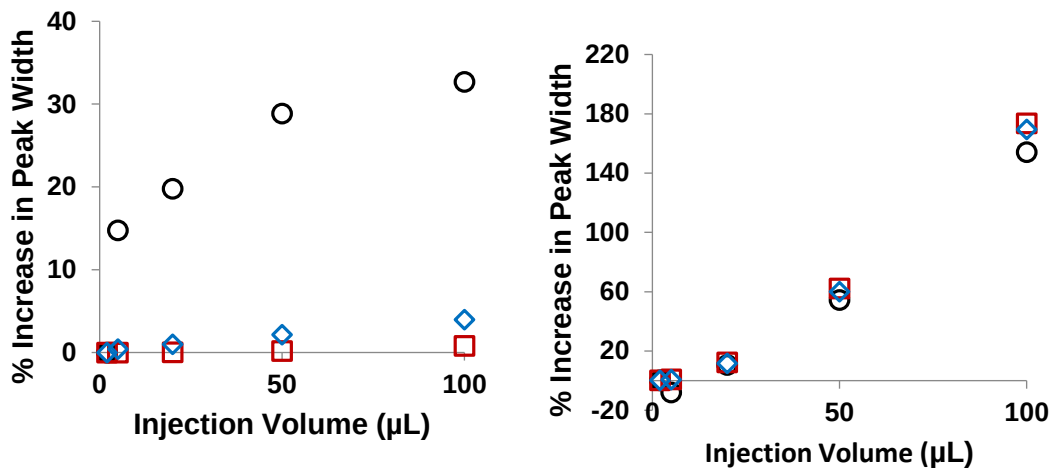

Figure 4.6. Percent increase in peak width for pentylbenzene (AB5) as a function of injection volume. Samples are in (A) 50% and (B) 90% (v/v) ACN for an eluent containing 70% (v/v) ACN. Black open circles are experimental, red open squares are for simulation and blue open diamonds are for theory (equations 3.22-3.25).

4.4. Incorporation of experimental injection profiles and solvent mismatch under gradient conditions

The work in this section explains the incorporation of experimentally acquired injection profiles in place of symmetric rectangular injection profiles. Also, we show extension of the previous effort by enabling simulation of separations under conditions involving both gradient elution and sample/mobile phase solvent mismatch, and variable sample loop filling. When a sample is injected, the material (analyte and solvent) begins entering the column in the first plate, during the first time step. As the simulation proceeds, more sample continues to enter the first plate until enough time has elapsed (t_{inj}) such that:

$$t_{inj} = \frac{V_{inj}}{F} \tag{4.1}$$

where V_{inj} is the volume of sample that enters the column, and F is the flow rate of mobile phase through the column. This is straightforward in the case where a rectangular injection pulse is

assumed because the injection volume is well defined. In cases where more realistic injection profiles are used in the simulation (see Figure 4.7) equation 4.1 no longer applies, and we must consider the volume of solvent and moles of analyte injected as integrals over the entire profile; this is discussed in detail below.

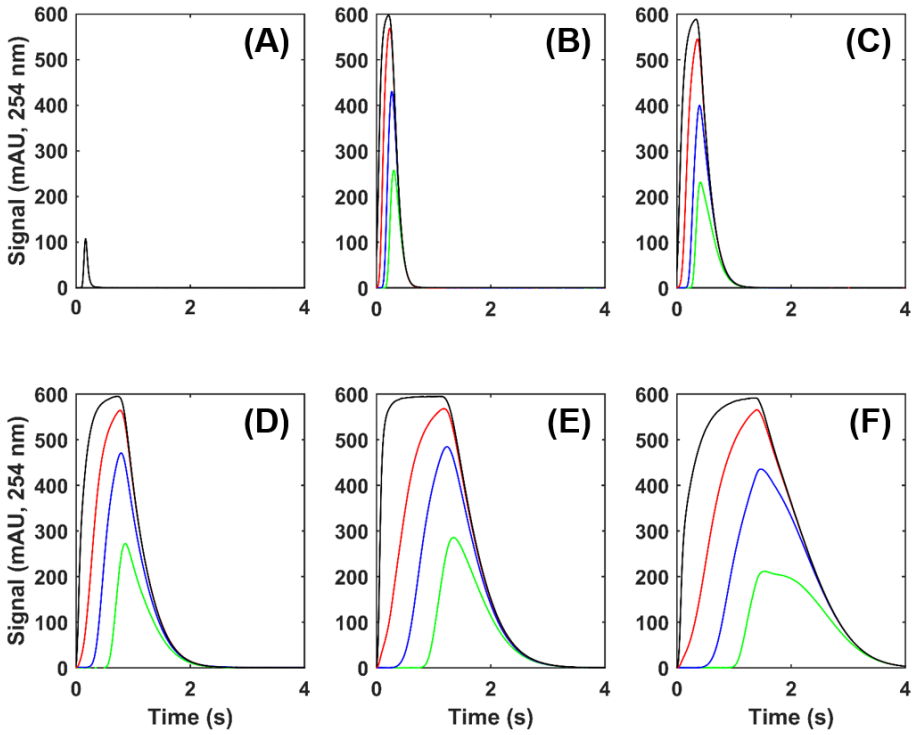

Figure 4.7. Experimentally measured injection profiles obtained from sample loops of different sizes, at different filling levels: (A) 0.4 µL; (B) 13.5 µL; (C) 20 µL; (D) 40 µL; (E) 60 µL; and (F) 80 µL. Filling levels were 25 (green), 50 (blue), 75 (red), and 100 (**black**) %, except for the 0.4 µL loop, which was filled to 200 %. Other conditions: Mobile phase, 50/50 ACN/water; injected sample was 10 µg/mL uracil in mobile phase; flow rate, 2.5 mL/min.

The most important difference between the model used in this work and the one described previously in Chapter 3 lies in the construction of the solvent profiles shown in Figure 4.8. In our previous work, we assumed rectangular injection profiles in cases of mismatch between the sample organic solvent composition and the starting point in the mobile phase gradient. In Figure 4.8, this is shown as the green trace, for the case of 100 % filling of a 40 µL loop with a sample containing

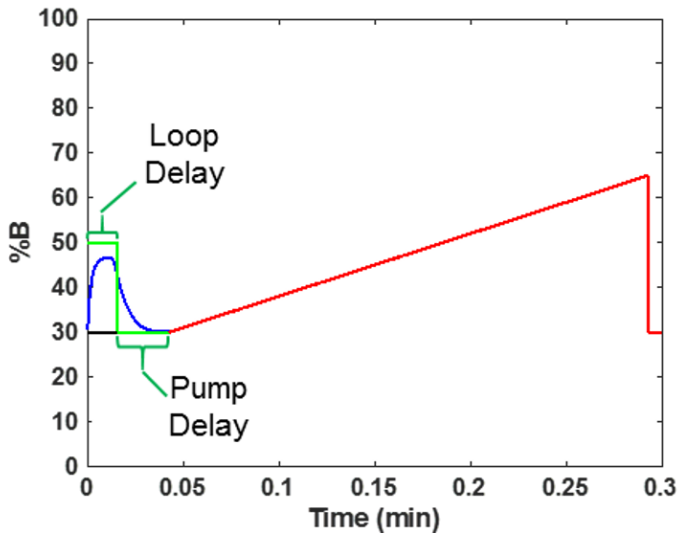

Figure 4.8. Graphic showing piecewise construction of solvent profiles (at column inlet) used in this work (here, for the specific case of 100% filling of a 40 μL loop). The red trace shows a simple linear solvent gradient over a gradient time t_G. The green and blue traces show rectangular or experimental injection profiles preceding the solvent gradient, respectively. The sample solvent is 20 % greater in organic composition relative to the initial mobile phase composition.

50 % ACN. In contrast, the blue trace shows the real, measured injection profile that is relevant to these conditions.

The overall solvent profile during the entire simulation, including injection (blue) and linear solvent gradient (red) is constructed as follows. First, we assume that the time required to travel the length of the sample loop ($t_{D,loop}$) is simply:

$$t_{D,loop} = \frac{V_{loop}}{F} \tag{4.2}$$

where V_{loop} is the experimentally determined loop volume. This, combined with the experimentally measured gradient delay time of the pump ($t_{D,pump}$) determines the total delay before the onset of the linear solvent gradient at the column inlet. During this pre-gradient period ($t_{D,loop} + t_{D,pump}$), the solvent composition is determined by the solvent composition of the sample, and the composition of the fluid that displaces the sample from the sample loop. The shape of this profile, $\phi_{t,injection}$, in

units of percent organic solvent composition, is calculated as follows. First, the appropriate injection profile, $S_{t,injection}$ (in mAU) is selected from the profiles shown in Figure 4.6. The x-axis (in time units) is converted to volume units by multiplying by the flow rate to give $S_{V,injection}$. The data are then interpolated to reflect the sampling interval, ΔV_{sim}, for the simulation conditions, which is calculated as

$$\Delta V_{sim} = \frac{V_M}{\left(L / \Delta z\right)} \tag{4.3}$$

Then, we calculate a ϕ profile as a function of volume that gives the final mobile phase composition profile for the injection ($\phi_{V,injection}$):

$$\phi_{V,injection} = \frac{S_{v,injection}}{A_v} V_{loop} (\phi_{sample} - \phi_o) + \phi_o \tag{4.4}$$

In doing so, the $S_{v,injection}$ profile is normalized by the area under this profile, A_v, which is in units of mAU·mL.

Finally, the *x*-axis for the $\phi_{V,injection}$ profile is converted to time, by dividing by the flow rate to give the mobile phase composition profile as a function of time $\phi_{t,injection}$. Note that because the $(\phi_{sample} - \phi_o)$ term in equation 4.4 can be negative, this results in a 'dip' in the mobile phase composition profile during injection in cases where the sample contains less organic solvent than the starting point in the solvent gradient. From this point forward, we define the following

$$\Delta\phi_{sample} = \phi_{sample} - \phi_o \tag{4.5}$$

The solvent composition due to the gradient is calculated as:

$$\begin{aligned} \phi_{t,gradient} &= 0 && \text{for t} < t_{D,loop} + t_{D,pump} \\ &= \frac{\left(\phi_f - \phi_o\right)}{t_G}\left(t - t_{D,loop} - t_{D,pump}\right) && \text{for t} \geq t_{D,loop} + t_{D,pump} \end{aligned} \tag{4.6}$$

These two profiles ($\phi_{t,injection}$ and $\phi_{t,gradient}$) are then added together to produce the overall mobile phase composition profile shown in Figure 4.8.

One final detail is important in the construction of these profiles. We have determined in other work not discussed here that when a sample of a known volume is pumped into a sample loop of known volume that some of the sample is lost out of the end of the loop when the filling level exceeds about 75 %. For example, if we push 40 μL of a sample from a syringe into a sample loop with a known volume of 40 μL (we refer to this as 100% filling), a fraction of the sample will be lost out of the end of the loop [77]. This is believed to be a result of axial dispersion of the leading edge of the solute band as it travels through the loop, such that some mass in the leading edge of the band leaves the end of the loop capillary before the entire sample volume has been pushed into the loop. It was determined that at 100 % filling, this loss is 7 %. At filling levels of 25, 50, and 75 %, no measureable losses are observed. A normalization similar to that described above was used to calculate the analyte injection profile, $m_{t,profile}$ that describes the initial mass profile for the analyte as it enters the column.

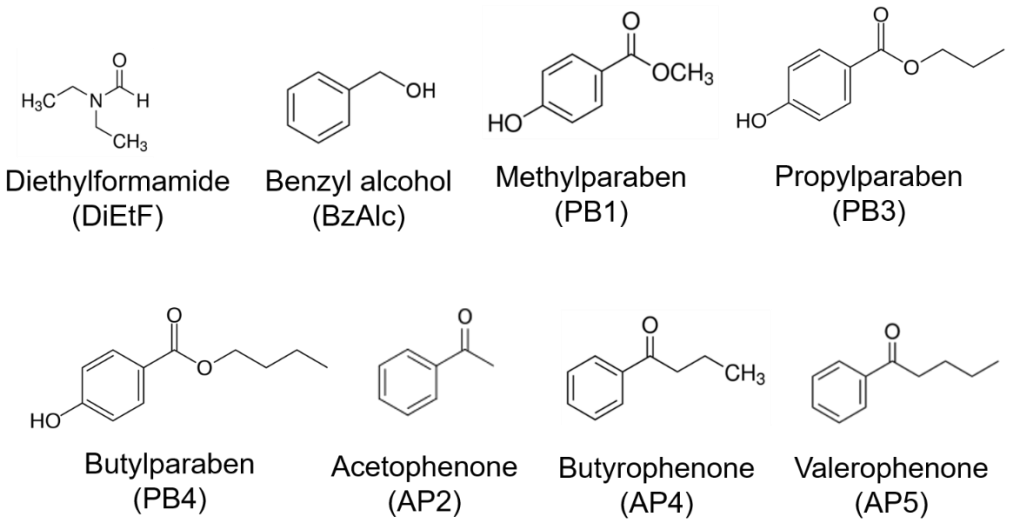

Figure 4.9. Structures and abbreviations for compounds used for the study discussed in section 4.4.

The plate numbers used for simulations were determined experimentally using isocratic conditions and a flow rate of 2.5 mL/min on a system with an extra-column variance of about 1 μL^2 (measured using a 150 nL injection of uracil, and peak width at half-height). A total of eight compounds were used in this study. The structures and abbreviations for these compounds are shown in Figure 4.9. The ACN/water composition of the mobile phase was adjusted to give a retention factor of about 2 for each compound, as this is close to the retention factor at the point of elution for the compounds and gradient conditions studied here. When the column was new the plate numbers for DiEtF and BzAlc were 1200, for the parabens (PB1, PB3, and PB4) 1350, and for the phenones (AP2, AP4, AP5) 1650. In the middle of the work to collect the experimental data under gradient elution conditions, and at the end, the column performance was re-evaluated under isocratic conditions. It was found that by the end of all of the gradient work the isocratic plate numbers had decreased by about 20 %. For the comparison of experimental and simulated retention times and peak widths (*i.e.*, Table 4.6, and Fig. 4.11), the isocratic plate numbers for each set of experiments related to a particular loop volume were estimated, assuming a consistent degradation in column performance over time. So, the initial plate numbers were used for simulations at 0.4, 13, and 20 μL. For the 40, 60, and 80 μL loop volumes, the plate numbers were 90, 85, and 80 % of the original plate numbers, respectively. Again, this was done to make the comparison of experimental and simulation results as fair as possible. Finally, simulations assumed a non-linear dependence of solute retention on organic solvent fraction of the mobile phase of the form described by Neue and Kuss [64] (see equation 3.19). Solute parameters for this dependence were determined experimentally, and are shown in Table 4.5.

Table 4.5. Neue-Kuss parameters for the solutes used in this work.

Solute	S_1[a]	S_2[a]	ln k_w[a]	s_E[b]	n[c]
DiEtF	27.36 (0.96)	2.772 (0.103)	3.132 (0.047)	7.61 x 10^{-3}	4
BzAlc	20.96 (0.54)	1.903 (0.064)	3.620 (0.030)	6.02 x 10^{-3}	4
PB1	26.95 (0.33)	1.955 (0.032)	5.150 (0.019)	3.75 x 10^{-3}	4
PB3	33.53 (2.49)	1.839 (0.138)	8.065 (0.260)	8.64 x 10^{-3}	5
PB4	34.57 (1.97)	1.694 (0.099)	9.290 (0.226)	1.17 x 10^{-2}	5
AP2	18.64 (0.43)	1.371 (0.041)	4.939 (0.035)	1.40 x 10^{-2}	7
AP4	22.73 (0.58)	1.239 (0.040)	7.624 (0.069)	3.14 x 10^{-3}	4
AP5	27.68 (3.69)	1.354 (0.186)	9.307 (0.527)	1.87 x 10^{-2}	5

a) Parameters obtained by fitting isocratic retention factors (*k*) to equation 3.19. Standard errors are given in parenthesis. Column - Zorbax SB-C18; Mobile phase – ACN/water; Temperature – 40 °C.
b) Standard error of the regression
c) Number of experimental data points used in the fit to equation 3.19.

4.4.1. Retention time and peak width

Early in this work we realized that the shape of the sample input profile had a strong influence on the shape of the simulated peaks and their widths, particularly at the 4.4 % height where the width is much more sensitive to peak asymmetry than at half-height. Figure 4.10 shows an example of the impact of the input profile on the peak shape observed in simulated chromatograms. Use of the rectangular injection profile produces peak shapes that are simply unrealistic, and typically underestimate the experimental peak width, especially near the base of the peak. For this reason, we have exclusively used the real injection profiles shown in Figure 4.7 for the simulations described in this section. We observe that using a rectangular input profile consistently leads to narrower, and therefore too optimistic, peak widths.

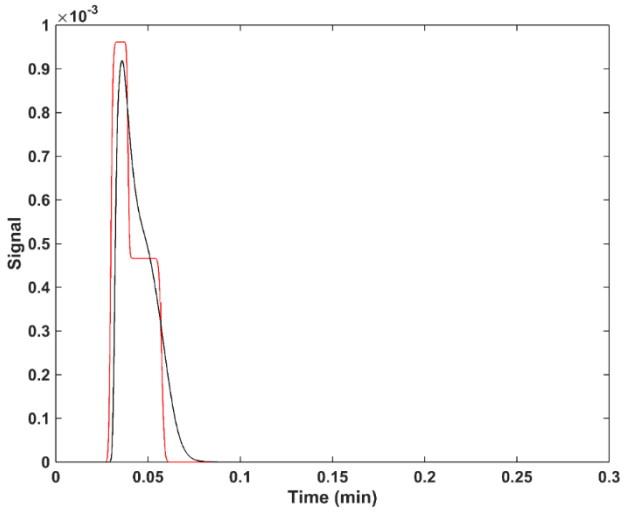

Figure 4.10. Comparison of the simulated chromatograms obtained for DiEtF using a rectangular (red) or experimental (**black**) injection profile. Conditions: Loop volume was 40 µL, with 100 % loop filling; injection of sample in 50/50 ACN/water. Other conditions: column, 30 mm x 2.1 mm i.d. Zorbax SB-C18, 3.5 µm; flow rate 2.5 mL/min; temperature, 40 ºC; gradient elution from 30-65 % ACN from 0-0.25 min.

Figure 4.11 shows a comparison of experimental and simulated chromatograms for separation of four of the eight test compounds (chosen simply to minimize peak overlap, while sampling the entire elution range), under three different test conditions that are more representative of those encountered in 2D-LC. In each case the loop volume was 40 µL, and the loop filling was 100 %. The sample composition was varied relative to the starting eluent composition used in the gradient. Table 4.5 provides a summary of the differences between experimental and simulated retention times and peaks widths for all of the conditions studied in this work. Overall we see that the simulation accurately captures the variation in the experimental chromatograms across this set of conditions. Most notable are the significant tailing of early eluting peaks, even in the case where $\Delta\phi$ is -0.2, and the 'table-top' shape of some of the severely broadened peaks (*e.g.*, peak 3 in Figure 4.11F). There are small differences in peak height between the experimental and simulated chromatograms. This is because in the simulations we assumed a uniform detector response independent of test solute chemistry, whereas these compounds have different molar absorption

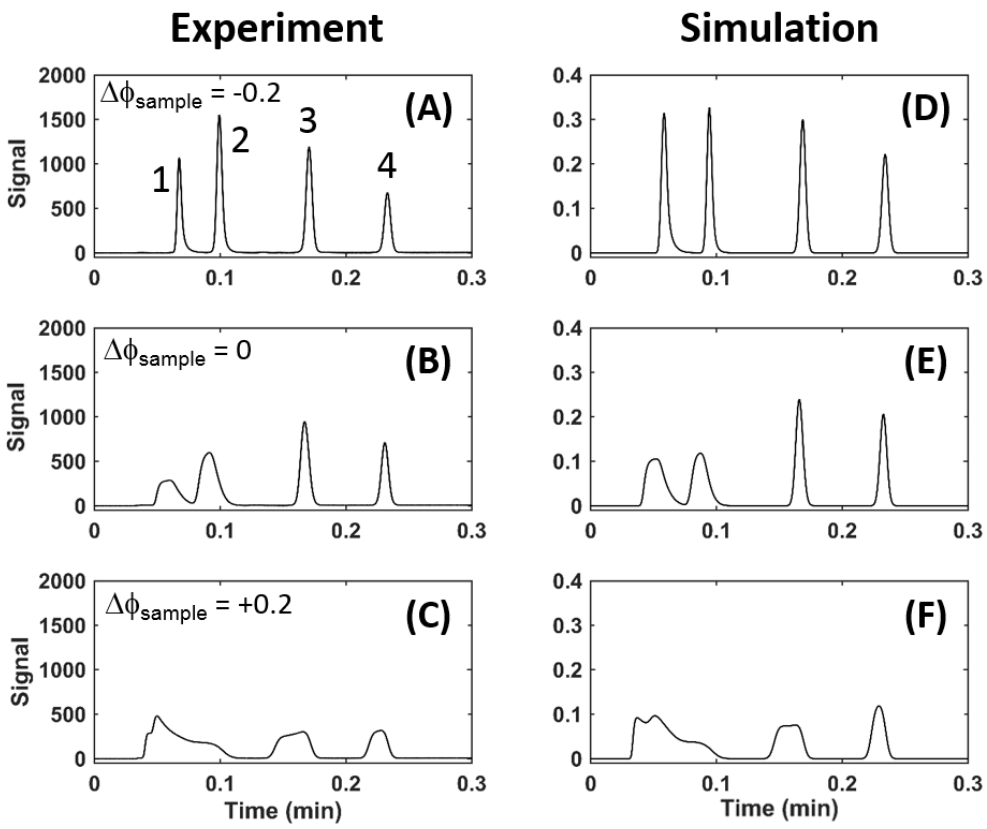

Figure 4.11. Comparison of experimental (A-C) and simulated (D-F) separations of (1) diethylformamide, (2) methylparaben, (3) propylparaben, and (5) butyrophenone. Loop volume was 40 µL, with 100 % loop filling. Panels A and D correspond to injections of sample in 10/90 ACN/water; B and E, 30/70 ACN/water; C and F, 50/50 ACN/water. Other conditions are as in Fig. 4.10. Experimental signals are due to absorption of UV light at 210 nm. The scale of the signal axis for the simulated chromatograms is arbitrary.

coefficients in real experiments. One noticeable difference between the experimental and simulated chromatograms, albeit mostly a difference in peak shape and not so much in peak width, is observed for peak 4 in Figures 4.11C and 4.11F. A second notable difference is in the shape of overlapped peaks 1 and 2 in Figures 4.11C and 4.11F. The main reason for this shape difference is that the difference in the retention times between peaks 1 and 2 is more pronounced in the simulations as compared to the experiments, which gives rise to more distinct peaks in the simulated chromatogram.

Table 4.6. Comparison[a] of simulated and experimental retention times and peak widths[b] at 100 % loop filling.

Loop size (µL)	**0.4**					**40**				
$\Delta\phi_{sample}$	**-0.2**	**-0.1**	**0**	**+0.1**	**+0.2**	**-0.2**	**-0.1**	**0**	**+0.1**	**+0.2**
t_R	0.5 / 0.7	0.4 / 0.7	0.6 / 0.7	0.7 / 0.8	0.4 / 0.6	-4.1 / -2.0	-4.0 / -1.8	-3.9 / -1.8	-1.9 / -0.7	-0.8 / -1.2
w_{50}	4.4 / 2.2	4.3 / 2.6	4.3 / 2.4	4.0 / 2.4	3.5 / 2.1	2.8 / 1.7	-0.9 / -2.1	-5.1 / -4.6	-11.1 / -9.3	-3.8 / -9.1
$w_{4.4}$	-2.7 / -4.2	-2.4 / -3.7	-2.9 / -4.0	-3.2 / -4.0	-3.4 / -3.1	0.8 / -1.1	-2.1 / -4.1	-4.7 / -5.6	-10.2 / -8.3	-7.9 / -8.7
Loop size (µL)	**13**					**60**				
$\Delta\phi_{sample}$	**-0.2**	**-0.1**	**0**	**+0.1**	**+0.2**	**-0.2**	**-0.1**	**0**	**+0.1**	**+0.2**
t_R	-3.8 / -1.0	-3.8 / -1.0	-3.8 / -0.9	-3.8 / -1.1	-4.0 / -1.2	-3.4 / -1.9	-3.7 / -2.2	-3.1 / -1.5	-1.0 / -1.1	-2.9 / -1.0
w_{50}	2.2 / 1.8	2.5 / 2.5	0.0 / 0.1	-3.8 / -2.8	-6.5 / -6.0	-5.9 / -3.6	-4.5 / -5.8	-8.0 / -7.8	-9.1 / -10.5	8.8 / -11.9
$w_{4.4}$	-3.1 / -4.3	-3.4 / -3.9	-3.9 / -5.1	-5.9 / -5.9	-8.1 / -7.1	-11.0 / -7.5	-8.3 / -8.1	-12.4 / -11.2	-12.4 / -12.4	-11.0 / -12.3
Loop size (µL)	**20**					**80**				
$\Delta\phi_{sample}$	**-0.2**	**-0.1**	**0**	**+0.1**	**+0.2**	**-0.2**	**-0.1**	**0**	**+0.1**	**+0.2**
t_R	-3.7 / -1.2	-3.7 / -1.2	-3.6 / -1.2	-3.5 / -1.2	-3.2 / -1.0	-3.4 / -0.3	-3.8 / -0.7	-3.1 / -0.5	-0.9 / 0.4	-2.9 / -0.3
w_{50}	-1.0 / -1.8	-1.9 / -1.9	-4.2 / -4.2	-6.3 / -6.5	-5.8 / -5.5	-5.3 / -4.8	-4.1 / -5.5	-7.8 / -9.2	-8.6 / -14.3	9.4 / -14.9
$w_{4.4}$	-6.0 / -7.1	-6.7 / -7.1	-7.4 / -7.3	-8.3 / -8.9	-8.8 / -7.4	-11.2 / -6.6	-8.4 / -6.2	-11.8 / -3.9	-11.9 / -12.6	-10.6 / -13.9

a. Mean and median differences are the upper and lower values in each cell, respectively. Each mean and median is calculated for the set of eight test solutes under a particular set of conditions. Percent difference is calculated as: $\left(\frac{Sim - Exp}{Exp}\right)*100$.

b. Peak widths measured at half-height (w_{50}) or 4.4 % height ($w_{4.4}$).

4.4.2. Effect of dilution

The simulation can also be used to inform 2D-LC method development decisions for targeted applications where detection sensitivity and/or resolution of critical pairs of peaks are the most important metrics of performance. In Figure 4.12 we plot average peak height for peaks 4 and 5 (AP2 and PB3), and resolution of that peak pair, as $\Delta\phi_{sample}$ and injection volume are changed. As expected, both the peak height and resolution decrease as the injection volume and $\Delta\phi_{sample}$ are increased. The simulation in this case assumes a constant number of moles of solute injected, independent of injection volume. As the peaks broaden with larger injection volume and $\Delta\phi_{sample}$, the peak height decreases because peak area is conserved. These plots are very effective tools for understanding that the combination of the sample matrix ($\Delta\phi_{sample}$ level) and the injection volume affects both detection sensitivity and resolution of particular pairs of peaks. Increasing the organic content of the sample and/or the injection volume generally leads to broadening of the peaks and loss of resolution, and in turn a loss of peak height. In these plots we've highlighted the positive effect of diluting the organic content of the sample by calling out the two points with red circles. The point at the lower left corresponds to a 40 µL injection of a sample containing 40 % ACN ($\Delta\phi_{sample}$ = +0.1). The resolution of the 4/5 peak pair is about 3.2 and the average height is about 0.0035 under these conditions. Now, if we simulate the dilution of this sample 1:1 with water, we know that the organic content will drop to 20 % ACN ($\Delta\phi_{sample}$ = -0.1), but in the process of doing so we also double the sample volume to 80 µL if we want to inject the same number of moles of analyte onto the column. The question, then, is how does the performance compare at this new condition, as measured by peak height and resolution? The arrows in the plots show that upon dilution we move from the purple point to the blue point, where the peak height has roughly

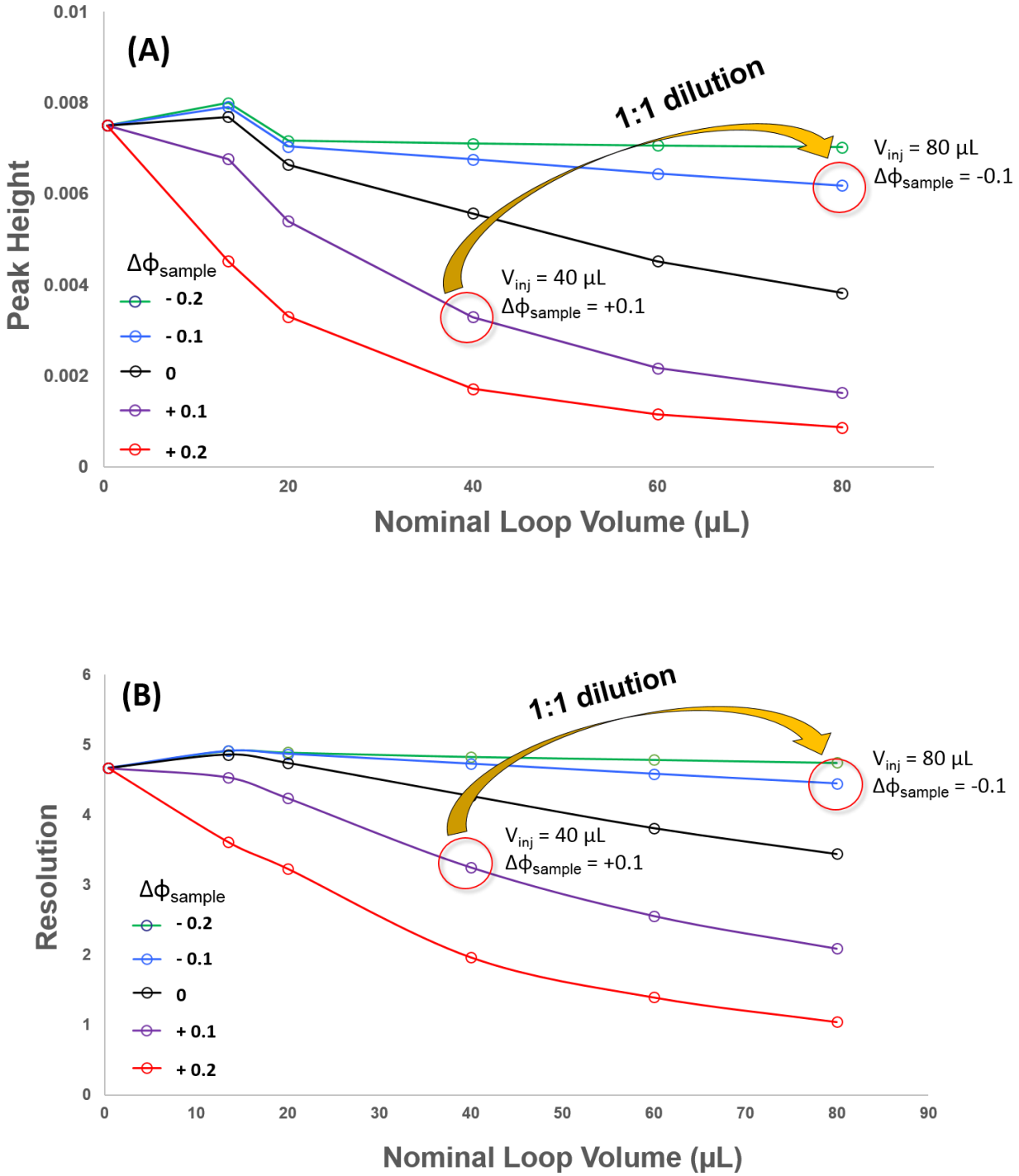

Figure 4.12. Peak height (A) and resolution (B) from simulation results vs. nominal loop volume (100% filling) for peaks 4 and 5 at different $\Delta\phi_{sample}$ levels. The peak height is taken as the average height of peaks 4 and 5. All other conditions are as in Figure 4.9.

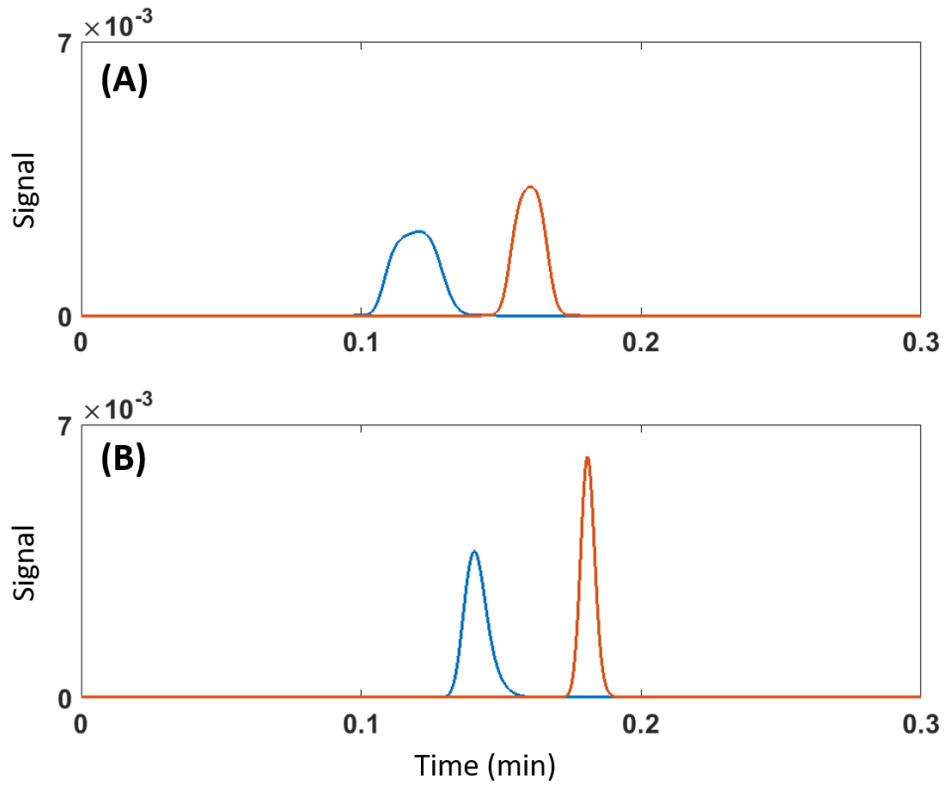

Figure 4.13. Simulation of peaks 4 and 5 for (A) nominal loop volume of 40 µL (100% filling) at $\Delta\phi_{sample}$ = +0.1 (B) nominal loop volume of 80 µL (100 % filling) at $\Delta\phi_{sample}$ = -0.1. All other conditions are same as Figure 4.10.

doubled, but at the same time the resolution has increased to about 4.6. The simulated chromatograms for each of these conditions are shown in Figure 4.13. This is a very powerful effect. In a practical application some of this resolution increase could be sacrificed for increased detection sensitivity by increasing the injection volume much further.

4.5. Effect of temperature

Along with mobile phase gradients, temperature is often controlled to further optimize the separation between analytes. The influence of temperature along with solvent composition on a chromatographic separation can be established by the use of the modified Neue-Kuss equation [64]:

$$\ln k = \ln k_{w,T} + \frac{D_{m,T}}{T} + 2\ln(1+S_2\phi) - \left(1+\frac{D_{m,T}}{T}\right)\frac{S_{1,T}\phi}{1+S_2\phi} \tag{4.7}$$

where T is the temperature in Kelvin, $D_{m,T}$ is the diffusion coefficient, and $k_{w,T}$ and $S_{1,T}$ are temperature dependent variables analogous to k_w and S_1 in the original Neue-Kuss model (equation 3.19). Diffusion coefficients at various temperatures and mobile phase compositions can be calculated based on the following empirical equation [78]:

$$D_{m,T} = D_{m,T'}\left(\frac{T\eta_{T'}}{T'\eta_T}\right) \tag{4.8}$$

where the diffusion coefficient $D_{m,T'}$ for the solute is known and the relationship of viscosity to mobile phase composition and temperature is defined as [79,80]:

$$\eta_T = 10^{[-2.533+742/T-0.452\phi+(235/T)\phi+1.573\phi^2-(691/T)\phi^2]} \tag{4.9}$$

Diffusion coefficients for solutes used in simulations are shown in Table 4.7.

Table 4.7. Diffusion coefficients for solutes used in simulations

Solute	Abbreviation	$D_{m,37\,°C}$ (cm^2/s)
Hydroxyacetophenone	HP2	9.80×10^{-6}
Hydroxypropiophenone	HP3	9.06×10^{-6}
Hydroxybutyrophenone	HP4	7.04×10^{-6}
Methylparaben	PB1	1.09×10^{-5}
Ethylparaben	PB2	9.80×10^{-6}
Propylparaben	PB3	9.06×10^{-6}
Butylparaben	PB4	7.04×10^{-6}

[1]Diffusion coefficient measured at 30 °C from references [81,82] converted to 37 °C using equation 4.8 [20].

Simply updating our existing simulation program with equation 4.7 allowed for retention prediction at a specified column temperature. The viscosity and diffusion coefficients at 70 ºC and ϕ = 0.242 (isocratic data from reference [22] Table S2) were calculated using equations 4.8 and 4.9. The Δz for simulations was obtained from the plate height calculated using the reduced van Deemter parameters given in reference [22] Table S2 (A = 0.66; B = 10.2; C = 0.095). Figure 4.14

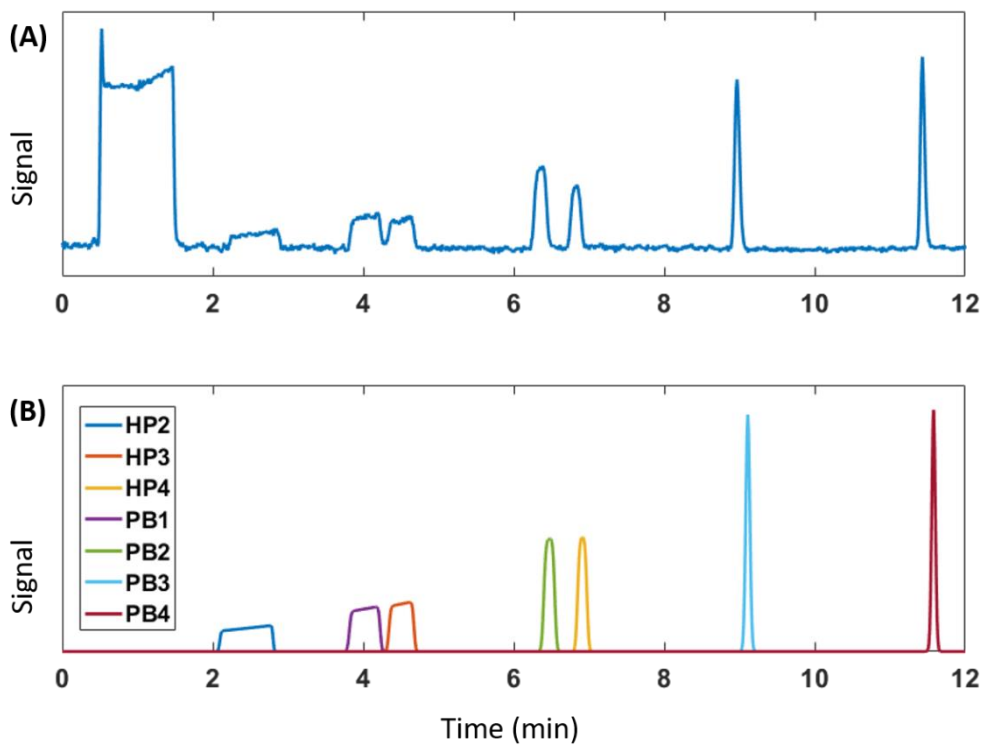

Figure 4.14. Experimental (A) and simulated (rectangular injection) (B) chromatograms collected for gradient separations of hydroxyphenones and parabens at 70 ºC. Conditions: capillary C_{18} column packed in-house (78 mm x 0.15 mm ID, 1.7 µm d_p), injection volume of 1500 nL, mobile phase gradient 95:5 to 55:45 10 mM H_3PO_4:ACN over 16 min at flow rate of 3.00 µL/min. Experimental data reproduced from [22], with permission.

shows comparison of simulation results (B) to the experimental data (A) [22]. The overall peak shape, retention time and peak widths agreed with experimental data reasonably well.

4.6. Conclusion

A finite difference scheme, based on the Craig model of chromatography, has been developed to solve the partial differential equations defining chromatographic elution for some specific systems of interest. It enables simulation of chromatographic peaks eluted under isocratic or gradient conditions including complex separation conditions where the mobile phase and sample solvents are not matched or where dilution causes increased injection volume. It also

possesses the versatility to use rectangular pulse or experimental injection profiles as well as different column temperatures. The analyte mass propagation down the column was calculated using estimates of local retention factor at regular spatial increments as the solute zone progresses along the column, as time increases. The approach is similar to that proposed by Czok and Guiochon [60] with an important distinction. The equations for non-steady state conditions in the original paper (applied to Langmuir isotherms) were in error and are corrected here and applied to both gradient mobile phase conditions and non-ideal injection conditions, which were not discussed in the original paper.

In this work, we have shown that both linear (LSS) and non-linear (Neue-Kuss) solvent strength models can be used to provide retention factors for the simulations. The accuracy of the simulation code was validated against LSS theory. The retention times obtained by simulation compared well to experimental results as well. Under sample/eluent solvent mismatch conditions (isocratic), the expected retention time trend was confirmed and the increases in the simulated peak widths were validated against predictions from theory. The simulation performance for linear mobile phase gradients with solvent mismatch was validated against experimental data. We have found that the injection profiles obtained from values in current use for 2D-LC are highly asymmetric. Therefore, it is necessary to use experimentally acquired injection profiles to achieve simulation prediction with accurate retention time, peak width and peak shape. Finally, the analysis of the simulation results yielded practical insights on the effect of dilution in 2D-LC method development. It was shown that detection sensitivity and resolution of peak pairs can increase with dilution of sample solvent to weaker composition compared to initial mobile phase composition despite the large injection volume.

The use of this simulation program can facilitate a deeper understanding of liquid chromatography and the development of new LC methods by reducing time-consuming trial-and-error experiments. In next chapter, we will explore a convolution technique developed to further speed up the simulation process.

Chapter 5: Convolution

This chapter has been adapted from L.N. Jeong, D.R. Stoll, P.W. Carr, S.C. Rutan, i*n preparation for submission to J. Chromatogr. A.*

5.1. Introduction

Although retention prediction using our simulation program is much faster than a trial-and-error approach for exploring the effects of various perturbations on the separation quality, full simulation can be slow due to the necessity of calculating results at each point in time and space. This is particularly the case for complex LC conditions such as volume overload and solvent mismatch. In order to develop a useful and practical simulator for method development in 2D-LC, these computations must be accelerated. One way to achieve this is to use a simulation on a short length of column – just long enough for the peak to develop its shape – and then mathematically convolve the resulting peak with the known closed form solution for the remainder of the column [83]. In this chapter we present a convolution approach as a way to achieve faster retention prediction and show that this method also allows for automation with low prediction error.

5.2. Closed form theory

Elution parameters for an analyte band including retention time and peak width have been expressed mathematically in previous theoretical studies [46,84,85]. The use of the LSS and

NK models has been shown to give reasonably accurate predictions for linear mobile phase gradient conditions [53]. Although the effect of different solvent strengths on retention time and peak widths has been explored previously [67,86–91], a definitive solution to sample solvent mismatch conditions is not yet available. Here we propose closed form expressions for approximate retention time and peak width prediction under non-ideal solvent mismatch conditions. Our theory is based on the previous theoretical developments by Blumberg [46,63] and a simplified representation of how the solvent and analyte bands travel along the distance of the column. The derivations for retention time and peak width calculations for sample solvent mismatch conditions are described in detail in Appendix B. The need for these closed form expressions is two-fold. First, with the availability of the simulator, we can characterize the exact limitations of closed form expressions. Secondly, for cases where many conditions are simulated, closed form expressions can provide estimates for parameters, such as the total time needed for simulation, that allow for automation of the simulation process.

5.2.1. Retention time calculation

Retention prediction for linear gradient mobile phase conditions under ideal injection conditions using closed form expressions has been shown previously in section 3.3. This can be extended to non-ideal injection conditions where the sample solvent and initial mobile phase composition are mismatched. In the presence of solvent mismatch, there are three contributions to retention: (1) the time it takes for half of the injection band to be loaded on to the column; (2) the elution time for the analyte band while it is eluting in the sample solvent; and (3) the elution time for the analyte band under linear mobile phase gradient conditions.

$$t_R = t_{R,1} + t_{R,2} + t_{R,3} \tag{5.1}$$

Tables 5.1 shows summary of derived equations that represent each contribution to the retention time under solvent mismatch conditions. The derivations are described in detail in Appendix B.

Table 5.1. Closed form equations for retention time calculations under solvent mismatch conditions

Contribution	Equation	Equation number
Injection	$t_{R,1} = \frac{t_{inj}}{2} = \frac{z_{inj}}{2u_m}$	B4
Elution in sample solvent	$t_{R,2} = t_{M,2}(1 + k_{ss})$	B9
Elution in gradient	$t_{R,3} = \frac{t_G(\phi_e - \phi_0)}{\Delta\phi} + t_{M,grad} + t_D$	B13

5.2.2. Peak width calculation

The peak width calculation is based on the previous expression of σ^2 as a sum of variances from the injection band width (i.e., extra-column effects) and the isocratic parts of the separation [63]:

$$\sigma_{tot} = \sqrt{\sigma_{grad}^2 + \Delta\sigma^2} \tag{5.2}$$

where $\Delta\sigma$ is the variance due to the finite injection bandwidth, as well as the contribution while the analyte elutes within the sample solvent and within the dwell time and σ_{grad} is the gradient peak width.

In order to calculate $\Delta\sigma$, we must consider the total bandwidth before the analyte experiences the gradient:

$$\sigma_b^2 = \sigma_{inject}^2 + \sigma_{sample}^2 + \sigma_D^2 \tag{5.3}$$

where σ_{inject}, σ_{sample}, and σ_D are the bandwidths of the injection itself, the band broadening during elution while in the sample solvent and the band broadening during the elution while in the dwell

volume, respectively. The band broadening in the sample solvent, σ_{sample}, was not included in the total bandwidth given in Chapter 3 (equation 3.22). It also should be noted that equation 3.22 was for isocratic conditions. Tables 5.2 shows equations that represent each bandwidth contribution.

Table 5.2. Closed form equations for calculation of bandwidth contributions before gradient

Contribution	Equation	Equation number
Injection	$\sigma_{inject} = \frac{k_o\left(k_{ss}+1\right)z_{1,f}}{k_{ss}\left(k_o+1\right)\sqrt{12}}$	B17
Band broadening during elution in sample solvent	$\sigma_{sample} = \sqrt{z_{2,m}\Delta z}$	B18
Band broadening during dwell time	$\sigma_D = \sqrt{z_D \Delta z}$	B19

The bandwidth σ_b conversion to peak width $\Delta\sigma$ and calculation for the gradient peak width σ_{grad} is similar to the closed form equations discussed in section 3.2.2. for LSS theory. All derivations for peak width calculation are described in detail in Appendix B.

5.3. Conditions studied

A large set of conditions were analyzed to compare the performance of closed form calculation and the convolution approach to full simulation. Retention prediction for eight compounds (structures and abbreviations shown in Figure 5.1) were studied. The sample solvent was either weaker, matching, or stronger (ϕ = 0.1, ϕ = 0.3, and ϕ = 0.5, respectively) compared to the initial mobile phase composition (ϕ_o = 0.3). Two different gradient times were used to produce shallow or steep gradient slopes (t_G = 0.5 min and t_G = 0.25 min, respectively). A set of 21 different injection volumes with corresponding injection profiles were used (rectangular injection profiles or experimental injection profiles obtained from different sample loops at different filling levels

as described in section 4.5). This resulted in 126 total condition combinations for each compound. With eight compounds, this results in a total of 1008 simulation conditions. Previous simulation *vs.* experimental data comparisons (Chapter 4) demonstrated accurate retention prediction using our simulation code. Therefore, closed form and convolution calculations were directly compared to the results from full simulation.

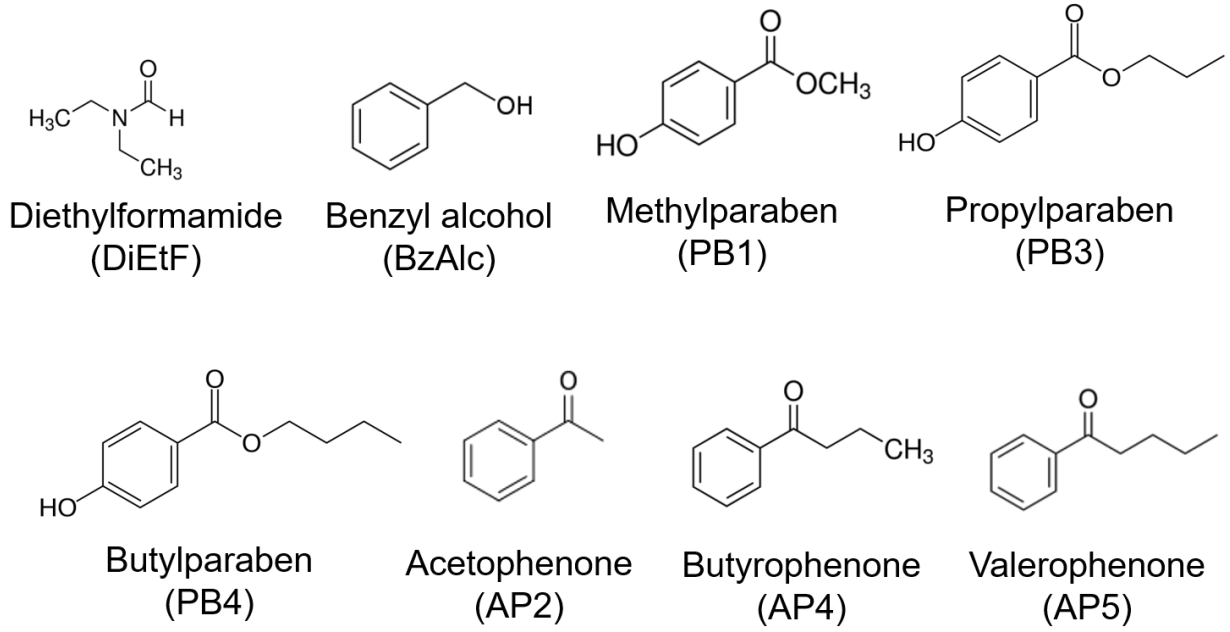

Figure 5.1. Structures and abbreviations for compounds used in the convolution study

5.4. Closed form retention predictions

Closed form calculation provides fast, almost instantaneous, retention prediction. For simple linear mobile phase conditions under ideal injection conditions (*i.e.*, rectangular injection with matching sample/eluent solvent composition), closed form predictions are reasonably accurate. As shown in Figure 5.2, for the 336 out of 1008 simulation conditions where the sample solvent and initial mobile phase composition are matching, the retention time and peak width prediction by closed form are in reasonable agreement with the full simulation results. Slight

deviations from the identity line for peak widths are observed for the largest injection volumes of the most weakly retained compounds (DiEtF and BzAlc). However, under non-ideal conditions with both solvent mismatch and volume overload, closed form prediction deviates from the simulation prediction. This is shown in Figure 5.3 where prediction results for all 1008 simulation conditions are compared. In general, the retention time predictions by closed form are shown to be reasonably accurate even for solvent mismatch conditions. However, the peak widths for first three eluting compounds under these conditions are predicted to be much broader than those predicted by simulation.

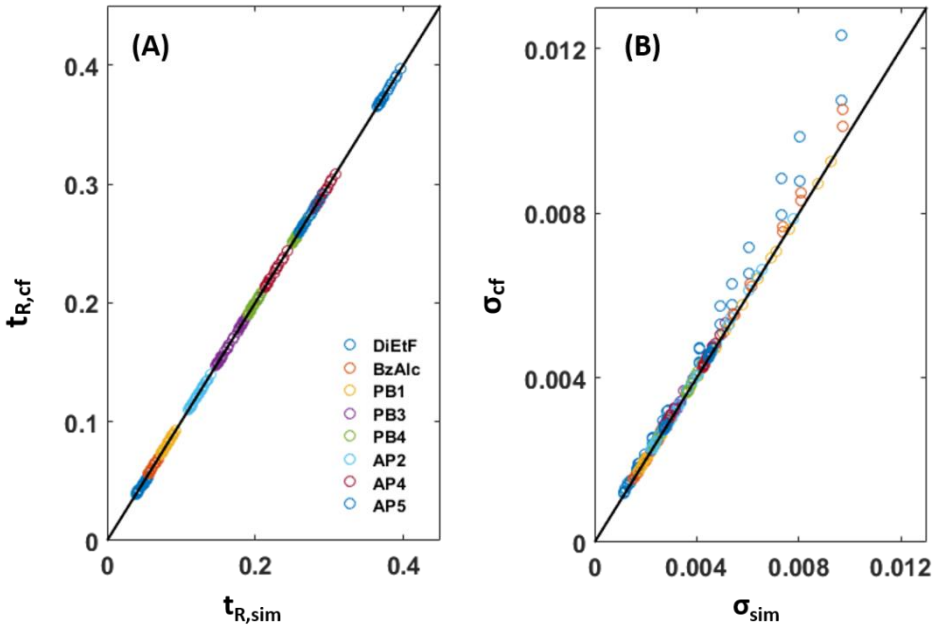

Figure 5.2. Comparison of retention prediction by closed form to full simulation using rectangular injection profiles (A) retention time and (B) peak width. These correspond to cases where the sample solvent is the same as the solvent composition at the start of the gradient.

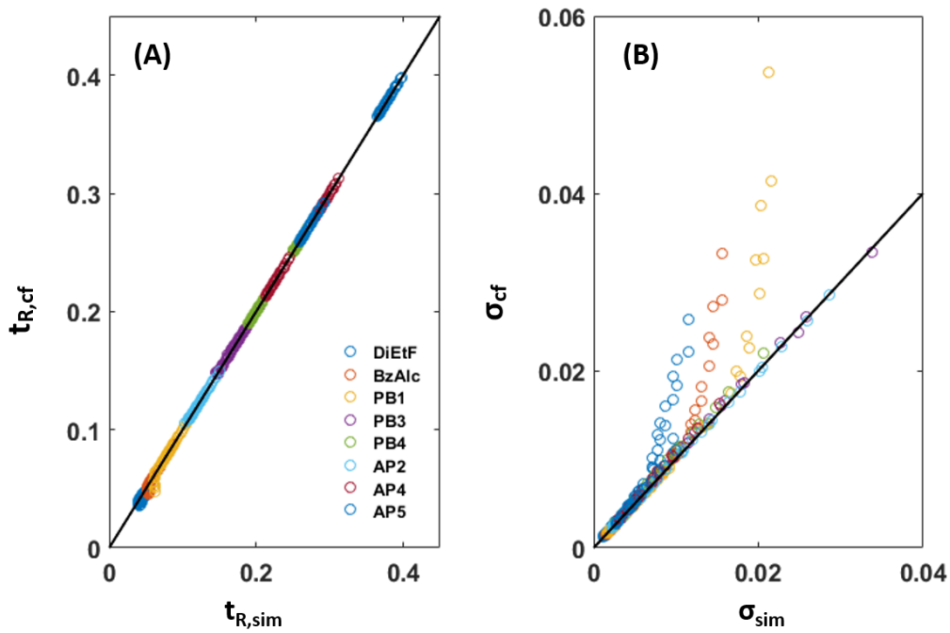

Figure 5.3. Comparison of retention prediction by closed form to full simulation using rectangular injection profiles (A) retention time and (B) peak width for all 1008 conditions.

The closed form calculation does not consider the injection band shape and therefore worse performance was expected for experimental injection profiles where the injection band is asymmetrical; thus, this comparison is not shown here. There is a need for a rapid prediction technique that can provide more accurate retention prediction for both rectangular and experimental injection profiles. Here we propose a convolution approach to speed up simulations without compromising the quality of simulation and to retain the ability to capture the tailing shapes introduced by the experimental injection profiles.

5.5. Convolution strategy

A convolution is a mathematical function that expresses the overlap of one function, *g*, as it is shifted over another function, *f*. It "blends" the two functions together [92]. The resulting convoluted function, *f***g*, is a modified function of the original function, *f*.

$$f(t) * g(t) = \sum_{\tau=-\infty}^{\infty} f(t)g(t-\tau) \tag{5.4}$$

For example, if we shift an exponential decay function *g* over a Gaussian function *f*, then we obtain an exponentially modified Gaussian function *f***g* as shown in Figure 5.4.

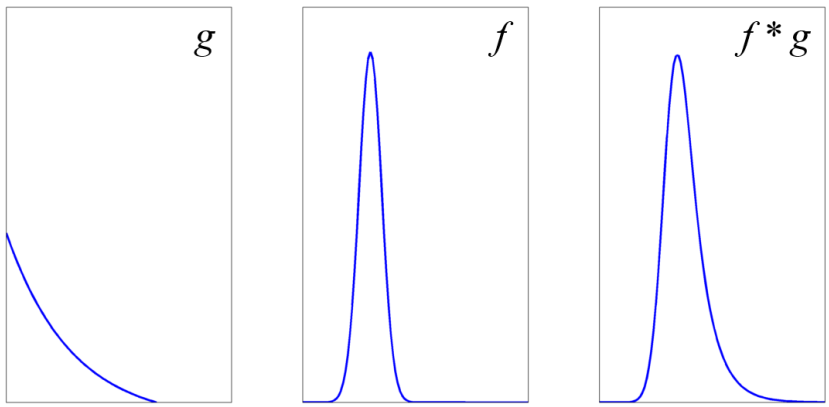

Figure 5.4. Convolution of a Gaussian function with an exponential decay function to produce an exponentially modified Gaussian function

For the purpose of chromatographic simulation, we adapt the convolution approach by dividing the column into two separate sections. As shown in Figure 5.5A, for the first section of the column C1, we perform a simulation. For the rest of the column length C2, we use a closed form calculation and produce a Gaussian peak from the calculated results. The obtained peaks are then convolved to give the expected chromatogram.

Convolution of two peaks involves three steps: (1) Fourier transform of both peaks; (2) multiplication in Fourier domain; and (3) inverse Fourier transform to get the resulting chromatogram. It is important to note that the distance for which simulation is required must be long enough so that the sample solvent surpasses the analyte band. In other words, $z_{2,f}$ must be equal to the distance at which the front end of the analyte band meets the tail end of the sample solvent band (Figure 5.6).

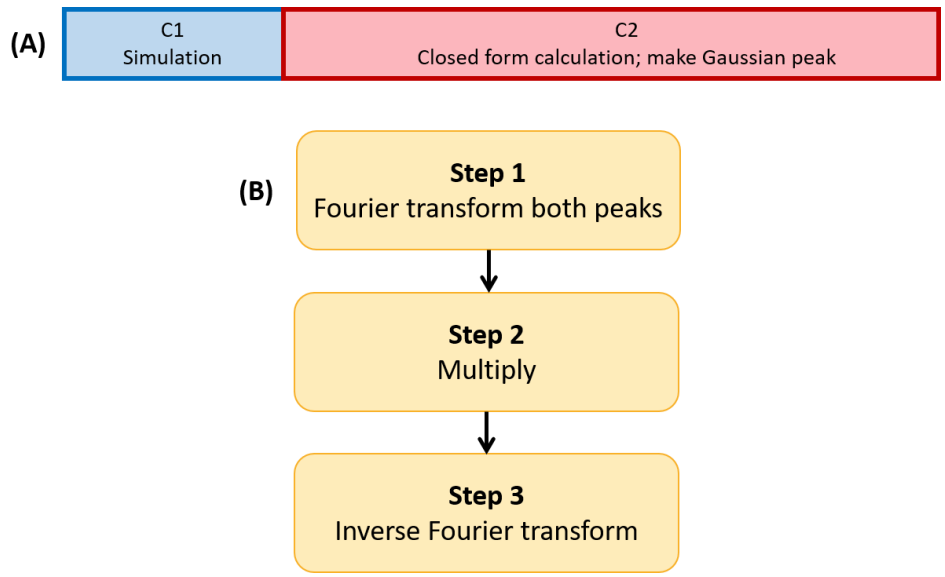

Figure 5.5. Convolution method applied to LC. (A) Two column segments for convolution approach: a full simulation is performed for first segment C1 and the known closed form solution for second segment C2 is used to make a Gausssian peak (B) Stepwise schematic of the convolution approach.

The time it takes for the tail end of the analyte band to travel from $z_{1,f}$ position to $z_{2,f}$ position (Figure 5.6A to 5.6B) is calculated as

$$t_2 = \frac{z_{2,f}}{u_m} = \frac{z_{2,f} - z_{1,f}}{u_{ss}} \tag{5.5}$$

Solving for $z_{2,f}$ after substituting for $z_{1,f}$ and u_{ss} using equations B5 and B6 yields

$$z_{2,f} = \frac{z_{inj}}{k_{ss}} \tag{5.6}$$

In other words, $z_{2,f}$ is simply double $z_{2,m}$ (Figure 5.6C).

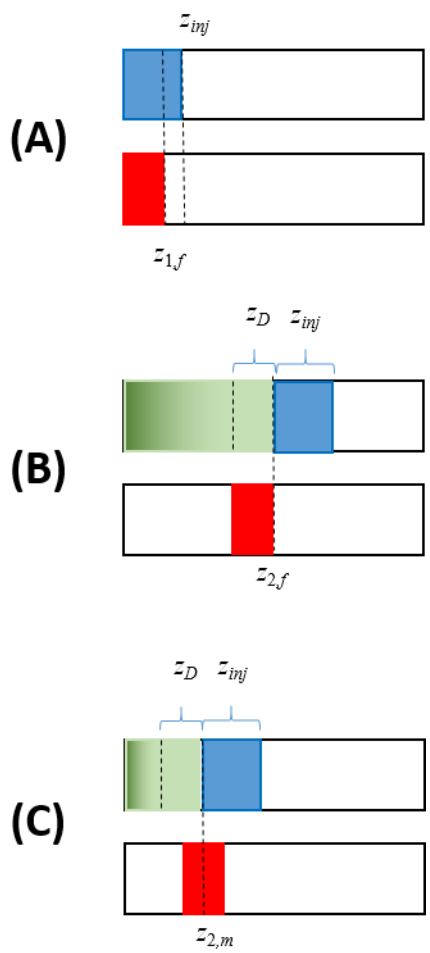

Figure 5.6. Relationship between $z_{1,f}$ (A), $z_{2,f}$ (B), and $z_{2,m}$ (C). Sample solvent band (blue), analyte band (red), and mobile phase gradient (green).

5.5.1. Feasibility testing

The feasibility of the convolution approach was determined by looking at a simple linear mobile phase gradient conditions without any solvent mismatch or volume overload. The retention of PEA on a 5 cm C_{18} column was simulated for a mobile phase gradient of 2 – 5 % ACN over 3 minutes. In order to perform convolution, we first divided the column into two separate sections. As shown in Figure 5.5A, for the first section of the column C1, we performed simulation and for the rest of the column length C2, we used closed form calculation and produced a Gaussian peak

from the calculated results. It is important to note that the peak widths of the simulated peak from C1 must be corrected before performing convolution. This peak adjustment was performed using the series of peak width equations presented in Appendix B.

First, it is important to recognize the initial mobile phase composition for C2 is equal to the mobile phase composition at elution from C1 ($\phi_{o,2} = \phi_{e,1}$). The remainder of the change in organic composition, the void time, and the gradient time ($\Delta\phi_2$, $t_{m,2}$, and $t_{G,2}$, respectively) are calculated to produce the new dimensionless gradient slope $b^{\dagger}$ for C2

$$b_2^{\dagger} = \frac{S^{*}\Delta\phi_2 t_{m,2}}{t_{G,2}} \tag{5.7}$$

where S^* is the slope of ln k vs ϕ plot at elution as defined in equation B25.

The bandwidth 'introduced' into C2 is equal to the bandwidth contribution at the exit of C1, which is obtained from the conversion of simulated peak width ($\sigma_{t,1}$) with its elution velocity (u_e)

$$\sigma_{b.2,entrance} = \sigma_{t,1,exit} u_e \tag{5.8}$$

This conversion was achieved by converting the time axis for C1 chromatogram to a distance axis for the introduction onto the C2 so that the simulated C1 chromatogram has the same axis as the C2 chromatogram. Subsequently, the peak width at the end of C2 is calculated by converting the band width at the C2 exit to a peak width by dividing by the elution velocity for C2

$$\Delta\sigma^2 = \frac{\sigma_{b,2,exit}}{u_{e,2}} \tag{5.9}$$

It is essential to perform this step ($\sigma_{t,1}$ conversion to $\Delta\sigma$) to obtain the correct overall peak width prediction.

Once peaks from both column sections C1 and C2 are obtained, we can proceed with the convolution approach. As schematic in Figure 5.5B shows, we first perform Fourier transform on both peaks (blue and red peaks in Figure 5.7A), then multiply them together (point-wise), and finally the inverse Fourier transform returns the convoluted peak (the green peak in Figure 5.7A).

The retention prediction with convolution is shown to have good agreement in retention time and peak width to the full simulation result, as shown in Figure 5.7. Because the convolution approach proved to provide accurate retention prediction for this simple linear mobile phase gradient condition, we believed that this approach had the potential to be applied to more complicated separation conditions faced in 2D-LC. We moved on to looking at the 1008 simulation conditions described in section 5.3.

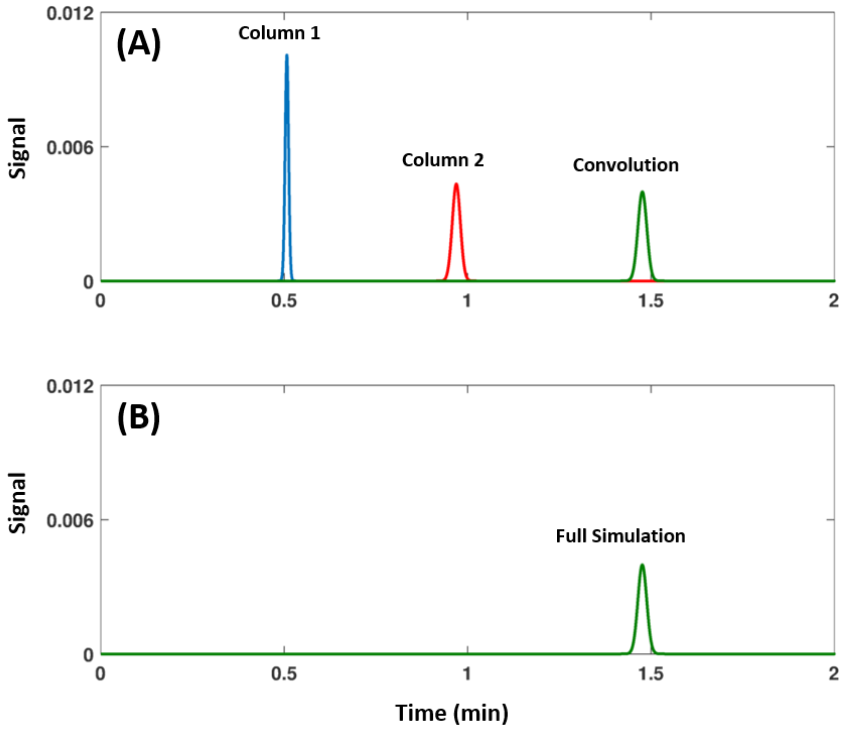

Figure 5.7. Comparison of (A) convolution to (B) full simulation in prediction of PEA retention on 5 cm C_{18} column under 2 % - 5 % ACN gradient over 3 minutes

5.5.2. Automated convolution approach

Automation is key to a rapid simulation prediction. In order to automate the convolution method, the overall simulation time and column lengths were estimated for each condition using the closed form calculations. Since closed form predictions were shown to deviate significantly for solvent mismatch conditions (Figure 5.3), we estimated total simulation time and length to be 5σ greater than retention time and distance at which the sample solvent escapes the analyte band:

$$t_{sim} = t_{R,cf} + 5\sigma_{cf} \tag{5.10}$$

$$L_{sim} = z_{2,f} + 5\sigma_b \tag{5.11}$$

where $t_{R,cf}$ and σ_{cf} are overall retention time and peak width prediction by closed form calculation, and $z_{2,f}$ is the position of the column when the front end of the analyte band meets the tail end of the sample solvent band (equation 5.6) and σ_b is overall band width calculated from equation 5.3. The convolution approach is useful because it reduces length and time required for simulation resulting in less overall computation time. The convolution approach does not provide any significant advantage over full simulation at L_{sim} lengths of greater than 90 % of the total column length. Therefore, we set a threshold for convolution program to only operate up to L_{sim} length of 90 % of the total column length and suggest full simulation under any conditions which do not fit this criterion.

We first tested the automated convolution approach performance using rectangular injection profiles. The comparison of 854 conditions (where convolution approach was deemed useful) with full simulation results show better agreement in retention time and peak width compared to closed form prediction (Figure 5.8). The greatest differences in retention time and peak widths for the rectangular injection profiles were 2.7 % and 9.4 %, respectively. Our

convolution method proved to be very effective even when asymmetric experimental injection profiles were used (Figure 5.9). All retention time and peak width predictions using convolution approach when using experimental injection profiles exhibited less than 5.5 % and 17 % difference compared to the full simulation results, respectively. The biggest difference resulted for earlier eluting compounds under stronger sample solvent conditions. We suspect that this is due to underestimation of L_{sim} by the closed form expressions. Despite this shortcoming, we believe that our fully automated convolution program will allow chromatographers to exhaustively search for the most optimal separation condition within reasonable amount of time.

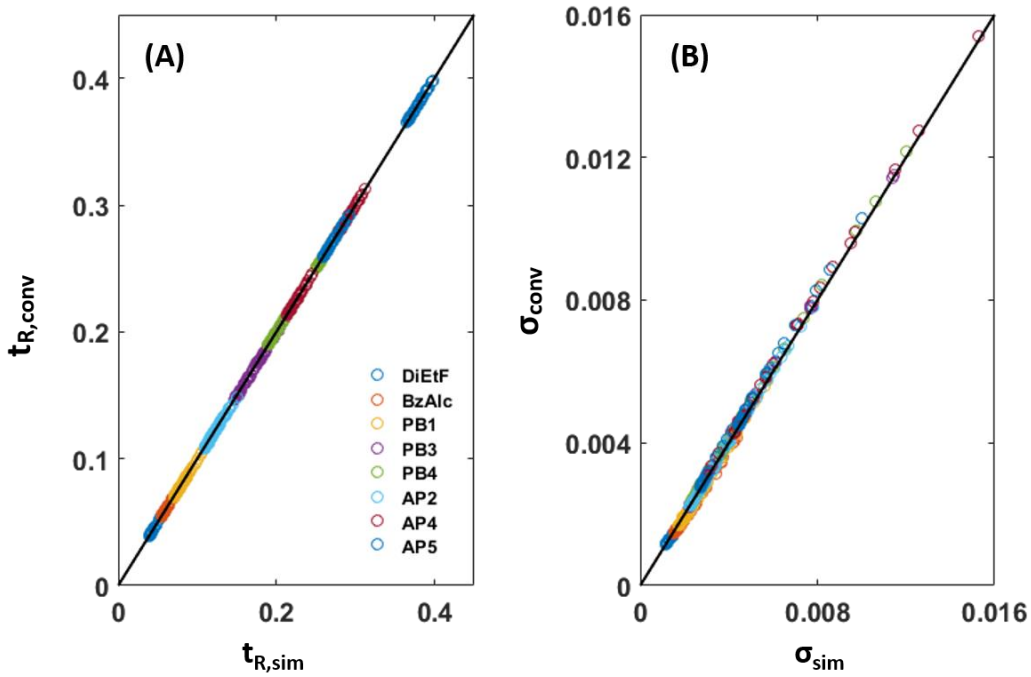

Figure 5.8. Comparison of retention prediction by convolution to full simulation (A) retention time and (B) peak width using rectangular injection profiles. Only the 854 conditions where convolution is useful are plotted.

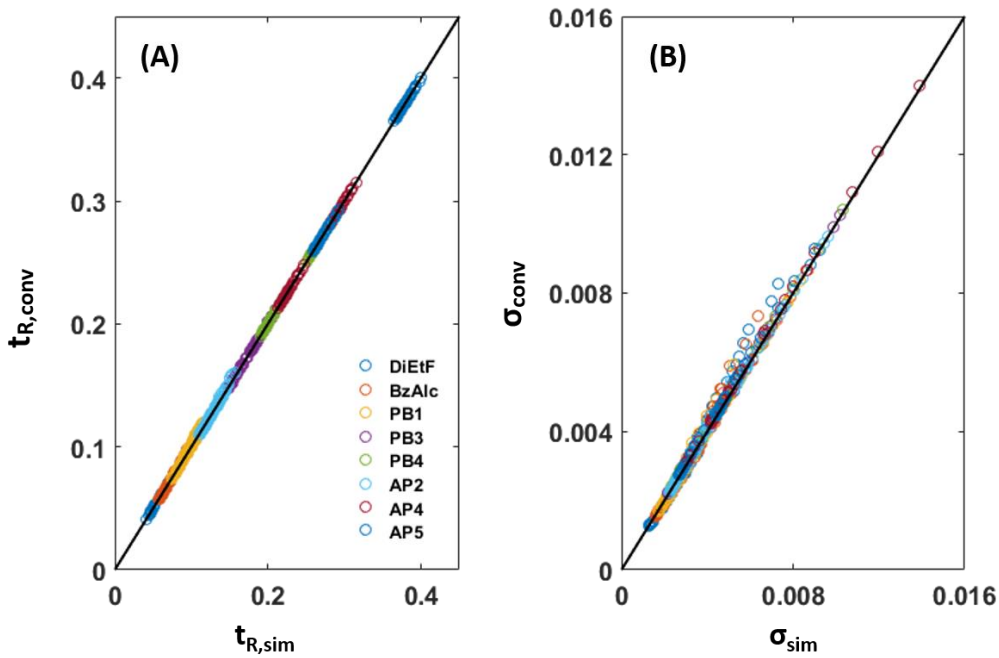

Figure 5.9. Comparison of retention prediction by convolution to full simulation (A) retention time and (B) peak width using experimental injection profiles. Only the 854 conditions where convolution is useful are plotted.

The computation times for the full simulation and the convolution approach for each condition were recorded for comparison. The average elapsed time for each compound when using the experimental injection profiles is shown in Table 5.3. The speed increase factor ranged from 2.2 to 13 depending on the solute. Retention predictions for the 854 conditions were achieved in 34 minutes with full simulation whereas prediction using the convolution approach was complete in 4.4 minutes, which is almost eight times faster than running full simulations.

Table 5.3. Comparison of average computation time when using experimental injection profiles

Compound	Full simulation average elapsed time (s)	Convolution average elapsed time (s)	Increase factor
DiEtF	1.0	0.47	2.2
BzAlc	1.3	0.43	3.1
PB1	1.5	0.36	4.1
PB3	2.5	0.20	12
PB4	3.0	0.26	11
AP2	2.0	0.31	6.6
AP4	3.2	0.29	11
AP5	3.6	0.28	13

*Computer used: Dell Precision T3600 with an Intel Xeon E5-1620 CPU at 3.60 GHz and 32.0 GB of RAM

5.6. Conclusion

In this study, we have extended our simulation program with the capability to accelerate retention prediction. We have proposed a set of closed form equations to provide approximate retention prediction for gradient elution separations with large injection volumes that have solvent compositions that differ from the starting mobile phase compositions. Although these equations predicted retention time and peak width with reasonable accuracy under volume overload conditions, the results deviated significantly for solvent mismatch condition commonly faced in 2D-LC separations.

In this chapter we have described a convolution approach to speed up the simulation process without the loss of prediction accuracy in retention time, peak width and peak shape. This approach reduces the column length required for simulation and uses the known, closed form solution for retention prediction for the remainder of the column length. In turn, the overall computation time is decreased. Complete automation of this approach allowed for exploration of wide range of separation conditions and resulted in eight-fold speed increase compared to full simulation. Also, retention time predictions achieved by convolution resulted in small differences compared to full simulation (greatest difference 2.7 % for rectangular injections and 5.5 % for experimental injections). The convolution approach has a great potential for development and optimization of LC methods.

Chapter 6: Stationary Phase Gradients

This chapter has been adapted from L.N. Jeong, S.G. Forte, S.C. Rutan, *in preparation for submission to J. Chromatogr. A.*

Section 6.5 has been adapted, with permission, from V.C. Dewoolkar, L.N. Jeong, D.W. Cook, K.M. Ashraf, S.C. Rutan, M.M. Collinson, *Anal. Chem.* 88 (2016) 5941–5949.

6.1. Introduction

There is a great interest in the development of different stationary phases such as monoliths, superficially porous particles, and mixed mode materials to enhance the separation performance of liquid chromatography (LC) [6,93,94]. The majority of the current method development efforts for LC separation often involve selecting one stationary phase and optimization of the mobile phase. However, it has been shown that a change in ligand type or bonding density in stationary phase can also provide varied separation selectivity [95–98]. A stationary phase with a gradient (or multiple gradients) in ligand density could provide improved separation for mixtures difficult to separate with conventional methods by providing unique selectivity.

The development of stationary phase gradients could also have a great impact on the development of comprehensive two-dimensional liquid chromatography (LCxLC). One of the issues in LCxLC method development is the existence of a solvent mismatch between the first

dimension (^{1}D) effluent and second dimension (^{2}D) initial mobile phase composition [71,74,75,99,100]. When using rapid gradients in the second dimension with a diode array detector (DAD), refractive index changes cause large backgrounds such as an injection ridge (from solvent mismatch) and sloping baselines, which can be problematic for achieving accurate quantitation [101,102]. Use of a stationary phase gradient may enable the use of an isocratic mobile phase in the ^{2}D which could be very useful in minimizing these background signals.

Stationary phase optimized selectivity liquid chromatography (SOSLC) is a technique to optimize separation selectivity by tuning stationary phase compositions [103,104]. The optimal stationary phase combination is determined by predicting the column combination that will result in highest degree of overall separation and shortest analysis time based on retention data for the mixture components on individual phases. This development has been commercialized as POPLC (Bischoff Chromatography) [105] and many studies have reported unique separation selectivity which resulted in improved separation [106–108]. However, these serially connected columns provide discontinuous step gradients with the possibility of void volumes between column sections which may cause peak broadening [109].

In recent studies, a simple and inexpensive method for preparation of continuous gradient on thin layer chromatography (TLC) plates was used to improve the separation of mixtures [96–98]. The controlled rate infusion (CRI) method, in which a functionalizing reagent is infused in a time dependent manner across the plate, was employed to prepare gradients in amine and amine/phenyl concentration on silica TLC plates and improved resolution was seen, relative to a plain silica plate or a fully functionalized silica plate [96,97]. Additionally, the CRI method has recently been used to prepare LC stationary phases with a gradient in the density of amine functionality on silica monoliths [110]. Because there is the capability of tuning the gradient

preparation, it would be advantageous to simulate the chromatographic behavior of these gradient systems, in order to guide the synthesis of novel gradient stationary phases for LC separations. The SOSLC prediction algorithm assumes that the retention factors are additive for serially connected columns. In our algorithm, the local retention factor for specific combinations of stationary phase ligands is calculated for more accurate prediction of overall retention. In addition, our simulations allow for consideration of both stationary phase and mobile phase gradients.

It is important to note that in this work we use Neue-Kuss theory to obtain parameters that should be able to predict retention for all mobile phase compositions on the corresponding stationary phase. Then, in principle, we can use any type of mobile phase gradient or injection solvent mismatch profile we like, hence being able to explore many conditions not explicitly described by closed-form theory. Also, our program allows for the evolution of the chromatogram to be captured in the form of movies and/or snapshots of the analyte distribution over time and/or distance to facilitate a better understanding of the separation process under complicated circumstances.

6.2. Stationary phase gradient theory

Gritti and Guichon have developed a closed form theory for retention on a column with a linear gradient in the stationary phase retention factor, which results in the following prediction of the retention time [111]:

$$t_R = \frac{L}{u_m}\left(1 + k_o + a\frac{L}{2}\right) \tag{6.1}$$

where L is the column length, u_m is the mobile phase velocity, k_o is the retention factor at the start of the gradient and a is the slope of the linear stationary phase gradient defined as

$$k(z) = k_o + az \tag{6.2}$$

Here, z is the incremental distance along the column length, so that $k(z)$ represents the local retention factor as a function of column length. These authors also formulated an expression for the band width for a gradient stationary phase [111]. While the original paper included two expressions for the band width considering both the case for 'band compression' or with 'no band compression' [111], Blumberg has subsequently shown that only the 'band compression' equation is correct [112,113]. The band width for a linear stationary phase gradient is therefore given by

$$\sigma_z = \sqrt{HL\frac{1 + p(L) + \frac{p(L)^2}{3}}{(1 + p(L))^2}} \tag{6.3}$$

where H is the plate height and $p(L)$ is given by

$$p(L) = \frac{aL}{1 + k_o} \tag{6.4}$$

The band width expressed by equation 6.3 can be converted to peak width by dividing by the band velocity at elution ($u_e = u_m/1+k(L)$), which results in the following expression

$$\sigma_t = \frac{1 + k(L)}{u_o}\sqrt{HL\frac{1 + p(L) + \frac{p(L)^2}{3}}{(1 + p(L))^2}} \tag{6.5}$$

While we have designed our code to accommodate any type of stationary phase gradient (*i.e.*, step, exponential or custom), the closed form solution for the linear gradient offers us a convenient means to validate our code.

The simulation code was written based on the Craig model, where the continuous chromatographic process is explained by describing the separation process in terms of discrete distance and time segments. As discussed in Chapter 4, Czok and Guiochon's approach was

adapted to simulate solute retention for linear (Linear Solvent Strength (LSS) theory [45]) and non-linear (Neue-Kuss [64]) models for the dependence of retention factor on solvent strength for linear mobile phase gradients. We present here an addition to the simulator's capability with the development of simulations for customized stationary phase gradients.

As illustrated before in Chapter 3, the local retention factor must be calculated for simulation of any LC conditions. According to Neue-Kuss theory, the local retention factor (k) can be predicted as a function of mobile phase composition (ϕ) (equation 3.19) [64]:

$$k = k_w (1 + S_2\phi)^2 \exp\left[\frac{-S_1\phi}{1 + S_2\phi}\right] \tag{6.6}$$

where S_1 is the slope of ln k versus ϕ, S_2 is the curvature coefficient, and k_w is the solute retention factor for a purely aqueous mobile phase. Ideally, the k_w parameter in this relationship depends only on interactions of the selected solute with stationary phase, while the S_1 and S_2 parameters depend only on the interactions of the selected solute with the mobile phase. While this is undoubtedly an oversimplification, in principle, this formula offers a convenient means of determining a local retention factor as a function of any mobile phase/stationary phase ligand concentration that should be at least approximately valid.

The S_1, S_2, and k_w for each solute must be experimentally determined independently for columns of each functionality. In the present work, we accomplished this by using nonlinear least squares fitting of the isocratic retention times (t_R) and mobile phase compositions (ϕ) on columns with the corresponding stationary phases to equation 6.6.

In order to perform stationary phase gradient simulations, common S_1 and S_2 values need to be obtained for each solute. While there are a number of reasons why the S_1 and S_2 values of a compound might differ significantly for two separate columns, one possible reason is a difference

in the stationary phase volumes. In order to adjust for this discrepancy, the gradient retention times on one column can be adjusted using the following relationship

$$t_{R_{1,corr}} = \frac{V_{stat_2}}{V_{stat_1}}(t_{R_1} - t_{m_1}) + t_{m_2} \tag{6.7}$$

where $\frac{V_{stat_2}}{V_{stat_1}}$ is the ratio of volumes of the stationary phases in the two columns. This relationship is optimized by finding a stationary phase volume ratio that produces the most similar S_1 and S_2 values across all solutes. These corrected retention times can then be utilized to calculate a set of theoretical NK parameters (k_{w1}, k_{w2}, S_1 and S_2) that can be used to implement the simulations.

By utilizing the NK parameters acquired by fitting the isocratic experimental data on the individual reference columns, gradient stationary phase simulations can be generated in an attempt to model the retention factors for this new method for selectivity adjustment [110]. As expected, we demonstrate that the application of the Craig model can accurately generate simulations that illustrate the potential of gradient stationary phases for the control of chromatographic selectivity.

6.3. Validation of retention time and peak width for linear stationary phase gradients

The theoretical predictions for the retention time (equation 6.1) and peak width (equation 6.3) from the Gritti-Guiochon theory [111] were compared to our simulation results. The simulation and calculations were carried out assuming a small molecule with S = 10 and the following parameters: u_m = 0.5 cm/s, L = 15 cm, H = 10 μm, k_o = 0 (retention factor at the beginning of the gradient) and k_f = 2.4 (retention factor at the end of the gradient). The retention time from the simulation agreed to within 0.0038 % to the retention time from theory (t_R = 1.100 min). The

simulated peak width (σ = 0.0094162 min) was in also in good agreement with the Gritti and Guiochon theory, as corrected by Blumberg (σ = 0.0094163 min) [111,112].

6.4. Phase-optimized liquid chromatography (POPLC)

6.4.1. Experimental

A group of ten amphetamines was selected to characterize the performance of the gradient simulations. The structures, names, and abbreviations for these compounds are shown in Figure 6.1. Each of the amphetamine standards was purchased from Grace Discovery Sciences (Columbia, MD). The samples analyzed using LC were prepared at varying concentrations in order to reduce the magnitude of tailing and column overload. The isocratic data were collected on a system composed of a binary pump, an autosampler, a column thermostat, and a diode array detector (DAD) in an Agilent 1260 system (Agilent Technologies). The separations were carried out using a POPLC ProntoSil 100-3-C_{18} SH-2 column (80 x 4.6 mm, 3 µm) and a POPLC ProntoSil 100-3-Phenyl-2 column (80 x 4.6 mm, 3 µm) with 10 mM potassium phosphate buffer at pH 2.5 and acetonitrile. The Neue-Kuss parameters S_1, S_2 and k_w values were estimated using nonlinear least squares regression of the isocratic retention times obtained from the experimental data of each amphetamine on each column fit to equation 6.6. Common S_1 and S_2 values were determined by correcting the C_{18} column retention times by optimizing the ratio of the stationary phase volumes (equation 6.7). The retention of amphetamines under various isocratic and gradient conditions was simulated with these extracted parameters.

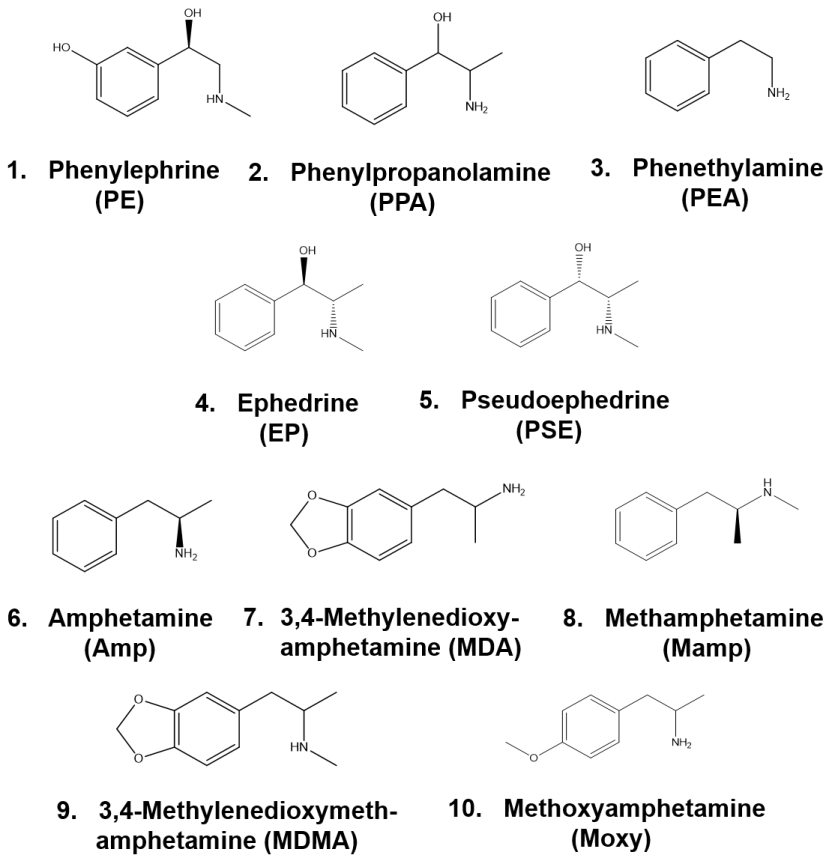

Figure 6.1. Structures and abbreviations for ten amphetamines

6.4.2. Simulation codes

All simulation codes were written in the Matlab program (Mathworks, Natick, MA) version R2016a. Non-linear regression to obtain the parameters necessary to implement simulations was accomplished using the function lsqnonlin found in the Matlab Optimization Toolbox.

6.4.3. Determination of Neue-Kuss Parameters

The Neue-Kuss (NK) parameters were calculated for each amphetamine from the experimental data. Initially, the NK parameters for each compound were calculated independently for each column. The S_1 values should be indicative of the mobile phase – analyte interactions, therefore it is expected that the S_1 and S_2 values would remain constant between the two columns as long as the mobile phase was the same. However, the S_1 values between the two columns differed by a significant amount. Although this observation was not surprising, due to the approximate nature of equation 6.6, one possible reason for this difference is differences in the stationary phase volumes due to the different stationary phase group sizes. Therefore, fits were carried out to achieve a common S_1 value. Also, the S_2 value represents the curved relationship of retention factor on organic composition and is expected to be common between two stationary phases. The retention times on the C_{18} column was corrected to match the same stationary phase volume of the phenyl column using the relationship shown by equation 6.7. The optimized common S_1 and S_2 values and k_w values of each column were then calculated and are shown in Table 6.1. The k_w values for each stationary phase were combined to give the k_w for the gradient stationary phase using the following equation:

$$k_{w,grad} = f_{C_{18}} k_{w,C_{18}} + f_{phen} k_{w,phen} \tag{6.8}$$

where f_{C18} and f_{phen} are the fractions of C_{18} and phenyl functional groups on the gradient column at a particular position, z, along the column, and $k_{w,C18}$ and $k_{w,phen}$ are the solute retention factors for a purely aqueous mobile phase on the individual corresponding stationary phase columns. The local retention factor (*i.e.*, at each position on the gradient column) for each solute was calculated using the fitted parameters shown in Table 6.1.

Table 6.1. Combined linear solvent-strength parameters for the amphetamine for C_{18} and phenyl based columns from fits to equation 6.7

Number	Amphetamine	S_1[a,b]	S_2[a,b]	$k_{w,phen}$[a]	$k_{w,C18}$[a]
1	PE	8.20 (1.1)	-0.147 (0.20)	1.55 (0.09)	1.9 (0.11)
2	PPA	15.9 (3.0)	1.36 (0.43)	4.07 (0.61)	6.6 (0.97)
3	PEA	20.4 (3.0)	2.02 (0.40)	6.11 (0.89)	9.9 (1.4)
4	EP	25.4 (3.9)	2.47 (0.45)	9.11 (1.6)	15.0 (2.6)
5	PSE	29.1 (4.3)	2.83 (0.48)	11.4 (2.1)	18.1 (3.4)
6	Amp	25.9 (4.0)	2.30 (0.47)	13.3 (2.4)	25.0 (4.5)
7	MDA	30.3 (4.4)	2.58 (0.48)	22.9 (4.4)	39.3 (7.6)
8	Mamp	25.2 (3.6)	2.11 (0.43)	17.9 (3.0)	33.2 (5.5)
9	MDMA	28.8 (4.3)	2.46 (0.46)	34.5 (6.5)	64.0 (12)
10	Moxy	30.8 (3.8)	2.34 (0.42)	29.1 (4.9)	48.3 (8.1)

[a]Standard errors of the parameters are given in parentheses. Conditions to fit to equation 6.6 were ϕ = 0.1 to 0.5 in 0.05 increments, t_M = 0.6302 min.

[b]Common S_1 and S_2 values were achieved using the following stationary phase volume ratio: $\frac{V_{phenyl}}{V_{C_{18}}} = 1.4$

6.4.4. Stationary phase gradient simulations

Simulations for the retention of ten amphetamines were performed on three types of stationary phase gradients with an isocratic mobile phase (ϕ = 0.10). The stationary phase gradient shapes used for the simulations are shown in Figure 6.2. The solid curve represents the relative concentration of the phenyl groups, and the dashed curve represents the relative concentration of the C_{18} groups on the stationary phase. Each of these gradients provides 50 % phenyl groups and 50 % C_{18} groups for the solutes to interact with. The resulting simulated chromatograms were identical regardless of the gradient shape. Also, reversing the order of the gradient (*i.e.*, reversing

the simulated flow direction) did not change the retention time or peak width. The invariance of the peak widths upon shift in flow direction was alluded to by Giddings as early as 1963 [114]. These results indicate that the retention of an analyte depends on the composition of stationary phase (*i.e.*, how many of each functional group the analyte is exposed to), not the shape or the direction of the stationary phase gradient. This finding of a lack of peak compression on a stationary phase gradient with isocratic mobile phase is contradictory to the conclusions of Gritti *et al.* [28]. These authors concluded that the use of a stationary phase gradient alone can improve the resolution, meaning the directionality of the gradient will affect peak width. A closer examination of their conclusions, as prompted by Blumberg [112], reveals that their conclusions were based on band widths, not peak widths. Bassanese *et al.* [115] recently reported a successful gradient modification of a commercial monolithic silica column and claimed that the column efficiency depended on the flow direction. This conclusion was solely based on one gradient column. In contrast, our investigation of reversing the column direction by simulation showed no change in the retention time or peak widths. However, even with lack of peak compression, a separation improvement is still possible using a stationary phase gradient by providing a variation in chromatographic selectivity.

The retention behavior of these compounds was further characterized using a set of nine different exponential stationary phase gradients (see for example Figure 6.2C), and the simulated chromatograms were compared to those obtained for the pure phenyl and pure C_{18} columns to determine the dependence of the chromatographic selectivity on the stationary phase composition. An exponential gradient shape was chosen because when controlled rate infusion is used to generate stationary phase gradients, the coupling of the functional groups is under kinetic

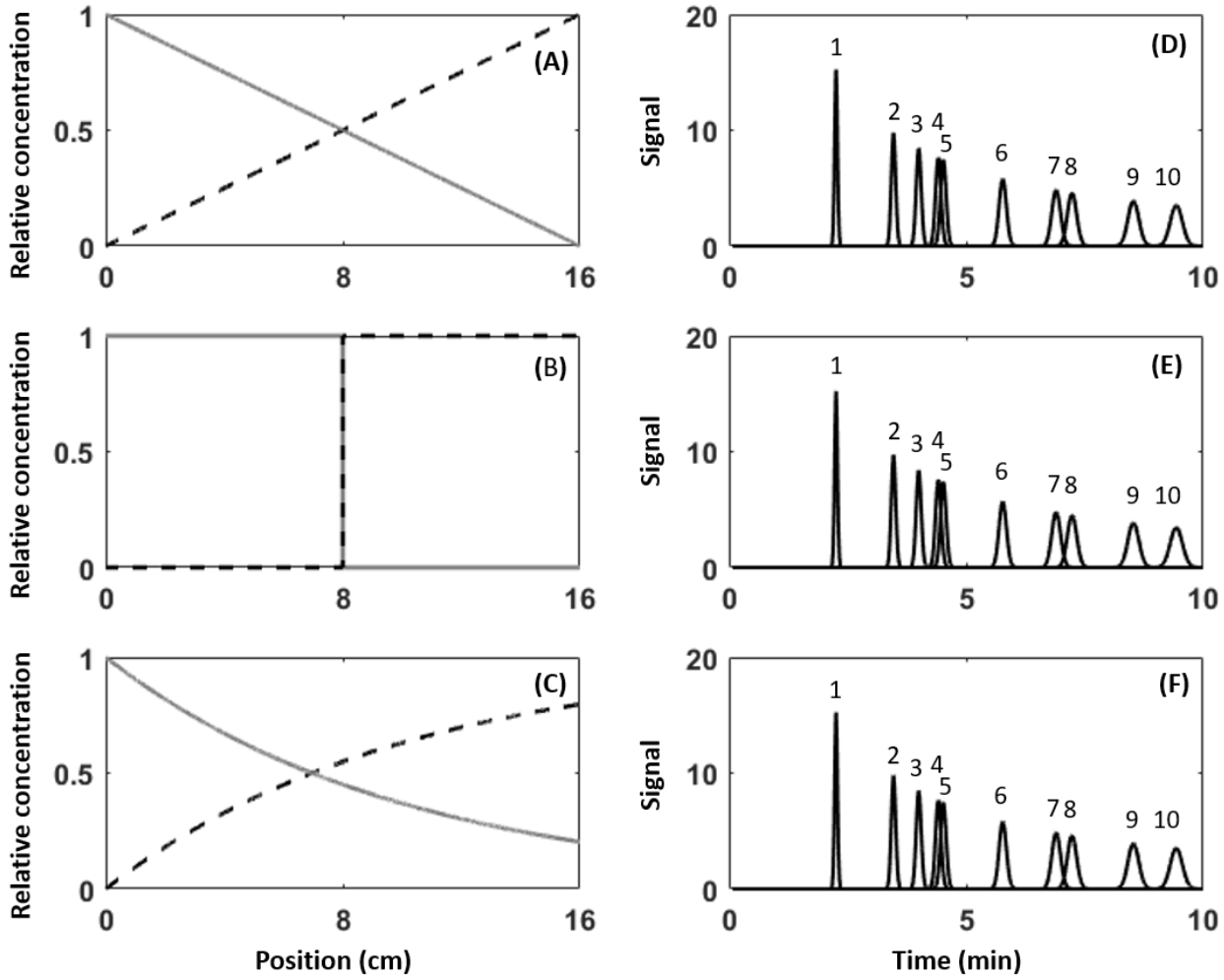

Figure 6.2. Relative concentration of phenyl (dashed curves) and C_{18} (solid curves) functional groups for simulated phenyl/C_{18} gradients: (A) linear gradient, (B) step gradient, and (C) exponential gradient. Resulting simulated chromatogram with isocratic mobile phase composition ($\phi = 0.1$) of each stationary phase gradient (D), (E), (F), respectively. Amphetamine elution order is as listed in Table 1.

control, such that in some cases, exponential gradient shapes are observed [96]. The overall gradient composition varied from 10 % to 90 % phenyl at 10 % increments. The exponential coefficient needed to achieve each target composition was calculated using the vpasolve function in the Symbolic Math Toolbox in Matlab. The determination of the effect of a stationary phase gradient on the chromatographic selectivity was performed by looking specifically at the four peaks, as shown in Figure 6.3. The retention times of PSE and MDA were affected to a lesser

degree than those of EP and Mamp with an increase in phenyl content in the stationary phase. This resulted in increased resolution of the first pair (EP and PSE) and decreased resolution of

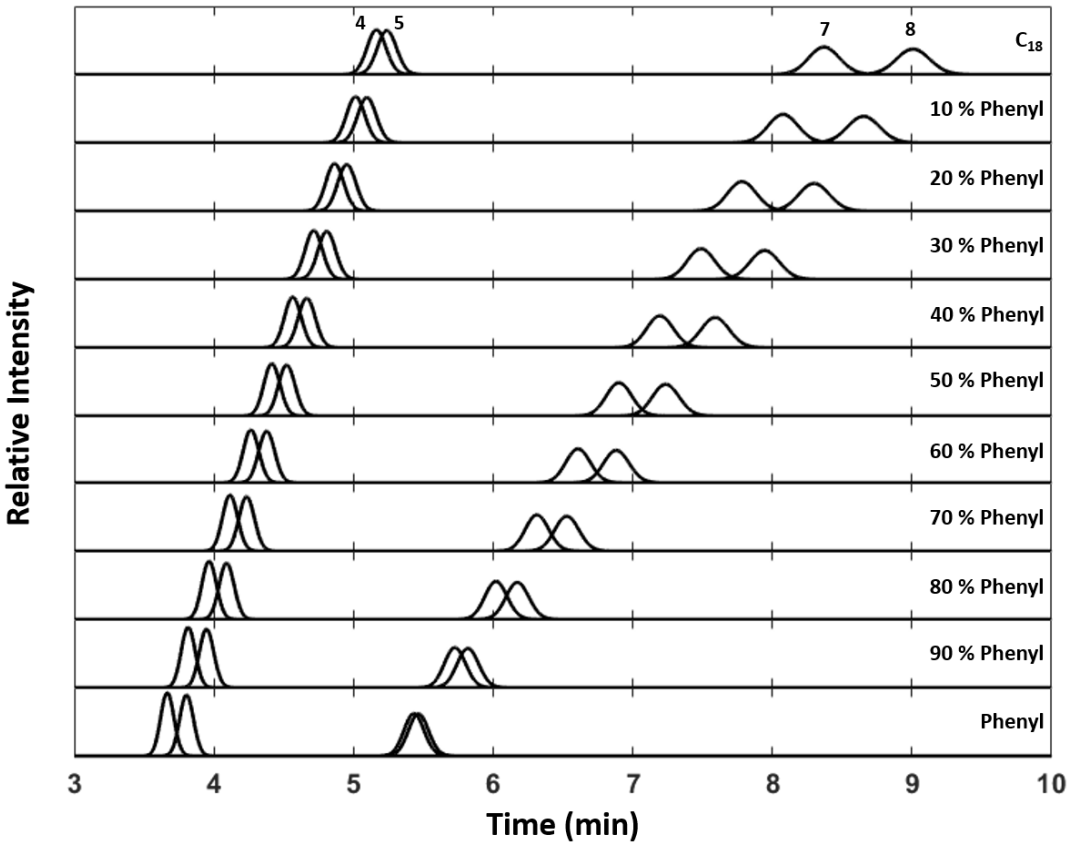

Figure 6.3. Simulation of four amphetamines: 4. EP, 5. PSE, 7. MDA and 8. Mamp on 11 different stationary phases with isocratic mobile phase composition ($\phi = 0.1$) with varying C_{18}/phenyl composition. The gradient columns were simulated to have exponential profiles.

the second peak pair (MDA and Mamp) as the proportion of phenyl groups on the column increased. Figure 6.3 clearly shows the benefit of using a mixed mode stationary phase over a single column chemistry, phenyl or C_{18}. The first peak pair (EP and PSE) is better separated on the phenyl column whereas the second peak pair (MDA and Mamp) is better separated on the C_{18} column. The use of traditional phenyl and C_{18} columns for separation of this mixture will require

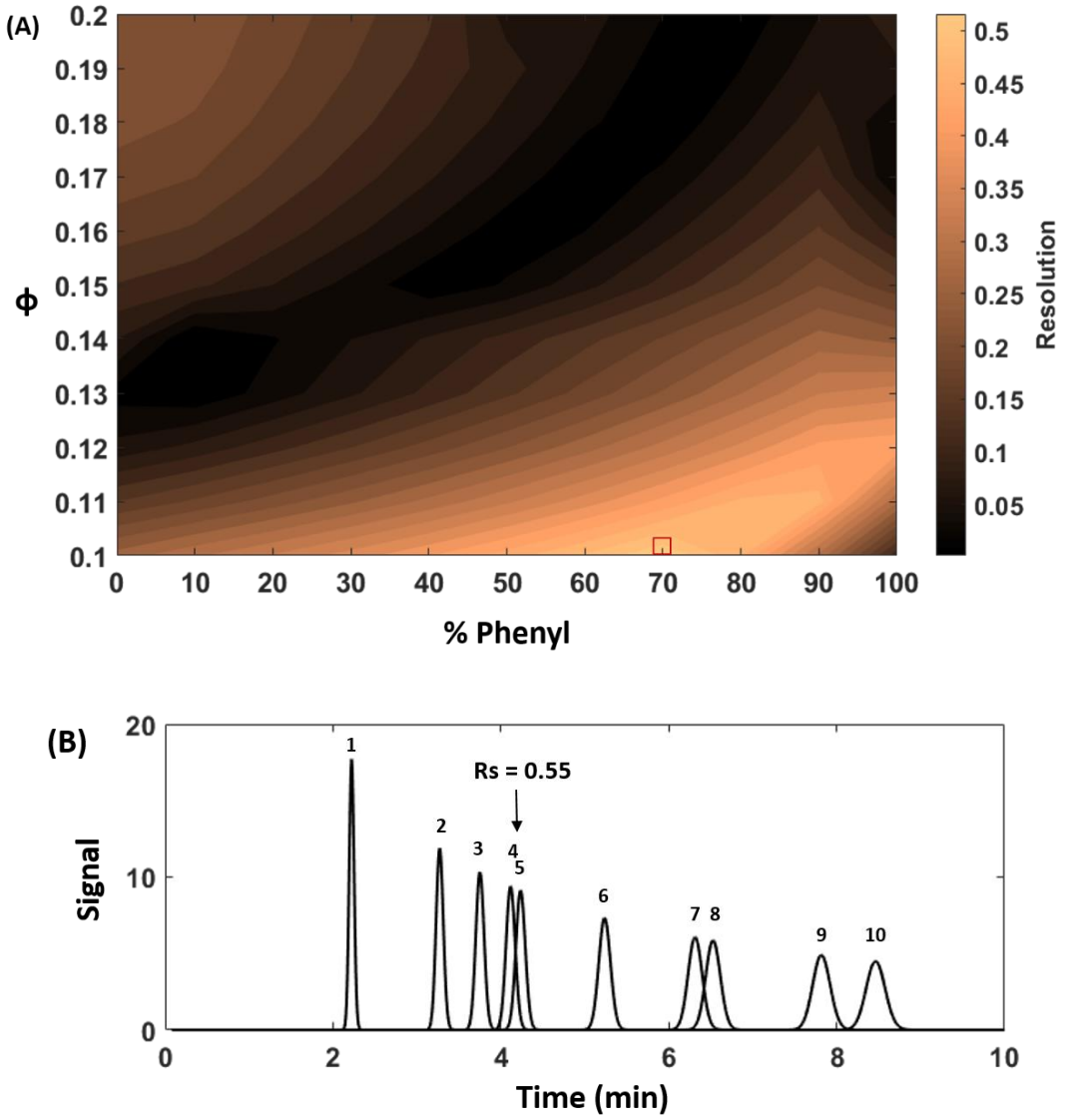

Figure 6.4. Predicted separation of ten amphetamines by varying stationary phase composition and ϕ. (A) Resolution map with optimum separation condition marked with a red square, (B) simulation using the optimum separation conditions 70 % phenyl gradient column and $\phi = 0.1$. The peak numbers correspond to the amphetamines shown in Figure 6.1. Resolution of the critical pair is marked with an arrow.

two serially connected columns. However, the use of a gradient column with approximately 70 % phenyl allows for a separation on a single column with resolution greater than 0.5 for all peaks.

It is evident that there must be an optimum condition for separation of these ten amphetamines. In order to investigate the effect of stationary phase and mobile phase composition on overall resolution, the retention of each compound for different combination of two parameters,

the stationary and mobile phase compositions, was calculated in Excel. Then the 'critical' pair (i.e., most overlapped peak pair) resolution values for each stationary phase and mobile phase composition combination were plotted to create the resolution map shown in Figure 6.4 to identify the conditions for maximum resolution.

6.4.5. Comparison of simulation to experimental data

The stationary phase gradient simulation program was validated against experimental data under isocratic and mobile phase gradient conditions. Retention predictions acquired by our simulation code were compared against the prediction from the POPLC optimization software and were shown to provide superior predictions for retention. The POPLC optimization software only takes a training set data for each column at the specific mobile phase condition to provide simply additive retention. On the other hand, our simulation program uses training set data collected for a range of mobile phase compositions and fits the NK parameters that best predict the retention time within this range. A comparison of the simulated and experimental chromatograms is given in Figure 6.5. Additionally, as shown in Table 6.2, the smallest percent difference for retention time achieved by POPLC optimization software (4.3 %) is approximately the largest percent difference achieved by our simulation code for an isocratic separation condition at $\phi = 0.2$.

Table 6.2. Experimental and simulated retention data for amphetamines separated under isocratic elution conditions[a]

Solute	$t_{R,exp}$ (min)	Simulation % difference[b]	POPLC software % difference[b]
PE	1.682	2.2	11.2
PPA	2.132	4.5	10.7
PEA	2.342	3.5	8.0
EP	2.390	3.3	7.9
PSE	2.384	3.1	7.4
Amp	2.750	2.3	6.9
MDA	2.958	1.0	5.1
Mamp	3.168	1.8	5.4
MDMA	3.365	1.5	4.3
Moxy	3.494	1.6	4.5

[a]The isocratic condition was 20 % ACN and injection volume was 5 µL.
A rectangular injection profile were used for simulations.
[b] $\% \text{ difference} = {(\text{sim} - \text{exp})}/{\text{exp}} * 100$

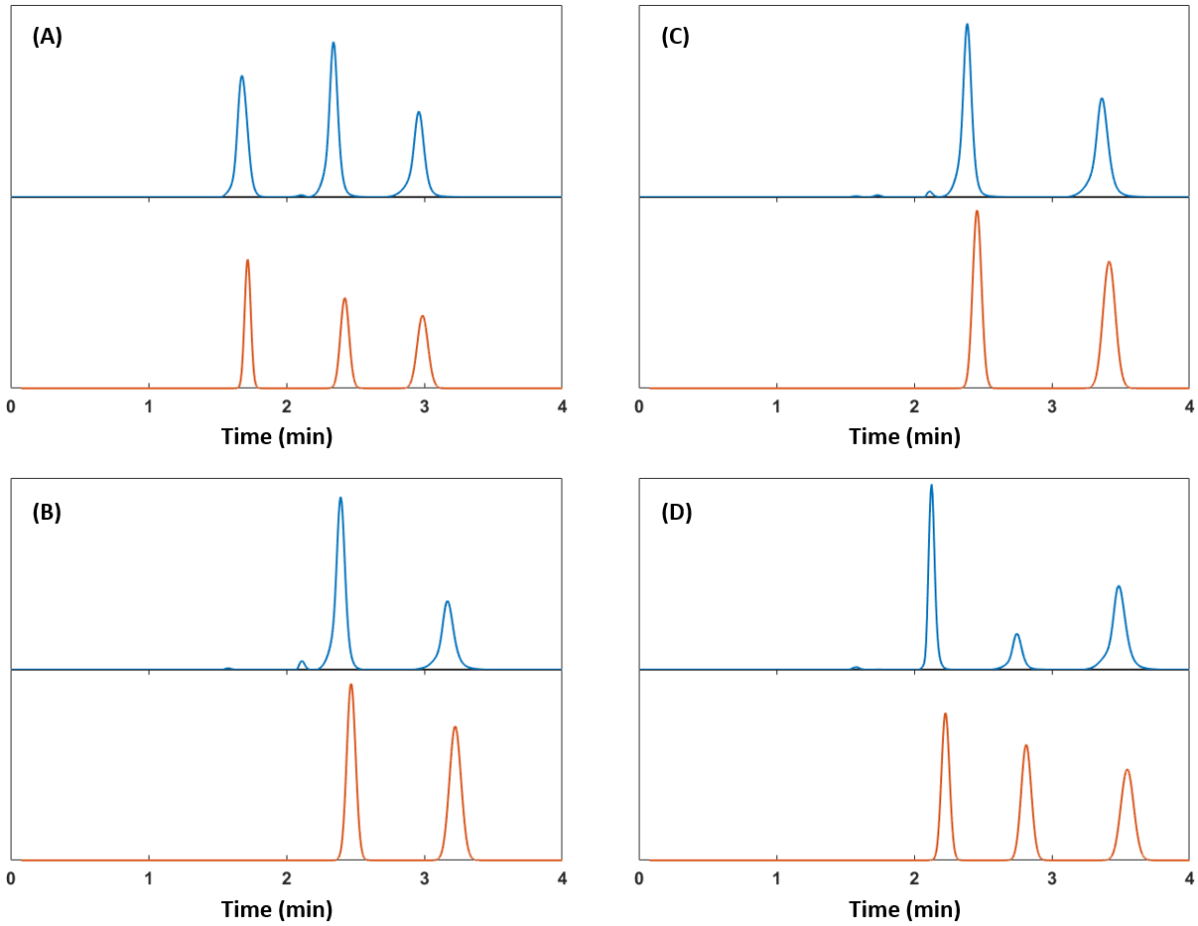

Figure 6.5. Comparison of experimental (blue) and simulated (orange) separations of (A) PE, PEA, and MDA; (B) EP and Mamp; (C) PSE and MDMA; and (D) PPA, Amp, and Moxy. Isocratic separation condition at ϕ = 0.2. Experimental signals relative intensity. The scale of the signal axis for the simulated chromatograms is arbitrary.

The SOSLC method has been adapted to provide retention predictions for mobile phase gradients [116], the current version of POPLC optimization software provided with the column kit does not contain this feature. The optimization software for combined gradients can be obtained from the Bischoff website [117]. This software only provides the most optimal combination of column segments under a given mobile phase gradient. Therefore, the specific combined gradient condition tested in this study could not be simulated with the optimization software for comparison. Also, the linear gradient prediction algorithm by De Beer *et al.* [116] uses discrete isocratic stages to represent a linear gradient. This discontinuous approach is only applicable for segmented stationary phase gradients. As shown in Chapter 4, our simulation program offers the flexibility to simulate variety of different conditions from simple linear mobile phase gradients to gradients with large injection volume and mismatching solvent. Our program can easily simulate a mobile phase gradient applied to a stationary phase gradient column with any shape. Figure 6.6 shows comparison of this combined gradient simulation with experimental data. The greatest retention time difference was only 4.2 %.

The peak width prediction with our simulation code was not as accurate as retention time prediction. Figure 6.5 and 6.6 shows the experimental peaks fronting overall. The use of rectangular injection profile which produces Gaussian peaks in our simulation are expected to have errors. However, even the use of experimental injection profile is not expected to completely resolve this issue. The fronting peaks are believed to be due to the nature of the POPLC connection with the PEEK cartridge segments. Even with careful handling, variation is introduced with every reassembly of the column configuration. In fact, every disassembly and reassembly resulted in significant difference in the measured t_M (data not shown here). These fronting effects were confirmed to be due to void volumes present in POPLC in a previous study [7]. In this study, Ortiz-

Bolsico *et al*. compared the connection of ACE columns with zero-dead-volume (ZDV) connectors to the column connectors used with the POPLC system and found that they could recreate the fronting peak shape obtained from the POPLC system by loosely connecting the ACE columns. Several other previous studies with the POPLC system have shown similar fronting peaks [118,119]. Discontinuous gradient assembly, which requires constant handling, causes inconsistencies between analysts and day-to-day analysis. Our lab, in collaboration with the Collinson lab, has been working on synthesizing continuous stationary phase gradients. Our simulation code can provide guidance for the selection of the stationary phase composition and shape along with insights into possible neighboring ligand effects that can arise from having multiple functionalities in close proximity to each other. In the next section, we explain the synthesis and characterization of continuous amine gradient column along with comparison of our simulation retention prediction to the experimental data.

Table 6.3. Experimental and simulated retention data for amphetamines separated under gradient elution conditions[a]

Solute	$t_{R,exp}$ (min)	Simulation % difference[b]
PE	2.200	2.7
PPA	3.304	4.0
PEA	3.807	3.2
EP	4.225	1.5
PSE	4.329	1.0
Amp	5.385	0.8
MDA	6.394	-2.1
Mamp	6.630	-1.0
MDMA	7.749	-4.1
Moxy	8.336	-4.2

[a]Gradient conditions: ϕ_o = 0.1 to ϕ_f = 0.15 over t_G = 10 min, the injection volume was 5 µL, and the stationary phase gradient had a step profile. A rectangular injection profile were used for simulations.

[b] $\% \text{ difference} = {(\text{sim} - \text{exp})}/{\text{exp}} * 100$

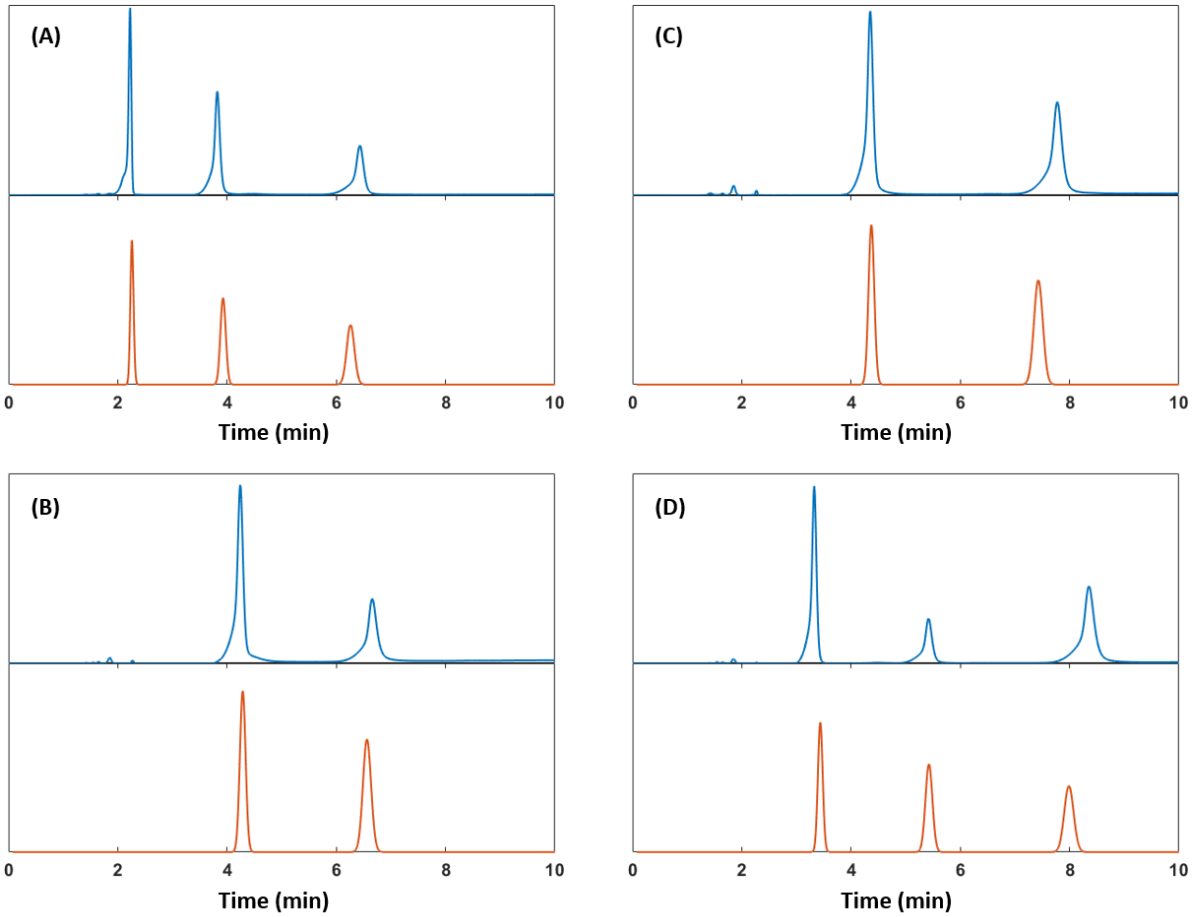

Figure 6.6. Comparison of experimental (blue) and simulated (orange) separations of (A) PE, PEA, and MDA; (B) EP and Mamp; (C) PSE and MDMA; and (D) PPA, Amp, and Moxy. Gradient separation condition: ϕ_o = 0.1 to ϕ_f = 0.15 over t_G = 10 min. Experimental signals are relative intensity. The scale of the signal axis for the simulated chromatograms is arbitrary.

6.5. In-house built continuous amine stationary phase gradients

Since additional connections must be made, serially connected columns such as POPLC have issues with excess void volume. These discontinuous gradients also do not allow for cooperative interactions to take place with strategically positioned functional groups on a surface with complementary functional groups on the analytes. Recently, a few reports of continuous

gradient stationary phases have appeared in the literature as a means to improve the selectivity of separations. The Collinson group has demonstrated the usefulness of continuous stationary phase gradients in thin layer chromatography (TLC) plates via separation of mixtures of acids and bases, over the counter drugs, water and fat-soluble vitamins, and metal ions [95–97]. Gradient stationary phases have also been prepared on polymeric capillary monoliths for electrochromatography [119–121]. These gradient stationary phases showed better performance and resolution of solutes compared to homogenously modified stationary phases. Bassanese *et al.* have recently reported the modification of a commercial silica monolithic column to form a gradient stationary phase, which they claimed gave different efficiencies, depending on the direction of the flow relative to the gradient direction [114]; however, this observation goes against well-established theory that peak compression should not occur on gradient stationary phases [111]. In this particular study, only one commercial column was modified, the results from the elemental characterization of the gradient profile were inconclusive, and no comparisons made to results obtained on uniformly modified columns. A peak parking method did give some indirect evidence of the presence of a gradient. Clearly, more in-depth studies with more replicates and controls need to be performed to confirm or deny the presence of this phenomenon and the usefulness of continuous gradient stationary phases in the field of chromatography.

We have recently reported a successful creation of continuous amine gradient on a monolithic silica column via controlled rate infusion (CRI) [109]. The amine gradient columns were carefully evaluated for their ability to alter analyte retention relative to a uniformly modified stationary phase. The presence of the amine and the gradient of its surface concentration changes along the length of the column were characterized using X-ray photoelectron spectroscopy (XPS). To demonstrate the application of these gradient stationary phases in the field of chromatography,

the stability, efficiency, and reproducibility associated with the separation of both nucleobases and weak acid/weak bases were established. Direct comparisons were made between the unmodified, uniformly modified, and gradient stationary phases, and the results demonstrate the promise that continuous gradient stationary phases have in separation science.

6.5.1. Experimental LC conditions

The synthesized monolithic column assembly was attached to an LC (HP1090, Hewlett Packard) via a reducing union. The analysis was done on three different types of columns: unmodified (bare silica columns), uniformly modified amine columns and amine gradient columns. Because the stationary phases consisted of silanol and amine functionalities, hydrophilic interaction liquid chromatography (HILIC) [122–126] was performed using 90 % ACN and 10 % aqueous buffer. For the separation of pyrimidine nucleobases consisting of uracil (40 µg/mL) and cytosine (200 µg/mL), an ammonium acetate buffer (10 mM; pH 3.64) was used. For the weak acid/weak base mixture consisting of benzoic acid, 3-aminobenzoic acid, 4-aminophenol and 2-aminopyridine (each at 20 µg/ mL), the buffer was ammonium formate (20 mM; pH 3.08). The separation of the nucleobases was carried out in duplicate at flow rates from 0.1 mL/ min to 1 mL/ min to produce van Deemter curves. The separation of the weak acid/weak base mixture was performed in duplicate at a constant flow rate of 0.5 mL/min. The dead volume was determined for each individual column using toluene as a marker. The flow rate used for dead volume determination was 0.5 mL/ min.

6.5.2. LC data analysis

Calculations of retention time and peak widths were performed using MATLAB version R2013a (Mathworks, Inc., Natick, MA). Data files were converted from Agilent .D files to MATLAB .mat files using ACD/Lab Spectrus Processor (Advanced Chemical Development, Inc., Toronto, Canada). The individual analyte signals were separated from each other and from the background [127] using an in-house program to perform multivariate-curve resolution-alternating least squares (MCR-ALS). Briefly, MCR-ALS extracts pure contributions from the instrumental data (*i.e.*, the pure chromatographic and spectral profiles of each analyte and the background) by taking advantage of the full spectral dimension in the data. For more information the reader is referred to a book chapter by Rutan, de Juan, and Tauler [128] and publications by Tauler *et al.* [129,130]. A MCR-ALS program with graphical user-friendly interface developed by Tauler *et al.* is available for download [131]. The pure chromatographic profiles of the analytes were then used for the calculation of retention time and peak width.

Since the obtained chromatographic peaks were not Gaussian (*i.e.*, they were asymmetric), the retention times were calculated using statistical moments calculation [132]. The first moments were used for determination of the retention factors, after correction of the extra column volume, V_{ext}. The precision of second and higher moments suffer from inconsistent determination of baseline. Therefore, the efficiency of each monolithic column (N_{sys}) was determined using the Foley-Dorsey equation, which is based on the properties of a well-accepted peak model known as the exponentially modified Gaussian (EMG) function [133]

$$N_{SYS} = \frac{41.7(t_R / w_{10})^2}{B / A + 1.25} \tag{6.11}$$

where w_{10} is the width at 10 % of the maximum, t_R is the retention time derived from the peak maximum, and B/A is the asymmetry factor at 10 % of peak maximum, where $B>A$. Finally, van Deemter plots were generated by plotting the plate height ($H = L/N_{SYS}$) versus linear velocity (u_m).

6.5.3. LC characterization

Two different mixtures were used to evaluate the chromatographic performance of the three different types of columns used in this work. One set of mixtures contained our first test compounds, uracil and cytosine, and the second set consisted of a mixture of four weak acids and bases, shown in Figure 6.7. Collectively, these mixtures will establish the stability, degree of

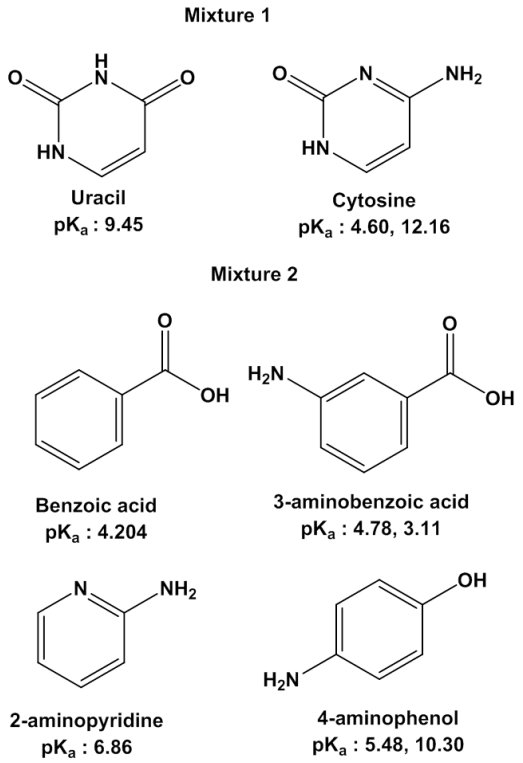

Figure 6.7. Structures and pKa's of analyzed compounds [134]

retention, column efficiency, and reproducibility of an amine gradient stationary phase for LC and provide a proof-of-principle demonstration of its promise in controlling analyte retention.

The first test mixture consisted of uracil and cytosine. HILIC conditions were employed for their separation due to the polar nature of these compounds, which show retention with both amine and silica functionalities under HILIC conditions. In this study, the mobile phase was acetonitrile: ammonium acetate buffer (10 mM; pH 3.64) (90:10 v/v). Chromatographic separations were carried out on multiple columns of each type: unmodified, uniformly modified and amine gradient. The reproducibility of column preparation was tested by carrying out separation at different times and on different days. A representative set of chromatograms for these two compounds on the three different monolithic columns is shown in Figure 6.8.

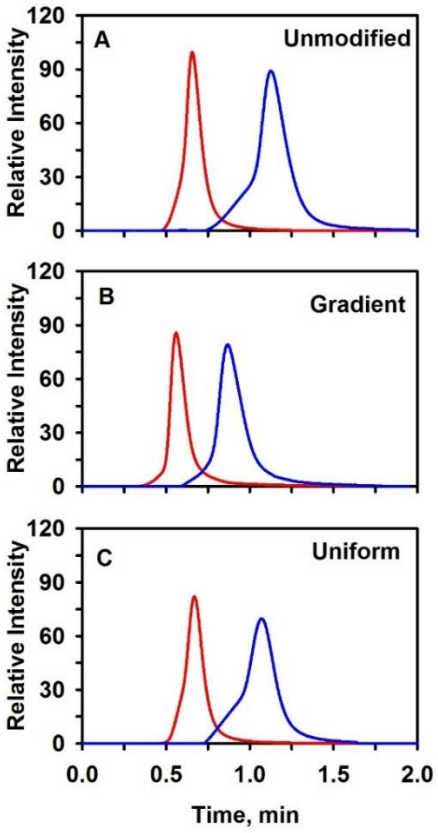

Figure 6.8. Stacked chromatograms of uracil (red) and cytosine (blue) standards on (A) unmodified, (B) gradient, and (C) uniformly modified monolithic columns. The chromatograms are normalized to represent a 5.8 cm column in each case.

Figure 6.8 A, B and C shows the chromatograms on unmodified, amine gradient and uniform columns, respectively. All three chromatograms for the three different columns showed the same pattern for elution of uracil and cytosine, which is in agreement with previous work using HILIC on commercial columns [135]. Both uracil and cytosine are weakly retained on these columns, and both compounds show distorted peak shapes, particularly fronting. The most likely explanation for this is small imperfections in the cladding that may result in non-uniform flow paths for the mobile phase and/or possible microscopic cracking of the monolithic bed.

From the chromatograms, retention times were measured and the retention factor for each of the nucleobases calculated. The chromatographic runs were undertaken on 11 amine gradient columns and 5 each of the unmodified and uniform monoliths. These values are shown in Figure 6.9. Standard deviations in the retention factors ranged from 0.06 to 0.16 for uracil and cytosine. No significant differences in retention on the three different columns were noted. The higher retention of cytosine on both the amine and silica phases as compared to uracil is consistent with literature reports using commercial columns [135,136].

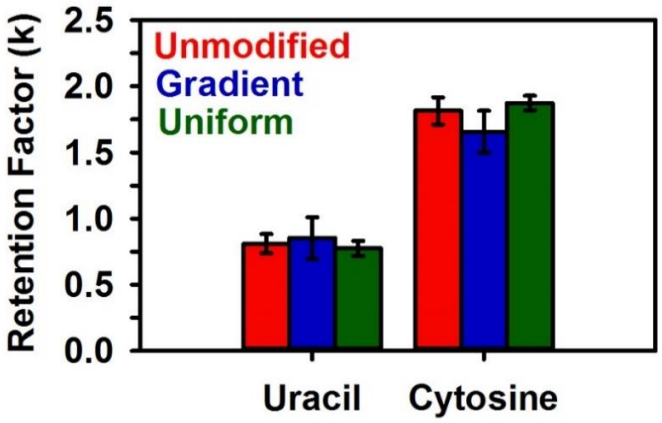

Figure 6.9. Retention factors for uracil and cytosine on unmodified ($n = 5$), gradient ($n = 11$), and uniformly modified monolithic columns ($n = 5$).

The efficiency of each column type (unmodified, uniformly amine modified and amine gradient monoliths) was determined using the uracil/cytosine mixture at a flow rate range from 0.1 mL/min to 1.0 mL/min (0.1 mL/min increments) in replicates. The retention time of each peak was calculated using the first central moment and the plate number (N_{SYS}) was calculated using the Foley-Dorsey equation (equation 6.12). The plate number was then converted to plate height, H, using each column length. The van Deemter plots for each column type were created by plotting H versus linear velocity, u_m, as shown in Figure 6.

Overall, the van Deemter plots are flat and have no significant differences between plate heights over the entire range of linear velocities studied or between the gradient, uniform, and unmodified monolithic columns. The relatively flat shapes of the van Deemter plots are reasonable based on previous literature reports [137,138]. The flatter van Deemter curves are thought to be due to reduced C term mass transfer, which may result from the presence of more through pores in monolithic columns that reduces the amount of stagnant mobile phase [139].

To evaluate whether peak compression influences the separation, we analyzed 3-aminobenzoic acid on an amine gradient column, reversing the column between runs. If peak compression occurs as a result of the stationary phase gradient, it is expected that the retention time and peak widths would show a difference when flow occurs from high amine to low amine concentration versus low to high amine concentration. No significant change in peak width was observed (p = 0.2). Differences in retention times (calculated by statistical moments) were found to be insignificant at a confidence level of 0.01, which was chosen due to the imperfect peak shapes as discussed in a previous section. Using replicates within and between different columns, the only observed differences can be attributed to errors introduced by the column fittings (data not shown). This agrees with Blumberg's assertion, based on Giddings' theory, that peak compression does not occur

in stationary phase gradients [111]; however, more thorough studies need to be performed in order to definitively determine the absence or presence of peak compression on stationary phase gradients.

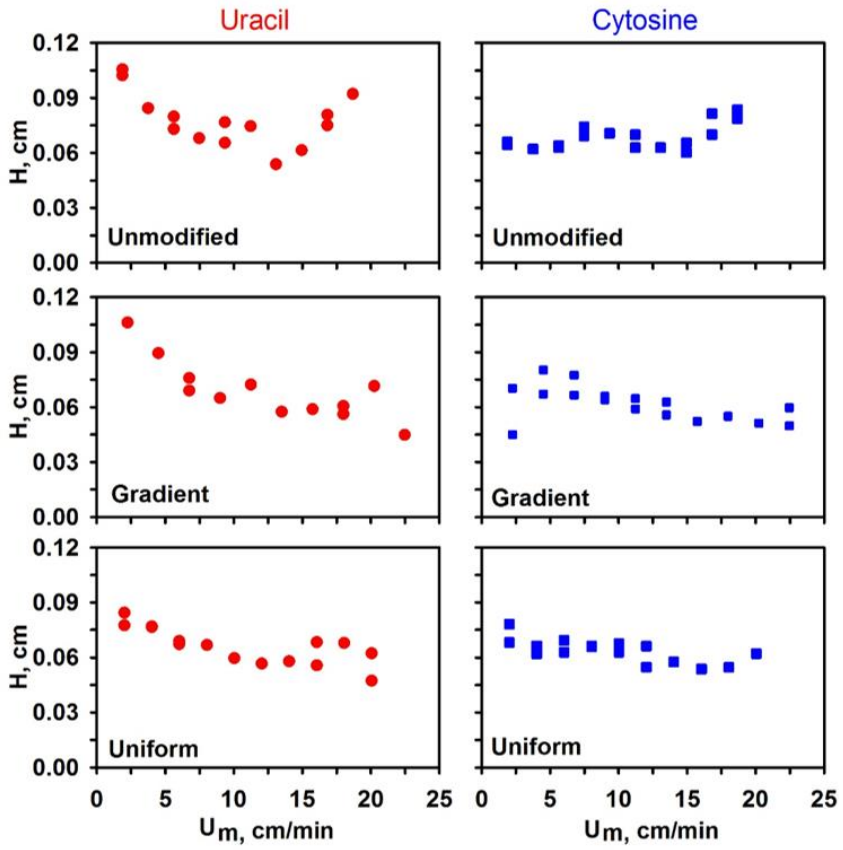

Figure 6.10. Van Deemter plots of uracil (blue circles) and cytosine (red squares) on unmodified, gradient and uniformly modified monolithic columns.

Given no significant difference in retention was noted for the uracil/cytosine mixture, a second mixture was studied. This mixture consists of four acids and bases, Figure 6.7 B, which is the same mixture that was used to demonstrate the advantages of a gradient amine stationary phase for planar chromatography in previous work [95]. In that work, on TLC plates ABA and BA

showed the strongest retention while 2-APy was least retained. The compound that was most sensitive to the modification of the TLC plate was 2-APy, where it was most retained on the unmodified plate. Complete separation was only achieved when the mixture was spotted on the low amine end of the gradient plate [95]. Figure 6.11 shows the stacked MCR-ALS resolved chromatograms of this mixture on unmodified, uniformly modified, and gradient monolithic columns. The time axis for uniform amine chromatogram was normalized to represent a 5.8 cm column for direct comparison to the other chromatograms. The mobile phase used was acetonitrile:ammonium formate buffer (20 mM; pH 3.08) 90:10 v/v.

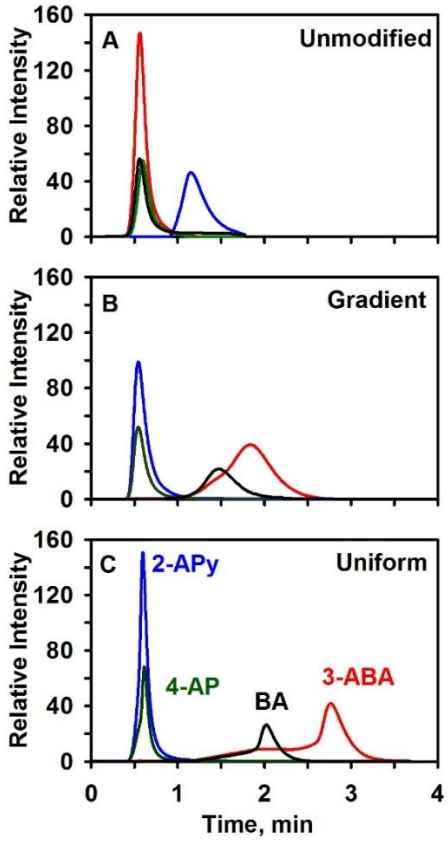

Figure 6.11. Stacked chromatograms resolved by MCR-ALS of 3-ABA (red), BA (black), 2-APy (blue) and 4-AP (green), on unmodified, gradient, and uniformly modified monolithic columns. The chromatograms are scaled to represent a 5.8 cm column in each case.

The chromatogram from the unmodified monolithic column in Figure 6.11 A shows two well separated peaks, with three of the four compounds (BA, 3-ABA and 4-AP) co-eluting. The most basic compound in this mixture, 2-APy, is partially retained due to interactions with the slightly acidic silanol groups. For the amine modified monolithic columns, Figure 6.11 B and C, however, the more acidic compounds (BA, 3-ABA) are retained presumably through hydrogen bonding interactions between the carboxyl and amine groups. Separation takes place between BA and 3-ABA while 4-AP and 2-APy co-elute. These results are consistent with that observed for TLC whereby 4-AP and 2-APy were not strongly retained on the amine modified stationary phases while BA and 3-ABA were. What is particularly noteworthy is that the retention of BA and 3-ABA, in particular, is different for the uniformly modified *vs.* the gradient stationary phase. The acids exhibit greater retention on the uniformly modified column compared to that on the gradient column, consistent with the greater amount of amine on its surface. On the unmodified monolithic columns, neither compound was retained. Both BA and 3-ABA have acidic functionalities that can interact with the amine groups on the stationary phase. The small differences in retention between these two compounds on the gradient *vs.* uniformly modified monolith are attributed to the amine group on ABA, which is not present in BA. It is possible that the basic amine group in ABA interacts with the acidic silanol groups resulting in slightly greater retention. The retention factors for these data are shown in Figure 6.12. The chromatographic studies were done for 10 amine gradient, 5 unmodified and 3 uniformly modified columns. The standard deviations associated with the retention factors ranged from 0.2 to 0.5 for the acidic compounds on the amine modified columns, but were below 0.2 for the basic compounds and for all the compounds on the unmodified column.

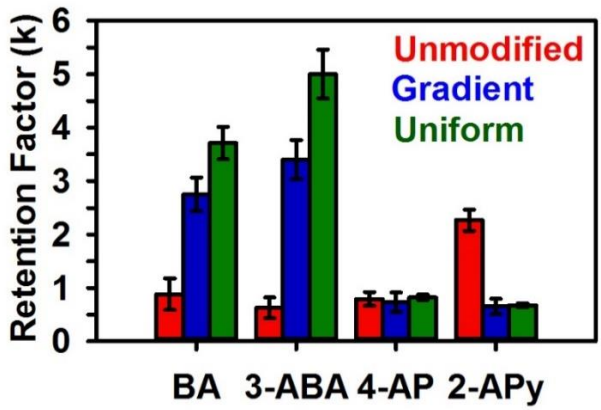

Figure 6.12. Retention factor for BA, 3-ABA, 4-AP and 2-APy on unmodified (n=5), gradient (n=10), and uniform (n=3).

6.5.4. Comparison of simulation to experimental data

We further compared the experimental data obtained for the gradient amine column to our simulation retention prediction results. The XPS data were used to estimate the amine fraction on the gradient column and these fractions were then used to simulate retention on an amine gradient column. The average N1s area for the amine gradient columns were compared to that of fully functionalized amine and bare silica columns. The amine gradient columns were estimated to have 65 % / 35 % of the characteristics of the fully functionalized amine column and bare silica column, respectively. This composition is denoted as 65 % amine and 35 % silica, from this point forward. The XPS data also indicated that the stationary phase gradient was linear along the length of the column, which dictated the shape of our simulated gradient. The retention factors of each compound were calculated from experimental retention factors measured on the bare silica and fully aminated monolithic columns using the following equation:

$$k_{\text{grad}} = f_{\text{silanol}} k_{\text{silanol}} + f_{\text{amine}} k_{\text{amine}} \tag{6.12}$$

These values were then used to calculate local retention factor for each compound on a gradient column with overall 65 % amine functionality. The simulation predictions for solute retentions on

a 5 cm length column with a 65 % amine gradient were compared to experimental results, and the differences are shown in Table 6.4.

As shown in Table 6.4, the simulation predictions were within the 95 % confidence interval of experimental retention data for most compounds. The simulation results fall outside of 95 % confidence intervals for 2-amino pyridine and cytosine. The simulated retention time for cytosine was slightly outside of the 95 % confidence interval; this result may be due to the fact all three types of columns (bare silica, fully aminated, and amine gradient) were found to provide cytosine with essentially the same retention. The greatest disagreement between experimental data and

Table 6.4. Experimental and simulated retention data for weak acids separated under gradient stationary phase and isocratic mobile phase elution conditions*

	Retention Time (min)		**Retention factor (*k*)**	
Solute	Experiment	Simulation	Experiment	Simulation
2-Amino pyridine	0.560 ± 0.030	0.758	0.655 ± 0.088	1.30
4-Amino phenol	0.589 ± 0.035	0.611	0.742 ± 0.103	0.807
Uracil	0.627 ± 0.028	0.610	0.854 ± 0.082	0.851
Cytosine	0.899 ± 0.030	0.958	1.66 ± 0.09	1.91
Benzoic acid	1.28 ± 0.06	1.25	2.77 ± 0.19	2.81
3-Amino benzoic acid	1.50 ± 0.08	1.50	3.42 ± 0.22	3.56

*The stationary phase gradient was estimated to be overall 65 % amine and 35 % silica. The mobile phase was 90 % acetonitrile mixed with acetate buffer (10 mM; pH 3.64) for uracil and cytosine; ammonium formate buffer (20 mM; pH 3.08) for weak acid/weak base mixture. The flow rate was 0.5 mL/min and the column length was 5 cm [110]. 95 % confidence intervals are shown.

simulation prediction was found for 2-aminopyridine, which had significant retention on bare silica columns (slightly acidic silanol groups) and minimal retention on the aminated columns. The experimental retention results on gradient amine columns suggest possibility of electrostatic repulsion between amine functional groups on the column and 2-aminopyridine which inhibits it from interacting with the negatively charged silanol groups. A limitation of our simulation code in the present form is that it does not incorporate any possible neighboring ligand effects between the

different functionalities and the solutes, which would result in retention prediction errors. However, this limitation can also aid in discovery of synergistic effects which result from the use of gradients in chemical functionalities. Any large discrepancies between the simulation predictions and the experimental data would indicate the presence of these interactions.

A resolution map as a function of percent amine functionality for the remaining compounds of mixture 2 (excluding 2-aminopyridine) is shown in Figure 6.13. As was observed in the experimental results, the best resolution was observed for the fully aminated column. Below 20 % amine concentration the resolution of all three compounds is not significantly different from zero. Despite the fact that a stationary phase gradient system did not show improved resolution in this case, these results demonstrate the feasibility of using stationary phase gradient simulations to predict the retention of compounds on lab-prepared gradient columns. Furthermore, this strategy can be used to aid in the design of future columns to ensure optimal separation conditions.

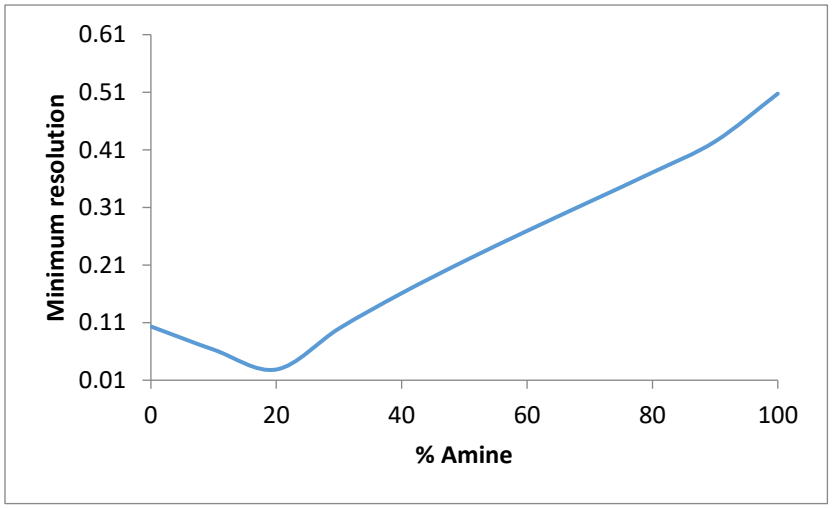

Figure 6.13. Resolution of critical pair for gradient columns with varying composition of amine calculated at 10 % increment of amine concentration at 90:10 ACN:ammonium acetate buffer (10 mM; pH 3.64).

6.6. Conclusion

In previous chapters, a general purpose simulation code was developed based on Craig model of chromatography which enabled simulation of gradient and isocratic conditions with solvent mismatch [53]. Here, an extension to this program was successfully developed to include simulation of linear and non-linear stationary phase gradients. The simulation code was validated by comparing the retention time and peak width results to closed form theory developed by Gritti and Guiochon [111]. Simulation of three different shaped gradients (linear, step, and exponential) with same C_{18}/phenyl composition resulted in identical chromatographic separations. The retention behavior of a solute depends on the total amount of each functional group it is exposed to and not the steepness or shape of the stationary phase gradient, in contrast to mobile phase gradients. Comparison of the chromatographic separation of ten amphetamines on eleven different C_{18}/phenyl gradients, ranging from 0 % to 100 % C_{18} composition clearly showed the advantage of a mixed mode stationary phase using a stationary phase gradient to tune the selectivity of the chromatographic separation. While it was determined that the shape of the gradient did not affect the selectivity or efficiency of the gradient, the controlled rate infusion method is a simple means for achieving such a mixed mode stationary phase.

The simulation code performance was tested through comparison of its retention prediction to experimental data of ten amphetamines on POPLC system consisting of C_{18} and phenyl functionalities. The retention time prediction errors for both isocratic and gradient elution were less than 5 % compared to the experimental data. The POPLC system produced fronting peaks which are attributed to introduction of additional void volume caused by difficult to control patented segmented PEEK connectors. Therefore, a greater difference was found for peak width prediction compared to experimental data. Despite these challenges with the POPLC system, our

simulation program displayed better retention prediction compared to the POPLC optimization software. Additionally, our simulator has the ability to simulate combined stationary phase and mobile phase gradients.

The simulator performance was also tested through comparison of its retention prediction to experimental data for six weak acids and bases on a gradient column with approximately 65 % coverage relative to a maximally aminated monolithic column and the retention of four of the six compounds were found to be in good agreement. In the case of 2-aminopyridine, the gradient experimental data suggested that the presence of electrostatic interactions between the protonated amine functionality and the analyte prevented access to the silanol groups. Any deviations between the results from the simulations and experimental data serve as evidence for neighboring ligand effects resulting from the use of a stationary phase gradient. Our group, in collaboration with the Collinson group [110] is currently investigating possible neighboring ligand effects of different functionalities on multi-component stationary phase gradient columns.

Chapter 7: Summary and Conclusions

As described in Chapter 1, a general purpose simulator was developed and improved with four goals in mind: (1) to support conventional LC method development with more flexibility and accuracy than currently available simulators; (2) to provide a better understanding of current problems faced in 2D-LC method development; (3) to automate and speed up simulation process; and (4) to support development of stationary phase gradient technology by providing a better understanding of how to tailor different separation selectivity. Chapters 4-6 have shown work completed towards achieving these goals.

7.1. Reflections on Chapter 4

The first and second goals were addressed in Chapter 4. A general purpose simulator was developed based on the Craig distribution model. According to Czok and Guiochon [32], the continuous chromatographic process can be discretized into distance and time segments, Δz and Δt, respectively. The retention factors for simulation are calculated at every position and time using linear (LSS) or non-linear (Neue-Kuss) solvent strength models. This allows for monitoring of mass propagation along the column. The simulation program was validated by comparison of the simulation results for five amphetamines under gradient elution to LSS theory calculations. The retention times and peak widths had good agreement with greatest difference of -0.019 % and -0.017 %, respectively. Two sets of training experiments were performed. The alkylbenzenes

were separated under isocratic conditions to extract Neue-Kuss model parameters for simulation. The amphetamines were separated under gradient conditions and LSS model parameters were extracted for simulation. It was found that training set for parameter extraction collected under gradient elution is ill-conditioned (*i.e.*, too many possible solutions) for Neue-Kuss model. The simulation results for alkylbenzenes and amphetamines under gradient elution were compared to experimental data. The retention time and peak width values were in reasonable agreement.

The simulation program capabilities were expanded by incorporation of a variety of different chromatographic conditions such as column temperature, large injection volume with sample solvent composition different from initial mobile phase condition, and the use of experimentally obtained injection profiles. These improvements were helpful in providing a better understanding of the effects of common separation conditions used in 2D-LC. It was found that the peak distortion and broadening resulting from large volume injection can be minimized when using a weaker sample solvent compared to the initial mobile phase condition. A weaker sample solvent encourages peak focusing and can provide increased sensitivity and resolution. This finding confirms current belief in 2D-LC method development.

The use of the Craig model involves calculating the retention factor at every position and time during the separation. Therefore, the simulation program not only yields retention time and peak width prediction, but also allows for monitoring of the analyte band and mobile phase composition during the chromatographic separation. This visualization ability offers better understanding of the chromatographic processes taking place inside the column, which is especially helpful for unusual separation conditions mentioned in Chapter 4. Although this is undoubtedly very powerful, the price we pay for obtaining this additional information is

computation time. A mathematical convolution approach to improve separation speed was explored in Chapter 5.

7.2. Reflections on Chapter 5

The third goal to accelerate the simulation program was addressed in Chapter 5. Due to the necessity of calculating the retention factor at each position and time, our simulation program can be slow. The convolution approach was applied to reduce the length of the column required for simulation. It was found that the analyte band stops developing its shape when the sample solvent band surpasses the analyte band. This distance was approximated using a set of closed form equations. The full simulation was performed for the first part of the column and the resulting peak was convolved with a known closed form solution for the remainder of the column length. Since the simulation program was validated and extensively evaluated in previous studies described in Chapter 4, the convolution prediction results were compared to full simulation results. The retention times and peak widths for full simulation *vs.* convolution were highly correlated. Since we made automation of the convolution approach possible by approximating simulation column length and time with closed form calculations, the correlation was worse when using experimental injection profile shapes. However, the retention time agreement was still within 5.5 %.

A comparison of the average computation time for each solute resulted in speed increase factors ranging from 2.2 to 13. Overall computation time for 854 simulations using convolution approach was almost eight times faster compared to performing full simulations. The decrease in computation time achieved by the convolution approach can provide a means to exhaustively search for the most optimal separation condition in a reasonable amount of time.

7.3. Reflections on Chapter 6

The fourth and final goal was addressed in Chapter 6. The simulation program was extended to simulate a non-constant stationary phase (*i.e.*, stationary phase gradient). The purpose of this development was to assist in the development of continuous stationary phase gradient columns by providing a better understanding of separation selectivity changes due to variation in the density of functional groups along the column length. The simulation program was evaluated using commercially available discontinuous stationary phase gradient known as POPLC. The Neue-Kuss simulation parameters were extracted for each column using isocratic training set data. It was found that the parameters S_1 and S_2 differed significantly for the two columns. This was believed to be due to the difference in stationary phase volumes. An approximate stationary phase volume ratio was determined (V_{phen}/V_{C18} = 1.4) and common S_1 and S_2 values were determined by correcting the C_{18} column retention times with this ratio. The comparison of our simulation results for isocratic and mobile phase gradient conditions resulted in retention time differences that were no greater than 4.5 %. This performance was superior to isocratic retention prediction results obtained from the optimization software included in POPLC kit which resulted in retention time differences of up to 11.2 %. Although SOSLC was performed for mobile phase gradient elution previously [116], the current POPLC optimization software does not provide this feature. Despite the good agreement of simulation retention times to experimental data, the severe fronting peak shapes in POPLC system cannot be simulated. This fronting is believed to be due to the extra column volume resulting from imperfect connections of the POPLC column assembly. The patented PEEK cartridge segments produced inconsistent retention data with every disassembly and reassembly. Because these discontinuous segmented stationary phase gradient systems have

these above-mentioned disadvantages, we have collaborated with the Collinson lab to develop continuous stationary phase gradients.

The Collinson lab was successful at reproducibly creating stable amine gradient columns using their controlled rate infusion method. These columns clearly showed a change in separation selectivity compared to bare silica and fully aminated columns. The gradient shape and composition was determined using XPS and was found to be approximately 65 % amine/ 35 % silica on average. Using this stationary phase composition, we were able to simulate the retention of six probe solutes. The simulation results were within the 95 % confidence interval of the experimental data for four out of six compounds studied. We believe that the disagreement displayed between simulation and experiments indicate possible neighboring ligand effect due to two functionalities located in close proximity to each other.

7.4. Future work

It is undeniable that the simulation program developed in this work has the potential to greatly impact the method development in LC. The simulation program is relatively simple to use following instructions provided in Appendix D of this dissertation. However, it may not be very intuitive for inexperienced scientists such as students. Therefore, future work should include the development of graphic user interface (GUI), which will display inputs and outputs in much user friendly way.

A proof-of-concept study was presented in developing continuous stationary phase gradient for change in separation selectivity [110]. Currently our lab, in collaboration with the Collinson lab, are working on the development of continuous stationary phase gradients on packed columns using CRI in a constructive way and a destructive way using acid to cleave the functional

groups. Both studies have shown promising results, and we believe our simulation program can help in determining possible neighboring ligand effects on these gradient columns.

Although there are several different types of liquid chromatography simulators available, we believe that our simulator provides more flexibility with capability to simulate chromatographic conditions current simulators cannot handle. The Stoll lab is currently working on incorporating the effect of injection of a much weaker solvent prior to sample injection. This is an extension of the effect of dilution study presented in Chapter 4. It is also desirable to obtain and incorporate distance and time dependent temperature profiles. This will allow us to simulate the effect of temperature-assisted on-column solute focusing [20–22], where temperature at the head of the column is controlled to achieve lower temperature upon sample injection to focus the analyte band. It will also provide visualization of the temperature effect on the analyte band as it travels through sections of the column with different temperatures. We believe that the possibilities for expansion of the simulation program are virtually limitless and its ability to calculate retention factor at every position and time makes modeling relatively easy to explore a variety of different separation conditions faced by chromatographers.

List of References

[1] HPLC Separation Modes, Waters. (2017). http://www.waters.com/waters/en_US/HPLC-Separation-Modes/nav.htm?cid=10049076&locale=en_US (accessed July 6, 2017).

[2] Y. Mao, Selectivity Optimization in Liquid Chromatography Using the Thermally Tuned Tandem Column (T3C) Concept, University of Minnesota, 2001.

[3] Chromatographic Selectivity, Sigma-Aldrich. (2017). http://www.sigmaaldrich.com/analytical-chromatography/hplc/learning-center/chromatographic-selectivity.html (accessed July 6, 2017).

[4] T.L. Chester, Recent Developments in High-Performance Liquid Chromatography Stationary Phases, Anal. Chem. 85 (2013) 579–589. doi:10.1021/ac303180y.

[5] J.J. Kirkland, J.J. DeStefano, T.J. Langlois, Fused Core Particles for HPLC Columns, J. Am. Lab. 39 (2007) 18–21.

[6] X.-T. Peng, Z. Li, Y. Zhang, T. Liu, Q.-W. Yu, Y.-Q. Feng, Study of Retention Mechanism of a Mixed-Mode Stationary Phase and Its Application for the Simultaneous Determination of Ten Water- and Fat-Soluble Vitamins by HPLC–UV, Chromatographia. 76 (2013) 735–745. doi:10.1007/s10337-013-2486-7.

[7] C. Ortiz-Bolsico, J.R. Torres-Lapasió, M.J. Ruiz-Ángel, M.C. García-Álvarez-Coque, Comparison of two serially coupled column systems and optimization software in isocratic liquid chromatography for resolving complex mixtures., J. Chromatogr. A. 1281 (2013) 94–105. doi:10.1016/j.chroma.2013.01.064.

[8] D.R. Stoll, X. Li, X. Wang, P.W. Carr, S.E.G. Porter, S.C. Rutan, Fast, comprehensive two-dimensional liquid chromatography., J. Chromatogr. A. 1168 (2007) 3–43. doi:10.1016/j.chroma.2007.08.054.

[9] J.M. Davis, D.R. Stoll, Likelihood of total resolution in liquid chromatography: Evaluation of one-dimensional, comprehensive two-dimensional, and selective comprehensive two-dimensional liquid chromatography, J. Chromatogr. A. 1360 (2014) 128–142. doi:10.1016/j.chroma.2014.07.066.

[10] R.E. Majors, Multidimensional High Performance Liquid Chromatography, J. Chromatogr. Sci. 18 (1980) 571–579. doi:10.1093/chromsci/18.10.571.

[11] D.R. Stoll, Recent advances in 2D-LC for bioanalysis., Bioanalysis. 7 (2015) 3125–3142. doi:10.4155/bio.15.223.

[12] D.R. Stoll, J.D. Cohen, P.W. Carr, Fast, comprehensive online two-dimensional high performance liquid chromatography through the use of high temperature ultra-fast gradient elution reversed-phase liquid chromatography, J. Chromatogr. A. 1122 (2006) 123–137. doi:10.1016/j.chroma.2006.04.058.

[13] G. Guiochon, L.A. Beaver, M.F. Gonnord, A.M. Siouffi, M. Zakaria, Theoretical investigation of the potentialities of the use of a multidimensional column in chromatography, J. Chromatogr. A. 255 (1983) 415–437. doi:10.1016/S0021-9673(01)88298-4.

[14] J.C. Giddings, Two-dimensional separations: concept and promise, Anal. Chem. 56 (1984) 1258A–1270A. doi:10.1021/ac00276a003.

[15] R.E. Murphy, M.R. Schure, J.P. Foley, Effect of Sampling Rate on Resolution in Comprehensive Two-Dimensional Liquid Chromatography, Anal. Chem. 70 (1998) 1585–1594. doi:10.1021/ac971184b.

[16] J. V Seeley, Theoretical study of incomplete sampling of the first dimension in comprehensive two-dimensional chromatography, J. Chromatogr. A. 962 (2002) 21–27. doi:10.1016/S0021-9673(02)00461-2.

[17] J.M. Davis, D.R. Stoll, P.W. Carr, Effect of First-Dimension Undersampling on Effective Peak Capacity in Comprehensive Two-Dimensional Separations, Anal. Chem. 80 (2008) 461–473. doi:10.1021/ac071504j.

[18] J.M. Davis, D.R. Stoll, P.W. Carr, Effect of First-Dimension Undersampling on Effective Peak Capacity in Comprehensive Two-Dimensional Separations, Anal. Chem. 80 (2008) 461–473. doi:10.1021/ac071504j.

[19] P.W. Carr, J.M. Davis, S.C. Rutan, D.R. Stoll, Principles of Online Comprehensive Multidimensional Liquid Chromatography, in: E. Grushka, N. Grinberg (Eds.), Adv. Chromatogr., CRC Press, 2012: pp. 140–235.

[20] S.R. Groskreutz, S.G. Weber, Temperature-assisted on-column solute focusing: A general method to reduce pre-column dispersion in capillary high performance liquid chromatography, J. Chromatogr. A. 1354 (2014) 65–74. doi:10.1016/j.chroma.2014.05.056.

[21] S.R. Groskreutz, A.R. Horner, S.G. Weber, Temperature-Based On-Column Solute Focusing in Capillary Liquid Chromatography Reduces Peak Broadening from Pre-Column Dispersion and Volume Overload when Used Alone or with Solvent-Based Focusing, J. Chromatogr. A. 1405 (2015) 133–139. doi:10.1016/j.chroma.2015.05.071.

[22] S.R. Groskreutz, S.G. Weber, Temperature-assisted solute focusing with sequential trap/release zones in isocratic and gradient capillary liquid chromatography: Simulation and experiment, J. Chromatogr. A. 1474 (2016) 95–108. doi:10.1016/j.chroma.2016.10.062.

[23] L.R. Snyder, J.J. Kirkland, J.L. Glajch, Practical HPLC Method Development, 2nd ed., Wiley Interscience, New York, 2012.

[24] J.W. Dolan, D.C. Lommen, L.R. Snyder, Drylab® computer simulation for high-performance liquid chromatographic method development : II. Gradient Elution, J. Chromatogr. A. 485 (1989) 91–112. doi:10.1016/S0021-9673(01)89134-2.

[25] I. Molnar, Computerized design of separation strategies by reversed-phase liquid chromatography: development of DryLab software, J. Chromatogr. A. 965 (2002) 175–194. doi:10.1016/S0021-9673(02)00731-8.

[26] A.P. Schellinger, Y. Mao, P.W. Carr, Use of DRYLAB to Compare Octadecylsilane and Carbon Supports for Reversed-Phase Chromatography of Triazine Herbicide Test Solutes, Anal. Bioanal. Chem. 373 (2002) 587–594. doi:10.1007/s00216-002-1355-2.

[27] ChromSword Off-line, (2016). http://www.chromsword.com/offline/ (accessed September 5, 2017).

[28] J.W. Dolan, L.R. Snyder, M.A. Quarry, Computer simulation as a means of developing an optimized reversed-phase gradient-elution separation, Chromatographia. 24 (1987) 261–276. doi:10.1007/BF02688488.

[29] J.E. Eble, R.L. Grob, P.E. Antle, L.R. Snyder, Simplified Description of High-Performance Liquid Chromatographic Separation Under Overload Conditions, Based on the Craig Distribution Model. I. Computer Simulations for a Single Elution Band Assuming a Langmuir Isotherm, J. Chromatogr. 384 (1987) 25–44. doi:10.1016/S0021-9673(01)94659-X.

[30] S. Fasoula, C. Zisi, H. Gika, A.. Pappa-Louisi, P. Nikitas, Retention Prediction and Separation Optimization under Multilinear Gradient Elution in Liquid Chromatography with Microsoft Excel Macros, J. Chromatogr. A. 1395 (2015) 109–115. doi:10.1016/j.chroma.2015.03.068.

[31] L. Wang, J. Zheng, X. Gong, R. Hartman, V. Antonucci, Efficient HPLC Method Development using Structure-Based Database Search, Physico-Chemical Prediction and Chromatographic Simulation, J. Pharm. Biomed. Anal. 104 (2015) 49–54. doi:10.1016/j.jpba.2014.10.032.

[32] M. Czok, G. Guiochon, The Physical Sense of Simulation Models of Liquid Chromatography: Propagation through a Grid or Solution of the Mass Balance Equation?, Anal. Chem. 62 (1990) 189–200. doi:10.1021/ac00201a020.

[33] K. Horváth, J.N. Fairchild, K. Kaczmarski, G. Guiochon, Martin-Synge Algorithm for the Solution of Equilibrium-Dispersive Model of Liquid Chromatography, J. Chromatogr. A. 1217 (2010) 8127–8135. doi:10.1016/j.chroma.2010.10.035.

[34] K. Kaczmarski, D. Antos, Modified Rouchon and Rouchon-Like Algorithms for Solving Different Models of Multicomponent Preparative Chromatography, J. Chromatogr. A. 756 (1996) 73–87. doi:10.1016/S0021-9673(96)00584-5.

[35] G.L. Frey, E. Grushka, Numerical Solution of the Complete Mass Balance Equation in Chromatography, Anal. Chem. 68 (1996) 2147–2154. doi:10.1021/ac960220o.

[36] A. Felinger, Critical Peak Resolution in Multicomponent Chromatograms, Anal. Chem. 69 (1997) 2976–2979. doi:10.1021/ac970241y.

[37] M.Z. El Fallah, G. Guiochon, Comparison of Experimental and Calculated Results in Overloaded Gradient Elution Chromatography for a Single-Component Band, Anal. Chem. 63 (1991) 859–867. doi:10.1021/ac00020a010.

[38] M.Z. El Fallah, G. Guiochon, Gradient Elution Chromatography at Very High Column Loading : Effect of the Deviation from the Langmuir Model on the Band Profile of a Single Component, Anal. Chem. 63 (1991) 2244–2252. doi:10.1021/ac00020a010.

[39] A. Felinger, G. Guiochon, Rapid Simulation of Chromatographic Band Profiles on Personal Computers, J. Chromatogr. A. 658 (1994) 511–515. doi:10.1016/0021-9673(94)80043-X.

[40] A.M. Katti, M. Czok, G. Guiochon, Prediction of Single and Binary Profiles in Overloaded Elution Chromatography using Various Semi-Ideal Models, J. Chromatogr. 556 (1991) 205–218. doi:10.1016/S0021-9673(01)96222-3.

[41] L.R. Snyder, J.W. Dolan, D.C. Lommen, Drylab Computer Simulation for High-Performance Liquid Chromatographic Method Development I. Isocratic Elution, J. Chromatogr. A. 485 (1989) 65–89. doi:10.1016/S0021-9673(01)89133-0.

[42] ACD/LC & GC Simulator—Model and Optimize LC and GC Separation Methods, (2015). http://www.acdlabs.com/products/com_iden/meth_dev/lc_sim/ (accessed September 6, 2017).

[43] K.P. Xiao, Y. Xiong, F.Z. Liu, A.M. Rustum, Efficient Method Development Strategy for Challenging Separation of Pharmaceutical Molecules using Advanced Chromatographic Technologies, J. Chromatogr. A. 1163 (2007) 145–156. doi:10.1016/j.chroma.2007.06.027.

[44] ACD/ChromGenius, (n.d.). http://www.acdlabs.com/products/com_iden/meth_dev/chromgen/techinfo.php (accessed September 6, 2017).

[45] L.R. Snyder, J.W. Dolan, High-Performance Gradient Elution: The Practical Application of the Linear-Solvent-Strength Model, Wiley, New York, 2006.

[46] L.M. Blumberg, Theory of Gradient Elution Liquid Chromatography with Linear Solvent Strength: Part 1. Migration and Elution Parameters of a Solute Band, Chromatographia. 77 (2013) 179–188. doi:10.1007/s10337-013-2555-y.

[47] T. Baczek, R. Kaliszan, Computer Assisted Optimization of Reversed-Phase HPLC Isocratic Separations of Neutral Compounds, LCGC Eur. (2001) 2–6.

[48] Z. Ma, G. Guiochon, Application of Orthogonal Collocation on Finite Elements in the Simulation of Non-Linear Chromatography, Comput. Chem. Eng. 15 (1991) 415–426. doi:10.1016/0098-1354(91)87019-6.

[49] G. Guiochon, A. Felinger, D.G. Shirazi, A.M. Katti, Single-Component Profiles with the Equilibrium Dispersive Model, in: Fundam. Prep. Nonlinear Chromatogr., 2nd ed., Elsevier B.V., Amsterdam, 2006: pp. 471–529.

[50] W. Hao, B. Di, B. Yue, Q. Chen, S. Wu, P. Zhang, Equivalence Between the Equilibrium Dispersive and the Transport Model in Describing Band Broadening in Analytical Gradient Liquid Chromatography, J. Chromatogr. A. 1369 (2014) 191–195. doi:10.1016/j.chroma.2014.10.015.

[51] J.E. Eble, R.L. Grob, P.E. Antle, L.R. Snyder, Simplified Description of High-Performance Liquid Chromatographic Separation Under Overload Conditions, Based on the Craig Distribution Model. II. Effect of Isotherm Type and Experimental Verification of Computer Simulations for a Single Band, J. Chromatogr. 384 (1987) 45–79. doi:10.1016/S0021-9673(01)94660-6.

[52] J.E. Eble, R.L. Grob, P.E. Antle, L.R. Snyder, Simplified Description of High-Performance Liquid Chromatographic Separation Under Overload Conditions, Based on

the Craig Distribution Model. III. Computer Simulations for Two Co-eluting Bands Assuming a Langmuir Isotherm., J. Chromatogr. 405 (1987) 1–29. doi:10.1016/S0021-9673(01)81745-3.

[53] L.N. Jeong, R. Sajulga, S.G. Forte, D.R. Stoll, S.C. Rutan, Simulation of elution profiles in liquid chromatography - I: Gradient elution conditions, and with mismatched injection and mobile phase solvents, J. Chromatogr. A. 1457 (2016) 41–49. doi:10.1016/j.chroma.2016.06.016.

[54] L.N. Jeong, R. Sajulga, S.G. Forte, D.R. Stoll, S.C. Rutan, Erratum to "Simulation of elution profiles in liquid chromatography—I: Gradient elution conditions, and with mismatched injection and mobile phases solvents'' [J. Chromatogr. A 1457 (2016) 41–49], J. Chromatogr. A. 1478 (2016) 84. doi:10.1016/j.chroma.2016.11.025.

[55] L.N. Jeong, S.G. Forte, S.C. Rutan, Simulation of elution profiles in liquid chromatography - III: Stationary phase gradients, J. Chromatogr. A., in preparation.

[56] D.R. Stoll, R.W. Sajulga, B.N. Voigt, E.J. Larson, L.N. Jeong, S.C. Rutan, Simulation of elution profiles in liquid chromatography − II: Investigation of injection volume overload under gradient elution conditions applied to second dimension separations in two-dimensional liquid chromatography, J. Chromatogr. A. (2017). doi:10.1016/j.chroma.2017.07.041.

[57] G. Vivó-Truyols, S. van der Wal, P.J. Schoenmakers, Comprehensive Study on the Optimization of Online Two-Dimensional Liquid Chromatographic Systems Considering Losses in Theoretical Peak Capacity in First- and Second-Dimensions: A Pareto-Optimality Approach, Anal. Chem. 82 (2010) 8525–8536. doi:10.1021/ac101420f.

[58] D.R. Stoll, K. O'Neill, D.C. Harmes, Effects of pH Mismatch Between the Two Dimensions of Reversed-Phase×Reversed-Phase Two-Dimensional Separations on Second Dimension Separation Quality for Ionogenic Compounds—I. Carboxylic acids, J. Chromatogr. A. 1383 (2015) 25–34. doi:10.1016/j.chroma.2014.12.054.

[59] P.J. Schoenmakers, G. Vivó-Truyols, W.M.C. Decrop, A protocol for designing comprehensive two-dimensional liquid chromatography separation systems., J. Chromatogr. A. 1120 (2006) 282–90. doi:10.1016/j.chroma.2005.11.039.

[60] M. Czok, G. Guiochon, The physical sense of simulation models of liquid chromatography: propagation through a grid or solution of the mass balance equation, Anal. Chem. 62 (1990) 189–200. doi:10.1021/ac00201a020.

[61] A.P. Schellinger, P.W. Carr, A Practical Approach to Transferring Linear Gradient Elution Methods, J. Chromatogr. A. 1077 (2005) 110–119. doi:10.1016/j.chroma.2005.04.088.

[62] P.J. Schoenmakers, H.A.H. Billiet, R. Tijssen, L. De Galan, Gradient Selection in Reversed-Phase Chromatography, J. Chromatogr. 149 (1978) 519–537. doi:10.1016/S0021-9673(00)81008-0.

[63] L.M. Blumberg, Theory of Gradient Elution Liquid Chromatography with Linear Solvent Strength: Part 2. Peak Width Formation, Chromatographia. 77 (2013) 189–197. doi:10.1007/s10337-013-2556-x.

[64] U.D. Neue, H.-J. Kuss, Improved reversed-phase gradient retention modeling., J. Chromatogr. A. 1217 (2010) 3794–803. doi:10.1016/j.chroma.2010.04.023.

[65] A. Vaast, E. Tyteca, G. Desmet, P.J. Schoenmakers, S. Eeltink, Gradient-elution parameters in capillary liquid chromatography for high-speed separations of peptides and intact proteins., J. Chromatogr. A. 1355 (2014) 149–57. doi:10.1016/j.chroma.2014.06.010.

[66] A. Vaast, E. Tyteca, G. Desmet, P.J. Schoenmakers, S. Eeltink, Corrigendum to "Gradient-Elution Parameters in Capillary Liquid Chromatography for High-Speed Separations of Peptides and Intact Proteins," J. Chromatogr. A. 1355 (2014) 149–157. doi:10.1016/j.chroma.2014.06.010.

[67] T. Raglione, S.A. Tomellini, T.R. Floyd, N. Sagliano, R.A. Hartwick, Zone Compression Effects in High-Performance Liquid Chromatography, J. Chromatogr. 367 (1986) 293–300. doi:10.1016/S0021-9673(00)94850-7.

[68] S. Keunchkarian, M. Reta, L. Romero, C. Castells, Effect of Sample Solvent on the Chromatographic Peak Shape of Analytes Eluted under Reversed-Phase Liquid Chromatogaphic Conditions, J. Chromatogr. A. 1119 (2006) 20–8. doi:10.1016/j.chroma.2006.02.006.

[69] C.B. Castells, R.C. Castells, Peak Distortion in Reversed-Phase Liquid Chromatography as a Consequence of Viscosity Differences Between Sample Solvent and Mobile Phase, J. Chromatogr. A. 805 (1998) 55–61. doi:10.1016/S0021-9673(98)00042-9.

[70] P. Jandera, T. Hájek, P. Česla, Effects of the gradient profile, sample volume and solvent on the separation in very fast gradients, with special attention to the second-dimension gradient in comprehensive two-dimensional liquid chromatography, J. Chromatogr. A. 1218 (2011) 1995–2006. doi:10.1016/j.chroma.2010.10.095.

[71] B.J. Vanmiddlesworth, J.G. Dorsey, Quantifying injection solvent effects in reversed-phase liquid chromatography, J. Chromatogr. A. 1236 (2012) 77–89. doi:10.1016/j.chroma.2012.02.075.

[72] N.E. Hoffman, S.-L. Pan, A.M. Rustum, Injection of Eluites in Solvents Stronger than the Mobile Phase in Reversed-Phase Liquid Chromatography, J. Chromatogr. 465 (1989) 189–200. doi:10.1016/S0021-9673(01)92657-3.

[73] N.E. Hoffman, A. Rahman, Computation of Band Shape for Strong Injection Solvent and Weak Mobile Phase Combinations in Liquid Chromatography, J. Chromatogr. 473 (1989) 260–266. doi:10.1016/S0021-9673(00)91307-4.

[74] P.G. Stevenson, D.N. Bassanese, X.A. Conlan, N.W. Barnett, Improving peak shapes with counter gradients in two-dimensional high performance liquid chromatography, J. Chromatogr. A. 1337 (2014) 147–154. doi:10.1016/j.chroma.2014.02.051.

[75] D.R. Stoll, E.S. Talus, D.C. Harmes, K. Zhang, Evaluation of detection sensitivity in comprehensive two-dimensional liquid chromatography separations of an active pharmaceutical ingredient and its degradants, Anal. Bioanal. Chem. 407 (2015) 265–277. doi:10.1007/s00216-014-8036-9.

[76] J. Layne, T. Farcas, I. Rustamov, F. Ahmed, Volume-Load Capacity in Fast-Gradient Liquid Chromatography: Effect of sample solvent composition and injection volume on chromatographic performance, J. Chromatogr. A. 913 (2001) 233–242. doi:10.1016/S0021-9673(00)01199-7.

[77] Achieving Accuracy and Precision with Rheodyne Manual Sample Injectors, (1983).

[78] J. Zhang, Y. Liu, A. Jaquins-Gerstl, Z. Shu, A.C. Michael, S.G. Weber, Optimization for speed and sensitivity in capillary high performance liquid chromatography. The importance of column diameter in online monitoring of serotonin by microdialysis, J. Chromatogr. A. 1251 (2012) 54–62. doi:10.1016/j.chroma.2012.06.002.

[79] D. Guillarme, S. Heinisch, J.L. Rocca, Effect of temperature in reversed phase liquid chromatography, J. Chromatogr. A. 1052 (2004) 39–51. doi:10.1016/j.chroma.2004.08.052.

[80] J. Billen, K. Broeckhoven, A. Liekens, K. Choikhet, G. Rozing, G. Desmet, Influence of pressure and temperature on the physico-chemical properties of mobile phase mixtures commonly used in high-performance liquid chromatography, J. Chromatogr. A. 1210 (2008) 30–44. doi:10.1016/j.chroma.2008.09.056.

[81] T. Seki, J. Mochida, M. Okamoto, O. Hosoya, K. Juni, K. Morimoto, Measurement of Diffusion Coefficients of Parabens and Steroids in Water and 1-Octanol, Chem. Pharm. Bull. (Tokyo). 51 (2003) 734–736. doi:10.1248/cpb.51.734.

[82] K. Nishida, Y. Ando, H. Kawamura, Diffusion coefficients of anticancer drugs and compounds having a similar structure at 30 °C, Colloid Polym. Sci. 261 (1983) 70–73. doi:10.1007/BF01411520.

[83] L.N. Jeong, D.R. Stoll, P.W. Carr, S.C. Rutan, Simulation of elution profiles in liquid chromatography - IV: Convolution approach to accelerate simulation, J. Chromatogr. A., in preparation.

[84] L.R. Snyder, J.W. Dolan, J.R. Gant, Gradient elution in high-performance liquid chromatography, J. Chromatogr. A. 165 (1979) 3–30. doi:10.1016/S0021-9673(00)85726-X.

[85] E.S. Parente, D.B. Wetlaufer, Relationship between isocratic and gradient retention times in the high-performance ion-exchange chromatography of proteins, J. Chromatogr. 355 (1986) 29–40. doi:10.1016/S0021-9673(01)97301-7.

[86] L.R. Snyder, Principles of gradient elution, Chromatogr. Rev. 7 (1965) 1–51. doi:10.1016/0009-5907(65)80002-3.

[87] L.R. Snyder, D.L. Saunders, Optimized Solvent Programming for Separations of Complex Samples by Liquid-Solid Adsorption Chromatography in Columns, J. Chromatogr. Sci. 7 (1969) 195–208. doi:10.1093/chromsci/7.4.195.

[88] H. Poppe, J. Paanakker, M. Bronckhorst, Peak width in solvent-programmed chromatography, J. Chromatogr. A. 204 (1981) 77–84. doi:10.1016/S0021-9673(00)81641-6.

[89] J. De Vos, G. Desmet, S. Eeltink, A generic approach to post-column refocusing in liquid chromatography, J. Chromatogr. A. 1360 (2014) 164–171. doi:10.1016/j.chroma.2014.07.072.

[90] J. De Vos, S. Eeltink, G. Desmet, Peak refocusing using subsequent retentive trapping and strong eluent remobilization in liquid chromatography: A theoretical optimization study, J. Chromatogr. A. 1381 (2015) 74–86. doi:10.1016/j.chroma.2014.12.082.

[91] S.R. Groskreutz, S.G. Weber, Quantitative evaluation of models for solvent-based, on-column focusing in liquid chromatography, J. Chromatogr. A. 1409 (2015) 116–124. doi:10.1016/j.chroma.2015.07.038.

[92] E.W. Weisstein, Convolution, MathWorld. (2017). http://mathworld.wolfram.com/Convolution.html (accessed April 10, 2017).

[93] H. Sklenářová, P. Chocholouš, P. Koblová, L. Zahálka, D. Šatínský, L. Matysová, P. Solich, High-resolution monolithic columns - A new tool for effective and quick separation, Anal. Bioanal. Chem. 405 (2013) 2255–2263. doi:10.1007/s00216-012-6561-y.

[94] I. Ali, Z.A. Al-Othman, M. Al-Za'abi, Superficially porous particles columns for super fast HPLC separations, Biomed. Chromatogr. 26 (2012) 1001–1008. doi:10.1002/bmc.2690.

[95] C.A. Doyle, T.J. Vickers, C.K. Mann, J.G. Dorsey, Characterization of liquid chromatographic stationary phases by Raman spectroscopy Effect of ligand type, J. Chromatogr. A. 779 (1997) 91–112. doi:10.1016/S0021-9673(97)00404-4.

[96] B. Kannan, M.A. Marin, K. Shrestha, D.A. Higgins, M.M. Collinson, Continuous stationary phase gradients for planar chromatographic media, J. Chromatogr. A. 1218 (2011) 9406–9413. doi:10.1016/j.chroma.2011.10.075.

[97] V.C. Dewoolkar, B. Kannan, K.M. Ashraf, D.A. Higgins, M.M. Collinson, Amine-phenyl multi-component gradient stationary phases, J. Chromatogr. A. 1410 (2015) 190–199. doi:doi:10.1016/j.chroma.2015.07.089.

[98] S.L. Stegall, K.M. Ashraf, J.R. Moye, D.A. Higgins, M.M. Collinson, Separation of transition and heavy metals using stationary phase gradients and thin layer chromatography, J. Chromatogr. A. 1446 (2016) 141–148. doi:10.1016/j.chroma.2016.04.005.

[99] N.E. Hoffman, S.-L. Pan, A.M. Rustum, Injection of eluites in solvents stronger than the mobile phase in reversed-phase liquid chromatography, J. Chromatogr. A. 465 (1989) 189–200. doi:10.1016/S0021-9673(01)92657-3.

[100] N.E. Huffman, A. Rahman, Computation of band shape for strong injection solvent and weak mobile phase combinations in liquid chromatography, J. Chromatogr. A. 473 (1989) 260–266. doi:10.1016/S0021-9673(00)91307-4.

[101] D.W. Cook, S.C. Rutan, D.R. Stoll, P.W. Carr, Two dimensional assisted liquid chromatography – a chemometric approach to improve accuracy and precision of quantitation in liquid chromatography using 2D separation, dual detectors, and multivariate curve resolution, Anal. Chim. Acta. 859 (2015) 87–95. doi:10.1016/j.aca.2014.12.009.

[102] R.C. Allen, M.G. John, S.C. Rutan, M.R. Filgueira, P.W. Carr, Effect of background correction on peak detection and quantification in online comprehensive two-dimensional liquid chromatography using diode array detection, J. Chromatogr. A. 1254 (2012) 51–61. doi:10.1016/j.chroma.2012.07.034.

[103] S. Nyiredy, Z. Szucs, L. Szepesy, Stationary-Phase Optimized Selectivity LC (SOS-LC): Separation Examples, Chromatographia. 63 (2006) S3–S9. doi:10.1365/s10337-006-0833-7.

[104] S. Nyiredy, Z. Szucs, L. Szepesy, Stationary phase optimized selectivity liquid chromatography: Basic possibilities of serially connected columns using the "PRISMA" principle., J. Chromatogr. A. 1157 (2007) 122–30. doi:10.1016/j.chroma.2007.04.041.

[105] Bischoff Chromatography, Phase Optimized Liquid Chromatography - POPLC, (n.d.). http://poplc.de/index_en.html (accessed July 9, 2016).

[106] K. Chen, F. Lynen, M. De Beer, L. Hitzel, P. Ferguson, M. Hanna-Brown, P. Sandra, Selectivity optimization in green chromatography by gradient stationary phase optimized selectivity liquid chromatography., J. Chromatogr. A. 1217 (2010) 7222–30. doi:10.1016/j.chroma.2010.09.029.

[107] K. Chen, F. Lynen, R. Szucs, M. Hanna-Brown, P. Sandra, Gradient stationary phase optimized selectivity liquid chromatography with conventional columns, Analyst. 138 (2013) 2914. doi:10.1039/c3an36797e.

[108] S. Thürmann, D. Belder, Phase-optimized chip-based liquid chromatography, Anal. Bioanal. Chem. 406 (2014) 6599–6606. doi:10.1007/s00216-014-8087-y.

[109] T. Alvarez-Segura, J.R. Torres-Lapasió, C. Ortiz-Bolsico, M.C. García-Alvarez-Coque, Stationary phase modulation in liquid chromatography through the serial coupling of columns: A review, Anal. Chim. Acta. 923 (2016) 1–23. doi:10.1016/j.aca.2016.03.040.

[110] V.C. Dewoolkar, L.N. Jeong, D.W. Cook, K.M. Ashraf, S.C. Rutan, M.M. Collinson, Amine Gradient Stationary Phases on In-House Built Monolithic Columns for Liquid Chromatography, Anal. Chem. 88 (2016) 5941–5949. doi:10.1021/acs.analchem.6b00895.

[111] F. Gritti, G. Guiochon, Band broadening along gradient reversed phase columns: a potential gain in resolution factor., J. Chromatogr. A. 1342 (2014) 24–9. doi:10.1016/j.chroma.2014.03.025.

[112] L.M. Blumberg, Velocity gradients in static chromatography always broaden the peaks., J. Chromatogr. A. 1373 (2014) 216–219. doi:10.1016/j.chroma.2014.11.011.

[113] F. Gritti, G. Guiochon, Response to "Velocity gradients in static chromatography always broaden the peaks," J. Chromatogr. A. 1373 (2014) 220–221. doi:10.1016/j.chroma.2014.11.012.

[114] J.C. Giddings, Plate Height of Nonuniform Chromatographic Columns: Gas Compression Effects, Coupled Column, and Analogous Systems, Anal. Chem. 35 (1963) 353–356. doi:10.1021/ac60196a026.

[115] D.N. Bassanese, A. Soliven, X.A. Conlan, R.A. Shalliker, N.W. Barnett, P.G. Stevenson, A non-destructive test to assess the axial heterogeneity of in situ modified monoliths for HPLC, Anal. Methods. 7 (2015) 7177–7185. doi:10.1039/C4AY02812K.

[116] M. De Beer, F. Lynen, K. Chen, P. Ferguson, M. Hanna-Brown, P. Sandra, Stationary-Phase Optimized Selectivity Liquid Chromatography: Development of a Linear Gradient Prediction Algorithm, Anal. Chem. 82 (2010) 1733–1743. doi:10.1021/ac902287v.

[117] Bischoff Chromatography, LG POPLC® Optimizer Software, (2010). http://www.poplc.de/lgpoplcoptimizer_en.html (accessed August 21, 2017).

[118] M. Kuehnle, J. Rehbein, K. Holtin, B. Dietrich, M. Gradl, H. Yeman, K. Albert, Phase optimized liquid chromatography as an instrument for steroid analysis, J. Sep. Sci. 31 (2008) 1655–1661. doi:10.1002/jssc.200700604.

[119] J. Lu, M. Ji, R. Ludewig, G.K.E. Scriba, D. Chen, Application of phase optimized liquid chromatography to oligopeptide separations, J. Pharm. Biomed. Anal. 51 (2010) 764–767. doi:10.1016/j.jpba.2009.09.036.

[120] S. Currivan, D. Connolly, E. Gillespie, B. Paull, Fabrication and characterisation of capillary polymeric monoliths incorporating continuous stationary phase gradients, J. Sep. Sci. 33 (2010) 484–492. doi:10.1002/jssc.200900720.

[121] V. Pucci, M.A. Raggi, F. Svec, J.M.J. Fréchet, Monolithic columns with a gradient of functionalities prepared via photoinitiated grafting for separations using capillary electrochromatography, J. Sep. Sci. 27 (2004) 779–788. doi:10.1002/jssc.200401828.

[122] A. Maruška, A. Rocco, O. Kornyšova, S. Fanali, Synthesis and evaluation of polymeric continuous bed (monolithic) reversed-phase gradient stationary phases for capillary liquid chromatography and capillary electrochromatography, J. Biochem. Biophys. Methods. 70 (2007) 47–55. doi:10.1016/j.jbbm.2006.10.011.

[123] P. Jandera, Stationary and mobile phases in hydrophilic interaction chromatography: a review, Anal. Chim. Acta. 692 (2011) 1–25. doi:10.1016/j.aca.2011.02.047.

[124] P. Hemström, K. Irgum, Hydrophilic interaction chromatography, J. Sep. Sci. 29 (2006) 1784–1821. doi:10.1002/jssc.200600199.

[125] Y. Guo, S. Gaiki, Retention and selectivity of stationary phases for hydrophilic interaction chromatography, J. Chromatogr. A. 1218 (2011) 5920–5938. doi:10.1016/j.chroma.2011.06.052.

[126] Y. Guo, Recent progress in the fundamental understanding of hydrophilic interaction chromatography (HILIC), Analyst. 140 (2015) 6452–6466. doi:10.1039/C5AN00670H.

[127] B. Buszewski, S. Noga, Hydrophilic interaction liquid chromatography (HILIC)—a powerful separation technique, Anal. Bioanal. Chem. 402 (2012) 231–247. doi:10.1007/s00216-011-5308-5.

[128] E. Bezemer, S.C. Rutan, Analysis of three- and four-way data using multivariate curve resolution-alternating least squares with global multi-way kinetic fitting, Chemom. Intell. Lab. Syst. 81 (2006) 82–93. doi:10.1016/j.chemolab.2005.10.005.

[129] S.C. Rutan, A. de Juan, R. Tauler, Introduction to Multivariate Curve Resolution, Elsevier, 2009. doi:10.1016/B978-044452701-1.00046-6.

[130] R. Tauler, D. Barceló, Multivariate curve resolution applied to liquid chromatography—diode array detection, TrAC Trends Anal. Chem. 12 (1993) 319–327. doi:10.1016/0165-9936(93)88015-W.

[131] A. de Juan, J. Jaumot, R. Tauler, Multivariate Curve Resolution (MCR). Solving the mixture analysis problem, Anal. Methods. 6 (2014) 4964–4976. doi:10.1039/C4AY00571F.

[132] R. Tauler, A. de Juan, J. Jaumot, Multivariate Curve Resolution, (2017). http://www.mcrals.info/ (accessed August 13, 2017).

[133] C.F. Poole, The Essence of Chromatography, 1st ed., Elsevier Science, 2003.

[134] J.P. Foley, J.G. Dorsey, Equations for calculation of chromatographic figures of merit for ideal and skewed peaks, Anal. Chem. 55 (1983) 730–737. doi:10.1021/ac00255a033.

[135] W.M. Haynes, T.J. Bruno, D.R. Lide, Handbook of Chemistry and Physics, Internet v, CRC Press, Boca Raton, Florida, 2015.

[136] Y. Guo, S. Gaiki, Retention and selectivity of stationary phases for hydrophilic interaction chromatography, J. Chromatogr. A. 1218 (2011) 5920–5938. doi:10.1016/j.chroma.2011.06.052.

[137] B.A. Olsen, Hydrophilic interaction chromatography using amino and silica columns for the determination of polar pharmaceuticals and impurities, J. Chromatogr. A. 913 (2001) 113–122. doi:10.1016/S0021-9673(00)01063-3.

[138] Q.C. Wang, F. Svec, J.M.J. Frechet, Macroporous polymeric stationary-phase rod as continuous separation medium for reversed-phase chromatography, Anal. Chem. 65 (1993) 2243–2248. doi:10.1021/ac00065a013.

[139] R. Wu, L. Hu, F. Wang, M. Ye, H. Zou, Recent development of monolithic stationary phases with emphasis on microscale chromatographic separation, J. Chromatogr. A. 1184 (2008) 369–392. doi:10.1016/j.chroma.2007.09.022.

[140] N. Ishizuka, H. Kobayashi, H. Minakuchi, K. Nakanishi, K. Hirao, K. Hosoya, T. Ikegami, N. Tanaka, Monolithic silica columns for high-efficiency separations by high-performance liquid chromatography, J. Chromatogr. A. 960 (2002) 85–96. doi:10.1016/S0021-9673(01)01580-1.

[141] L.M. Blumberg, T.A. Berger, Variance of a Zone Migrating in a Non-Uniform Time-Invariant Linear Medium, J. Chromatogr. A. 596 (1992) 1–13. doi:10.1016/0021-9673(92)80197-3.

[142] L.M. Blumberg, Variance of a zone migrating in a linear medium. II. Time-varying non-uniform medium, J. Chromatogr. A. 637 (1993) 119–128. doi:10.1016/0021-9673(93)83204-6.

APPENDIX A

Derivation of Craig model for time and distant dependent retention factors

According to Blumberg [141,142], the change in total mass of an analyte in a non-uniform medium (i.e., a gradient) along the time domain can be expressed as the following differential equation with the analyte velocity and its dispersion both as functions of position

$$\frac{\partial m}{\partial t} = \frac{\partial^2}{\partial z^2}\left(Dm\right) - \frac{\partial}{\partial z}\left(u_a m\right) \tag{A1}$$

where m is the mass of analyte per unit length, t is time, z is distance, D is diffusivity and u_a is the analyte velocity. With the assumption of no diffusion, the equation is simplified to

$$\frac{\partial m}{\partial t} + \frac{\partial}{\partial z}\left(u_a m\right) = 0 \tag{A2}$$

where $u_a = u_m/(1+k)$. The mobile phase velocity, u_m, is assumed to be constant and is not included in the differential.

$$\frac{\partial m}{\partial t} + u_m \frac{\partial}{\partial z}\left(\frac{m}{1+k}\right) = 0 \tag{A3}$$

Because the retention factor remains in the differential, the effect of the change in analyte velocity along the column length is captured in this approach. The two differential terms are substituted with the following finite difference equations

$$\frac{\partial m}{\partial t} = \frac{m_{z,t} - m_{z,t-1}}{\Delta t} \tag{A4}$$

$$\frac{\partial m}{\partial z} = \frac{m_{z,t-1} - m_{z-1,t-1}}{\Delta z} \tag{A5}$$

Solving for $m_{z,t}$ by letting $u_m = \Delta z/\Delta t$ (uniform mobile phase velocity) and using retention factors specific for each time and position results in

$$m_{z,t} = m_{z,t-1}\left(\frac{k_{z,t-1}}{1+k_{z,t-1}}\right) + m_{z-1,t-1}\left(\frac{1}{1+k_{z-1,t-1}}\right) \tag{A6}$$

This equation differs from that provided by Czok and Guiochon

$$m_{z,t} = m_{z,t-1}\left(\frac{k_{z,t-1}}{1+k_{z,t}}\right) + m_{z-1,t-1}\left(\frac{1}{1+k_{z,t}}\right) \tag{A7}$$

We believe this is because they did not account for the distance dependence of the analyte velocity in equation A2. While Czok and Guiochon's formulation gave reasonable accuracy for peak retention times and widths, mass balance was not conserved with their formulation, and peak areas were incorrect, which caused us to investigate equation A7 in more detail, and to find the correct formulation, as represented by equation A6. Equation A6 gives accurate peak areas for all conditions tested by us to date.

In the model used here, the time vector at $z = L$ (from the time/space matrix) is taken as the time-based chromatogram, in the sense that each element of this vector at a given z,t coordinate contains the mass of analyte that passes to the detector. However, from a physical point of view, the only analyte mass that can pass to the detector (m_d) is the mass in the mobile phase (m_m) – this is inconsistent with the fact that the model does not explicitly differentiate between the mass in the mobile and stationary phases (*i.e.*, see the two components on the right-hand side of equation A6). Thus, the fraction of mass that is actually in the mobile phase at any time point in the chromatogram, $m_{L,t}$, must be calculated to produce a chromatogram with accurate peak heights and areas. These ideas are expressed by equation A8, where we recognize that the total mass at any

$m_{L,t}$ is the sum of masses in the mobile (m_m) and stationary (m_s) phases (and that $m_d = m_m$), and recognize that m_s is the product of m_m and the retention factor at elution (k_e).

$$m_{L,t} = m_m + m_s = m_d + k_e m_d = m_d(1 + k_e) \tag{A8}$$

$$m_d = \frac{m_{L,t}}{1 + k_e} \tag{A9}$$

APPENDIX B

Derivation of the closed form expressions for sample solvent mismatch conditions

B.1. Retention time calculation

The retention prediction for linear gradient mobile phase condition under ideal injection conditions using closed form expressions has been shown previously in section 3.3. This can be extended to non-ideal injection conditions where the sample solvent and initial mobile phase composition are mismatched. In the presence of solvent mismatch, there are three contributions to retention: (1) the time it takes for half of the injection band to be loaded on to the column; (2) the elution time for the analyte band while it is eluting in the sample solvent; and (3) the elution time for the analyte band under linear mobile phase gradient conditions.

$$t_R = t_{R,1} + t_{R,2} + t_{R,3} \tag{B1}$$

A derivation for each contribution is shown in detail below, and the different zone widths are illustrated in Figure B.1.

First, the injection time is given by:

$$t_{inj} = \frac{V_{inj}}{F} \tag{B2}$$

and the sample solvent injection band width is given by:

$$z_{inj} = u_m t_{inj} \tag{B3}$$

where u_m is the mobile phase velocity.

The first contribution to the retention time, t_{R1}, is equal to half the injection time or the time it takes for the midpoint of the band to reach the head of the column.

$$t_{R,1} = \frac{t_{inj}}{2} = \frac{z_{inj}}{2u_m} \tag{B4}$$

The width of the analyte band after injection has been completed (Figure B.1A) is calculated as

$$z_{1,f} = t_{inj}u_{ss} = \frac{z_{inj}u_{ss}}{u_m} = \frac{z_{inj}}{1+k_{ss}} \tag{B5}$$

where u_{ss} is the velocity of the analyte in the sample solvent defined as

$$u_{ss} = \frac{u_m}{(1+k_{ss})} \tag{B6}$$

The midpoint of the analyte band is positioned at half way point $\frac{z_{1,f}}{2}$.

Next, the time it takes for the midpoint of the analyte band to travel from $\frac{z_{1,f}}{2}$ to the position at which it lines up with the tail end of the sample solvent is calculated (Figure B.1B):

$$t_1 = \frac{z_{2,m}}{u_m} = \frac{z_{2,m} - \frac{z_{1,f}}{2}}{u_{ss}} \tag{B7}$$

Solving for $z_{2,m}$ from equation B7 yields

$$z_{2,m} = \frac{z_{inj}}{2k_{ss}} \tag{B8}$$

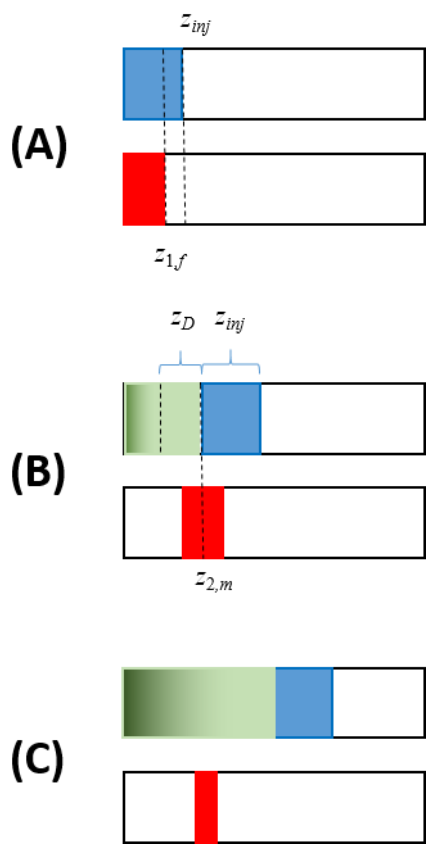

Figure B.1. Three contributions to retention: (A) injection; (B) elution from sample solvent; (C) elution in gradient. Sample solvent band (blue), analyte band (red), and mobile phase gradient (green).

The second contribution, the elution time of analyte band while in the sample solvent, is defined as

$$t_{R,2} = t_{M,2}(1 + k_{ss}) \tag{B9}$$

where $t_{M,2}$ is the fractional t_M corresponding to the distance $z_{2,m}$

$$t_{M,2} = \frac{z_{2,m}}{L} t_M \tag{B10}$$

The third and final component contributing to retention is due toelution in the mobile phase gradient and it can be calculated from Neue-Kuss theory [64]. The mobile phase composition at elution is calculated as (equation 3.21)

$$\phi_e = \frac{\phi_o + \frac{1+S_2\phi_o}{S_1}\ln\left(\frac{\Delta\phi k_w S_1}{t_G}\left(t_m - \frac{t_D}{k_o}\right)\exp\left(\frac{-S_1\phi_o}{1+S_2\phi_o}\right)+1\right)}{1-\frac{S_2(1+S_2\phi_o)}{S_1}\ln\left(\frac{\Delta\phi k_w S_1}{t_G}\left(t_m - \frac{t_D}{k_o}\right)\exp\left(\frac{-S_1\phi_o}{1+S_2\phi_o}\right)+1\right)} \tag{B11}$$

where k_w, S_1 and S_2 are parameters obtained from fitting retention time data to NK model (equation 3.19)

$$k = k_w(1+S_2\phi)^2 \exp\left[\frac{-S_1\phi}{1+S_2\phi}\right] \tag{B12}$$

The analogous expressions for LSS theory can be used instead of equations B11 and B12 if desired. The retention time for the gradient elution is calculated from ϕ_e, the initial organic composition of the gradient, ϕ_o, the gradient time, t_G, the delay time, t_D, and the change in mobile phase composition over t_G, $\Delta\phi$, as [64]

$$t_{R,3} = \frac{t_G(\phi_e - \phi_0)}{\Delta\phi} + t_{M,grad} + t_D \tag{B13}$$

where $t_{M,grad}$ is the remainder of the void time.

$$t_{M,grad} = t_M - t_{M,2} \tag{B14}$$

B.2. Peak width calculation

The peak width calculation is based on previous expression of σ^2 as a sum of variances from the injection band width (i.e., extra-column effects) and the isocratic parts of the separation [63]:

$$\sigma_{tot} = \sqrt{\sigma_{grad}^2 + \Delta\sigma^2} \tag{B15}$$

where $\Delta\sigma$ is the variance due to the finite injection bandwidth, as well as the band broadening contribution while the analyte elutes within the sample solvent (σ_{sample}) and within the dwell time (σ_D) and σ_{grad} is the gradient peak width.

In order to calculate $\Delta\sigma$, we must consider the total band width before the analytes experiences the gradient:

$$\sigma_b^2 = \sigma_{inject}^2 + \sigma_{sample}^2 + \sigma_D^2 \tag{B16}$$

where σ_{inject}, σ_{sample}, and σ_D are the bandwidths of the injection itself, the band broadening during elution while in the sample solvent and the band broadening during the elution while in the dwell volume, respectively. The σ_{inject} can be estimated as [67]:

$$\sigma_{inject} = \frac{k_o\left(k_{ss}+1\right)z_{1,f}}{k_{ss}\left(k_o+1\right)\sqrt{12}} \tag{B17}$$

The σ_{sample} and σ_D contributions are estimated as

$$\sigma_{sample} = \sqrt{z_{2,m}\Delta z} \tag{B18}$$

$$\sigma_D = \sqrt{z_D\Delta z} \tag{B19}$$

where z_D is equal to

$$z_D = u_o\left(t_D + t_{M,D}\right) \tag{B20}$$

where u_o is equal to the analyte velocity in the initial mobile phase composition and $t_{M,D}$ is given as

$$t_{M,D} = \frac{t_D}{k_o} \tag{B21}$$

The $\Delta\sigma$ is calculated as [63]:

$$\Delta\sigma = \frac{t_M\sigma_b}{L\mu_R\left(1+\omega_o b^{\dagger}\right)} \tag{B22}$$

or equivalently,

$$\Delta\sigma = \frac{\sigma_b(1+k_e)}{u_m} \tag{B23}$$

where ω_o is the analyte immobility in the initial mobile phase composition (equation 3.13),

$$\omega_o = \frac{k_o}{1+k_o} \tag{B24}$$

μ_R is the analyte mobility at elution (equation 3.14),

$$\mu_R = 1 - \frac{\omega_o}{1+\omega_o b^\dagger} \tag{B25}$$

and $b^\dagger$ is the dimensionless slope of the mobile phase gradient, analogous to the dimensionless slope as defined by Snyder for LSS theory [45], which is based on S (linear slope of ln k vs. ϕ plot). However, due to the curved nature of Neue-Kuss ln k vs. ϕ plot, we approximate the slope at elution by taking the derivative of ln k as a function of ϕ, and evaluate it at ϕ_e. This slope at elution is therefore given as:

$$S^* = \left(\frac{-2a}{1+a\phi_e}\right) + \left(\frac{B}{\left(1+a\phi_e\right)^2}\right) \tag{B26}$$

Then $b^\dagger$ can be calculated as

$$b^\dagger = \frac{t_{M,grad\ only}\Delta\phi S^*}{t_G} \tag{B27}$$

Finally, σ_{grad} is calculated as

$$\sigma_{grad} = G t_{M,grad\ only}\left(1+k_e\right)\sqrt{\frac{\Delta z}{z_{grad}}} \tag{B28}$$

where k_e is the retention factor at elution and $t_{M,grad\ only}$, z_{grad} and G are defined as

$$t_{M,grad\ only} = t_M - t_{M,2} - t_{M,D} \tag{B29}$$

$$z_{grad} = L - z_D - z_{2,m} \tag{B30}$$

$$G = \frac{1}{\left(1+\omega_o b^{\dagger}\right)} \sqrt{1+\omega_o b^{\dagger} + \frac{1}{3}\omega_o^2 b^{\dagger 2}} \tag{B31}$$

APPENDIX C

All simulation codes presented here are located in Virginia Commonwealth University's network R drive (R:\CHEM\Rutan_lab\Lena\Dissertation\Simulation package) and are reproduced here.

C.1. Simulation parameter fitting

The functions isotimefit_lss.m, isotimefit_nk.m, and gradtimefit_lss.m are used for parameter fitting when using only one stationary phase functionality. The functions isotimefit_lss_cS.m and isotimefit_nk_cBa.m are used for parameter fitting for stationary phase gradient with two different functionalities. These functions force the mobile phase dependent parameters to be common between the two columns.

isotimefit_lss.m

```
function [ferr]=isotimefit_lss(param,tm,phi,tr_exp)
S=param(1);
kw=param(2);
for n=1:size(tr_exp,1)
    logk=log(kw)-S*phi(n);
    k=exp(logk);
    tr_est(n)=tm*(k+1);
end
ferr=tr_exp-tr_est';
```

isotimefit_nk.m

```
function [ferr]=isotimefit_nk(param,tm,phi,tr_exp)
B=param(1);
a=param(2);
kw=param(3);
for n=1:size(tr_exp,1)
    logk(n)=log(kw)+2*log(1+a*phi(n))-(B*phi(n))/(1+a*phi(n));
    k(n)=exp(logk(n));
    tr_est(n)=tm*(k(n)+1);
end
ferr=tr_exp-tr_est';
```

gradtimefit_lss.m

```
function [ferr]=gradtimefit_lss(param,tD,tM,phiinit,delphi,tG,tR)
S=param(1);
kw=param(2);
for n=1:size(tR,1)
    logko=log(kw)-S*phiinit(n);
    ko=exp(logko);
```

```
    b=tM(n)*delphi(n)*S/tG(n);
    tRest(n)=(tM(n)/b)*(log(ko*b*(1-tD/(tM(n)*ko))+1))+tM(n)+tD;
endferr=tR-tRest'
```

isotimefit_lss_cS.m

```
function [ferr]=isotimefit_lss_cS(param,tm_stat1,phi_stat1,...
    tr_exp_stat1,tm_stat2,phi_stat2,tr_exp_stat2)
S=param(1);
kw_stat1=param(2);
kw_stat2=param(3);

for n=1:size(tr_exp_stat1,1)
    logk_stat1=log(kw_stat1)-S*phi_stat1(n);
    k_stat1=exp(logk_stat1);
    tr_est_phen(n)=tm_stat1*(k_stat1+1);
end
ferr=tr_exp_stat1-tr_est_phen';

for n=1:size(tr_exp_stat2,1)
    logk_stat2=log(kw_stat2)-S*phi_stat2(n);
    k_stat2=exp(logk_stat2);
    tr_est_stat2(n)=tm_stat2*(k_stat2+1);
end
ferr=[ferr; tr_exp_stat2-tr_est_stat2'];
```

isotimefit_nk_cBa.m

```
function [ferr]=isotimefit_nk_cBa(param,tm_stat1,phi_stat1,...
    tr_exp_stat1,tm_stat2,phi_stat2,tr_exp_stat2)
B=param(1);
a=param(2);
kw_stat1=param(3);
kw_stat2=param(4);

for n=1:size(tr_exp_stat1,1)
    logk_stat1=log(kw_stat1)+2*log(1+a*phi_stat1(n))...
        -(B*phi_stat1(n))/(1+a*phi_stat1(n));
    k_stat1=exp(logk_stat1);
    tr_est_stat1(n)=tm_stat1*(k_stat1+1);
end
ferr=tr_exp_stat1-tr_est_stat1';

for n=1:size(tr_exp_stat2,1)
    logk_stat2=log(kw_stat2)+2*log(1+a*phi_stat2(n))...
        -(B*phi_stat2(n))/(1+a*phi_stat2(n));
    k_stat2=exp(logk_stat2);
    tr_est_stat2(n)=tm_stat2*(k_stat2+1);
end
ferr=[ferr; tr_exp_stat2-tr_est_stat2'];
```

C.2. Setting up simulation parameters

The functions model_LSS.m and model_NK.m allows for importing of preset simulation parameters or manual input of new simulation parameters for either solvent strength model.

model_LSS.m

```
function [model] = model_LSS(S,kw,compound,column)

if exist('compound')

    x={'PE'; 'PPA'; 'PEA'; 'EP'; 'PSE'; 'Amp'; 'MDA'; 'Mamp'; 'Moxy';
'MDMA'};
    S  = [15.044 22.146 19.415 24.403 26.401 21.971 24.336 21.794 24.232
23.165];
    if isequal(column,'C18')
    kw = [0.95856 4.7170 4.7543 8.7610 10.973 12.114 18.606 16.801 21.888
23.986];
    elseif isequal(column,'Phen')
    kw = [0.73760 4.0337 3.9340 7.1185 8.5123 9.9955 13.423 13.252 17.222
16.547];
    else
    error('Error: column not found');
    end

    ind=strcmp(x,compound);
if ~ind
    error('Error: compound not found');
else
    field1='S';
    value1=S(ind);

    field2='kw';
    value2=kw(ind);

end

else
field1='S';
value1=S;

field2='kw';
value2=kw;
end
model=struct(field1,value1,field2,value2);
end
```

model_NK.m

```
function [model] = model_NK(kw,B,a,compound)

if exist('compound')

    x={'AB1'; 'AB2'; 'AB3'; 'AB4'; 'AB5'; 'DiEtF'; 'BzAlc'; 'PB1'; 'PB3';
'PB4'; 'AP2'; 'AP4'; 'AP5'};
    kw = [1011          5314         6203       8004       9262    22.91977
37.33757    172.4315     3181.156     10829.18    139.6305    2046.733
11014.85];
```

```
    B  = [18.59       23.97       19.95     16.82     14.71      27.36
20.96       26.95        33.53        34.57       18.64       22.73
27.68];
    a  = [1.0438      1.2379      0.9237    0.6486    0.4897     2.772
1.903       1.955        1.839        1.694       1.371       1.239
1.354];

    ind=strcmp(x,compound);
if ~ind
    error('Error: compound not found');
else

    field1='kw';
    value1=kw(ind);

    field2='B';
    value2=B(ind);

    field3='a';
    value3=a(ind);
end

else
field1='kw';
value1=kw;

field2='B';
value2=B;

field3='a';
value3=a;
end
model=struct(field1,value1,field2,value2,field3,value3);
end
```

C.3. Setting up simulation conditions

The functions conditions_iso.m and conditions_lin.m allows for setting up of all separation conditions for isocratic or mobile phase gradient elution, respectively. The conditions_lin.m function also constructs the analyte injection band profile and the mobile phase gradient profile.

conditions_iso.m

```
function [conditions] = conditions_iso(delz,Vm,F,L,time,Vinj,sample,phi)

%distance segment (equal to H)
field1='delz';
value1=delz;

%void volume
field2='Vm';
value2=Vm;
```

```
%flow rate
field3='F';
value3=F;

%void time
field4='tM';
tM=Vm/F;
value4=tM;

%column length
field5='L';
value5=L;

%time segment
field6='delt';
delt=delz/(L/tM)*60; %in seconds
value6=delt;

%total time for simulation
field7='time';
value7=time;

%injection volume (uL)
field8='Vinj';
value8=Vinj;

%number of injection slices (unitless)
field9='slices';
slices=floor(Vinj/1000/Vm*(L/delz));
value9=slices;

%sample solvent composition
field10='sample';
value10=sample;

%mobile phase composition
field11='phi';
value11=phi;

conditions=struct(field1,value1,field2,value2,field3,value3,...
    field4,value4,field5,value5,field6,value6,field7,value7,...
    field8,value8,field9,value9,field10,value10,field11,value11)
end
```

conditions_lin.m

```
function [conditions] = conditions_lin(delz,Vm,F,L,time,Vloop,fill,...
    inj_exptl,inj_prof,Vaxis,sample,phiinit,delphi,tG,tD,Mgrad)

%distance segment (equal to H)
field1='delz';
value1=delz;

%void volume
```

```
field2='Vm';
value2=Vm;

%flow rate
field3='F';
value3=F;

%void time
field4='tM';
tM=Vm/F;
value4=tM;

%column length
field5='L';
value5=L;

%time segment
field6='delt';
delt=delz/(L/tM)*60; %in seconds
value6=delt;

%total time for simulation
field7='time';
value7=time;

%loop size (mL)
field8='Vloop';
value8=Vloop;

%filling level (fraction)
field9='fill';
value9=fill;

%injection volume
field10='Vinj';
Vinj=Vloop*fill;
value10=Vinj;

%number of injection slices (unitless)
field11='slices';
slices=floor(Vinj/1000/Vm*(L/delz));
value11=slices;

%sample solvent composition
field12='sample';
value12=sample;

%initial mobile phase composition
field13='phiinit';
value13=phiinit;

%difference between sample and phiinit
field14='delphisam';
delphisam=sample-phiinit;
```

```
value14=delphisam;

%difference between final and initial mobile phase composition
field15='delphi';
value15=delphi;

%gradient time
field16='tG';
value16=tG;

%delay time
field17='tD';
value17=tD+(Vloop/1000)/F;

%rectangular injection=0; experimental injection=1
field18='inj_exptl';
value18=inj_exptl;

%experimental injection profile; only used when inj_exptl=1
field19='inj_prof';
value19=inj_prof;

%volume axis for experimental injection profile
field20='Vaxis';
value20=Vaxis;

field21='Mgrad'; %mobile phase gradient profile
field22='C_injProf'; %analyte injection profile

if exist ('Mgrad');
    value21=Mgrad;
else
tottime=time*60; %converts time to seconds
nt=floor(tottime/delt); %an integer number of time steps, rounding down
phifinal=phiinit+delphi; %final mobile phase solvent composition
mGradient=ones(1,nt)*phifinal; %initalizes mobile phase gradient profile
tgsteps=floor(tG*60/delt); %number of time steps occupied by the gradient
ntd=tD*60/delt; %number of time steps occupied by the void time
slope=delphi/tgsteps; %slope of the gradient
old_slice_axis=Vaxis/Vm*(L/delz); %converts volume axis to slice axis
scale1=0.00625/60*F; %determines volume/point in the gradient profile
scale2=L/(delz*Vm); %determines plates/void volume of column
ndelt_spacing=size(Vaxis,1)-1; %number of points needed for interpolation
new_points=floor(ndelt_spacing*scale1*scale2); %converts number of points
%for interpolation into number of plates
new_slice_axis=[1:new_points]; %new slice axis
C_injProf=zeros(1,nt); %preset C_injProf with zeros
for m=1:nt
    if m<=slices
        if inj_exptl==0
        mGradient(1,m)=sample;
        else
        mGradient(1,m)=phiinit;
        end
    elseif m>slices && m<=slices+ntd
```

```
        mGradient(1,m)=phiinit;
    elseif m>slices+ntd && m<=tgsteps+slices+ntd
        mGradient(1,m)=slope*(m-(slices+ntd))+phiinit;
        end
end
    if inj_exptl==1
    %interpolation (old to new slice axis)
    inj_prof_new=interp1(old_slice_axis,inj_prof,new_slice_axis);
    inj_prof_new(isnan(inj_prof_new))=0;
    %sample solvent profile
    Minj_prof=inj_prof_new*delphisam;
    %mobile phase gradient profile
    mGradient(1,1:new_points)=mGradient(1,1:new_points)+Minj_prof;
    %normalizes injection profile of the analyte
    Cinj_prof=inj_prof_new/sum(inj_prof_new);
    %analyte injection profile
    C_injProf(1,1:new_points)=C_injProf(1,1:new_points)+Cinj_prof;
    else
        inj=1;
        analyte=inj/slices;
        C_injProf(1,1:slices)=analyte;
    end
value21=mGradient;
value22=C_injProf;
end

conditions=struct(field1,value1,field2,value2,field3,value3,...
    field4,value4,field5,value5,field6,value6,field7,value7,...
    field8,value8,field9,value9,field10,value10,field11,value11,...
    field12,value12,field13,value13,field14,value14,field15,value15,...
    field16,value16,field17,value17,field18,value18,field19,value19,...
    field20,value20,field21,value21,field22,value22);
end
```

C.4. Isocratic simulation

The functions chromsim_isoLSS.m and chromsim_isoNK.m calls on previously constructed options structures model using models_LSS.m or models_NK.m and isocratic condition from conditions_iso.m to simulate a chromatogram.

chromsim_isoLSS.m

```
function [Cfinal,Mfinal,kp]=chromsim_isoLSS(model_LSS,conditions_iso)
kw=model_LSS.kw;
S=model_LSS.S;
sample=conditions_iso.sample;
slices=conditions_iso.slices;
phi=conditions_iso.phi;
tottime=conditions_iso.time*60;
totdist=conditions_iso.L;
u=totdist/conditions_iso.tM;
delt=conditions_iso.delz/u*60;
D1=0.5;
nz=round(totdist/conditions_iso.delz);
nt=floor(tottime/delt);
```

```
C1=zeros(nz,1);
C2=zeros(nz,1);
dM=zeros(nz,1);
dC=zeros(nz,1);
kp=zeros(1,nt);
Mfinal=zeros(1,nt);
Cfinal=zeros(1,nt);
M1=ones(nz,1)*phi;
M1(1,1)=-D1*sample+D1*phi+sample;
M1(2,1)=-2*D1*phi+D1*sample+D1*phi+phi;
pkprime(1:nz,1)=kw*exp(-S*M1(1:nz,1));
kp(1)=pkprime(nz,1);
inj=1;
analyte=inj/slices;
C_injProf=zeros(1,nt);
for m=1:slices
    C_injProf(1,m)=analyte;
end
D(:,1)=1./(2*(pkprime(:,1)+1).^2);
for m=1:nt
    if m<=slices
        M2(1,1)=sample;
    else
        M2(1,1)=phi;
    end
    for n=2:nz
        M2(n,1)=M1(n-1,1);
    end
    dM(1)=-D1*M2(1,1)+D1*M2(2,1);
    for n=2:nz-1
        dM(n,1)=-2*D1*M2(n,1)+D1*M2(n-1,1)+D1*M2(n+1,1);
    end
    dM(nz,1)=-2*D1*M2(nz,1)+D1*M2(nz-1,1)+D1*M1(nz,1);
    M2=M2+dM;
    C2(1,1)=C_injProf(1,m);
    kprime(1,1)=kw*exp(-S*M2(1,1));
    P1(1,1)=pkprime(1,1)/(pkprime(1,1)+1);
    P(1,1)=1/(kprime(1,1)+1);
    D(1,1)=1/(2*(pkprime(1,1)+1)^2);
    if D(1,1)>0.5 D(1,1)=0.5; end;
    C2(1,1)=P1(1,1)*C1(1,1)+C2(1,1);
    for n=2:nz
        kprime(n,1)=kw*exp(-S*M2(n,1));
        P(n,1)=1/(pkprime(n-1,1)+1);
        P1(n,1)=pkprime(n,1)/(pkprime(n,1)+1);
        D(n,1)=1/(2*(pkprime(n,1)+1)^2);
        C2(n,1)=P1(n,1)*C1(n,1)+P(n,1)*C1(n-1,1);
    end
    dC(1)=-D(1,1)*C2(1,1)+D(2,1)*C2(2,1);
    for n=2:nz-1
        dC(n,1)=-2*D(n,1)*C2(n,1)+D(n-1,1)*C2(n-1,1)+D(n+1,1)*C2(n+1,1);
    end
    dC(nz,1)=-2*D(nz,1)*C2(nz,1)+D(nz-1,1)*C2(nz-1,1)+D(nz,1)*C1(nz,1);
    C2=C2+dC;
    kp(1,m)=kprime(nz,1);
    pkprime=kprime;
    C1=C2;
```

```
    M1=M2;
    Cfinal(1,m)=C1(nz,1);
    Mfinal(1,m)=M2(nz,1);
end
Cfinal=Cfinal./(kp+1);
```

chromsim_isoNK.m

```
function [Cfinal,Mfinal,kp]=chromsim_isoNK(model_NK,conditions_iso)
kw=model_NK.kw;
B=model_NK.B;
a=model_NK.a;
sample=conditions_iso.sample;
slices=conditions_iso.slices;
phi=conditions_iso.phi;
tottime=conditions_iso.time*60;
totdist=conditions_iso.L;
delz=conditions_iso.delz;
tM=conditions_iso.tM*60;
u=totdist/tM;
delt=delz/u;
D1=1/2;
nz=round(totdist/delz);
nt=floor(tottime/delt);
C1=zeros(nz,1);
C2=zeros(nz,1);
pkprime=zeros(nz,1);
kprime=zeros(nz,1);
dM=zeros(nz,1);
dC=zeros(nz,1);
kp=zeros(1,nt);
Mfinal=zeros(1,nt);
Cfinal=zeros(1,nt);
M1=ones(nz,1)*phi;
M1(1,1)=-D1*sample+D1*phi+sample;
M1(2,1)=-2*D1*phi+D1*sample+D1*phi+phi;
if isscalar(kw)
    kw=kw*ones(nz,1);
end
pkprime(1:nz,1)=kw.*(1+a*M1(1:nz,1)).^2.*exp(-B*M1(1:nz,1)...
    ./(1+a*M1(1:nz,1)));
kp(1)=pkprime(nz,1);
inj=1;
analyte=inj/slices;
C_injProf=zeros(1,nt);
for m=1:slices
    C_injProf(1,m)=analyte;
end
D(:,1)=1./(2*(pkprime(:,1)+1).^2);
for m=1:nt
    if m<=slices
        M2(1,1)=sample;
    else
        M2(1,1)=phi;
    end
    for n=2:nz
        M2(n,1)=M1(n-1,1);
```

```
    end
    dM(1)=-D1*M2(1,1)+D1*M2(2,1);
    for n=2:nz-1
        dM(n,1)=-2*D1*M2(n,1)+D1*M2(n-1,1)+D1*M2(n+1,1);
    end
    dM(nz,1)=-2*D1*M2(nz,1)+D1*M2(nz-1,1)+D1*M1(nz,1);
    M2=M2+dM;
    C2(1,1)=C_injProf(1,m);
    kprime(1,1)=kw(1,1)*(1+a*M2(1,1))^2*exp(-B*M2(1,1)/(1+a*M2(1,1)));
    P1(1,1)=pkprime(1,1)/(pkprime(1,1)+1);
    P(1,1)=1/(kprime(1,1)+1);
    D(1,1)=1/(2*(pkprime(1,1)+1)^2);
    C2(1,1)=P1(1,1)*C1(1,1)+C2(1,1);
    for n=2:nz
    kprime(n,1)=kw(n,1)*(1+a*M2(n,1))^2*exp(-B*M2(n,1)/(1+a*M2(n,1)));
    P(n,1)=1/(pkprime(n-1,1)+1);
    P1(n,1)=pkprime(n,1)/(pkprime(n,1)+1);
    D(n,1)=1/(2*(pkprime(n,1)+1)^2);
    C2(n,1)=P1(n,1)*C1(n,1)+P(n,1)*C1(n-1,1);
    end
    dC(1)=-D(1,1)*C2(1,1)+D(2,1)*C2(2,1);
    for n=2:nz-1
        dC(n,1)=-2*D(n,1)*C2(n,1)+D(n-1,1)*C2(n-1,1)+D(n+1,1)*C2(n+1,1);
    end
    dC(nz,1)=-2*D(nz,1)*C2(nz,1)+D(nz-1,1)*C2(nz-1,1)+D(nz,1)*C1(nz,1);
    C2=C2+dC;
    kp(1,m)=kprime(nz,1);
    pkprime=kprime;
    C1=C2;
    M1=M2;
    Cfinal(1,m)=C1(nz,1);
    Mfinal(1,m)=M2(1,1);
end
Cfinal=Cfinal./(kp+1);
```

C.5. Mobile phase gradient simulation

The functions chromsim_lin_LSS.m and chromsim_lin_NK.m calls on previously constructed options structures model using models_LSS.m or models_NK.m and mobile phase gradient condition from conditions_lin.m to simulate a chromatogram. Both programs allow for an option of saving snapshots.

chromsim_lin_LSS.m

```
function[Cfinal,Mfinal,kp,time,Frames]=chromsim_lin_LSS(cond_lin,...
    model_LSS,movie_tstep)

kw=model_LSS.kw;
S=model_LSS.S;
slices=cond_lin.slices;
tottime=cond_lin.time*60;
totdist=cond_lin.L;
delz=cond_lin.delz;
delt=cond_lin.delt;
phiinit=cond_lin.phiinit;
```

```
delphi=cond_lin.delphi;
phifinal=phiinit+delphi;
sample=cond_lin.sample;
D1=1/2;
nz=round(totdist/cond_lin.delz);
nt=floor(tottime/delt);
Vm=cond_lin.Vm;
F=cond_lin.F;
Vloop=cond_lin.Vloop;
fill=cond_lin.fill;
inj_exptl=cond_lin.inj_exptl;
inj_prof=cond_lin.inj_prof;
Vaxis=cond_lin.Vaxis;
C1=zeros(nz,1);
C2=zeros(nz,1);
pkprime=zeros(nz,1);
kprime=zeros(nz,1);
dM=zeros(nz,1);
dC=zeros(nz,1);
kp=zeros(1,nt);
Mfinal=zeros(1,nt);
Cfinal=zeros(1,nt);
inj=1;
analyte=inj/slices;
C_injProf=zeros(1,nt);
for m=1:slices
    C_injProf(1,m)=analyte;
end
if isscalar(kw)
    kw=kw*ones(nz,1);
end
M1=ones(nz,1)*phiinit;
M1(1,1)=-D1*sample+D1*phiinit+sample;
M1(2,1)=-2*D1*phiinit+D1*sample+D1*phiinit+phiinit;
pkprime(1:nz,1)=kw.*exp(-S*M1(1:nz,1));
kp(1)=pkprime(nz,1);
D(:,1)=1./(2*(pkprime(:,1)+1).^2);

%establish movie time step
if exist('movie_tstep')
    mov=1;
figure('units','inches','position',[1 1 8 6]);
frvec=[1:movie_tstep:nt];
j=1;
else
    mov=0;
end

m=1;
while m<=nt %time loop
%call upon established mobile phase gradient profile
M2(1,1)=cond_lin.Mgrad(1,m);
    for n=2:nz
        M2(n,1)=M1(n-1,1);
    end
    dM(1)=-D1*M2(1,1)+D1*M2(2,1);
```

```
    for n=2:nz-1
        dM(n,1)=-2*D1*M2(n,1)+D1*M2(n-1,1)+D1*M2(n+1,1);
    end
    dM(nz,1)=-2*D1*M2(nz,1)+D1*M2(nz-1,1)+D1*M1(nz,1);
    M2=M2+dM;
    C2(1,1)=C_injProf(1,m);
    kprime(1,1)=kw(1,1)*exp(-S*M2(1,1));
    P1(1,1)=pkprime(1,1)/(pkprime(1,1)+1);
    P(1,1)=1/(kprime(1,1)+1);
    D(1,1)=1/(2*(pkprime(1,1)+1)^2);
    C2(1,1)=P1(1,1)*C1(1,1)+C2(1,1);
    for n=2:nz
        kprime(n,1)=kw(n,1).*exp(-S*M2(n,1));
        P(n,1)=1/(pkprime(n-1,1)+1);
        P1(n,1)=pkprime(n,1)/(pkprime(n,1)+1);
        D(n,1)=1/(2*(pkprime(n,1)+1)^2);
        C2(n,1)=P1(n,1)*C1(n,1)+P(n,1)*C1(n-1,1);
    end
    dC(1)=-D(1,1)*C2(1,1)+D(2,1)*C2(2,1);
    for n=2:nz-1
        dC(n,1)=-2*D(n,1)*C2(n,1)+D(n-1,1)*C2(n-1,1)+D(n+1,1)*C2(n+1,1);
    end
    dC(nz,1)=-2*D(nz,1)*C2(nz,1)+D(nz-1,1)*C2(nz-1,1)+D(nz,1)*C1(nz,1);
    C2=C2+dC;
    %k at elution is kprime at z=L
    kp(1,m)=kprime(nz,1);
    %reset previous time kprime equal to current kprime
    pkprime=kprime;
    %reset previous time analyte mass equal to current analyte mass
    C1=C2;
    %reset previous time mobile phase composition equal to
    %current mobile phase composition
    M1=M2;
    %final chromatogram equals mass at the end of the column
    Cfinal(1,m)=C2(nz,1);
    %final mobile phase profile equals mass at the end of the column
    Mfinal(1,m)=M2(nz,1);
%continue simulation if not returned to baseline
if m==nt
    if Cfinal(1,m)>1e-10
        time=(tottime+5)/60;
        cond_lin=conditions_linn2(delz,Vm,F,L,time,Vloop,fill,...
            inj_exptl,inj_prof,Vaxis,sample,phiinit,delphi,tG,tDm);
        nt=floor(time*60/delt);
        disp('Not long enough simulation time, more time needed.')
    end
end
%get frames for movie
if mov==1 && ismember(m,frvec)
zaxis=delz:delz:totdist;
    subplot(2,1,1); plot(zaxis,M2,'LineWidth',2);
    if phifinal==phiinit
        phiflim=phiinit+0.1;
    else
        phiflim=phifinal;
    end
    set(gca, 'XLim',[0 L]);
```

```
    set(gca,'YLim',[sample phiflim]);
    title(sprintf('time = %0.4f sec',delt*m))
    xlabel('Distance (cm)')
    ylabel('\phi')
    set(gca,'fontsize',18);
    subplot(2,1,2); plot(zaxis,C2,'r','LineWidth',2);
    set(gca,'YLim',[0 3*max(cond_lin.C_injProf)]);
    xlabel('Distance (cm)')
    ylabel('Analyte mass')
    set(gca,'fontsize',18);
    Frames(j)=getframe(gcf);
    j=j+1;
    elseif mov==0
    Frames=struct([]);
end
    m=m+1;
end
Cfinal=Cfinal./(kp+1); %area correction; divide Cfinal by (k at elution+1)
```

chromsim_lin_NK.m

```
function[Cfinal,Mfinal,kp,time,Frames]=chromsim_lin_NK(model_NK,...
    cond_lin,movie_tstep)

kw=model_NK.kw;
a=model_NK.a;
B=model_NK.B;
phiinit=cond_lin.phiinit;
delphi=cond_lin.delphi;
phifinal=phiinit+delphi;
time=cond_lin.time;
tottime=time*60;
L=cond_lin.L;
totdist=L;
delz=cond_lin.delz;
delt=cond_lin.delt;
Vm=cond_lin.Vm;
F=cond_lin.F;
Vloop=cond_lin.Vloop;
fill=cond_lin.fill;
inj_exptl=cond_lin.inj_exptl;
inj_prof=cond_lin.inj_prof;
Vaxis=cond_lin.Vaxis;
sample=cond_lin.sample;
D1=1/2;
nz=floor(totdist/delz);
nt=floor(tottime/delt);
phifinal=phiinit+delphi;
tG=cond_lin.tG;
tDm=cond_lin.tD-(Vloop/1000)/F;
C1=zeros(nz,1);
C2=zeros(nz,1);
pkprime=zeros(nz,1);
kprime=zeros(nz,1);
dM=zeros(nz,1);
dC=zeros(nz,1);
kp=zeros(1,nt);
```

```
Mfinal=zeros(1,nt);
Cfinal=zeros(1,nt);
if isscalar(kw);
    kw=kw*ones(nz,1);
end
M1=ones(nz,1)*cond_lin.phiinit;
M1(1,1)=-D1*cond_lin.sample+D1*cond_lin.phiinit+cond_lin.sample;
M1(2,1)=-
2*D1*cond_lin.phiinit+D1*cond_lin.sample+D1*cond_lin.phiinit+cond_lin.phiinit
;
pkprime(1:nz,1)=kw.*(1+a*M1(1:nz,1)).^2.*exp(-
B*M1(1:nz,1)./(1+a*M1(1:nz,1)));
kp(1)=pkprime(nz,1);
D(:,1)=1./(2*(pkprime(:,1)+1).^2);

%establish movie time step
if exist('movie_tstep')
    movie_tstep=floor(movie_tstep);
    mov=1;
figure('units','inches','position',[1 1 8 6]);
frvec=[1:movie_tstep:nt];
j=1;
else
    mov=0;
end

m=1;
while m<=nt %establish movie time step
%call upon established mobile phase gradient profile
    M2(1,1)=cond_lin.Mgrad(1,m);
    %mobile phase compsition for every distance point with dispersion
    for n=2:nz
        M2(n,1)=M1(n-1,1);
    end
    dM(1)=-D1*M2(1,1)+D1*M2(2,1);
    for n=2:nz-1
        dM(n,1)=-2*D1*M2(n,1)+D1*M2(n-1,1)+D1*M2(n+1,1);
    end
    dM(nz,1)=-2*D1*M2(nz,1)+D1*M2(nz-1,1)+D1*M1(nz,1);
    M2=M2+dM;
    C2(1,1)=cond_lin.C_injProf(1,m);
    kprime(1,1)=kw(1,1)*(1+a*M2(1,1))^2*exp(-B*M2(1,1)/(1+a*M2(1,1)));
    P1(1,1)=pkprime(1,1)/(pkprime(1,1)+1);
    P(1,1)=1/(kprime(1,1)+1);
    D(1,1)=1/(2*(pkprime(1,1)+1)^2);
    C2(1,1)=P1(1,1)*C1(1,1)+C2(1,1);
    %analyte mass for every distance point with dispersion
    for n=2:nz
        kprime(n,1)=kw(n,1)*(1+a*M2(n,1))^2*exp(-B*M2(n,1)/(1+a*M2(n,1)));
        P(n,1)=1/(pkprime(n-1,1)+1);
        P1(n,1)=pkprime(n,1)/(pkprime(n,1)+1);
        D(n,1)=1/(2*(pkprime(n,1)+1)^2);
        C2(n,1)=P1(n,1)*C1(n,1)+P(n,1)*C1(n-1,1);
    end
    dC(1)=-D(1,1)*C2(1,1)+D(2,1)*C2(2,1);
    for n=2:nz-1
```

```
        dC(n,1)=-2*D(n,1)*C2(n,1)+D(n-1,1)*C2(n-1,1)+D(n+1,1)*C2(n+1,1);
    end
    dC(nz,1)=-2*D(nz,1)*C2(nz,1)+D(nz-1,1)*C2(nz-1,1)+D(nz,1)*C1(nz,1);
    C2=C2+dC;

     %k at elution is kprime at z=L
    kp(1,m)=kprime(nz,1);
    %reset previous time kprime equal to current kprime
    pkprime=kprime;
    %reset previous time analyte mass equal to current analyte mass
    C1=C2;
    %reset previous time mobile phase composition equal to
    %current mobile phase composition
    M1=M2;
    %final chromatogram equals mass at the end of the column
    Cfinal(1,m)=C2(nz,1);
    %final mobile phase profile equals mass at the end of the column
    Mfinal(1,m)=M2(nz,1);

%continue simulation if not back down to baseline
if m==nt
    if Cfinal(1,m)>1e-10
        time=(tottime+5)/60;
        cond_lin=conditions_linn2(delz,Vm,F,L,time,Vloop,fill,...
            inj_exptl,inj_prof,Vaxis,sample,phiinit,delphi,tG,tDm);
        nt=floor(time*60/delt);
        disp('Not long enough simulation time, more time needed.')
    end
end
%get frames for movie
if mov==1 && ismember(m,frvec)
    zaxis=delz:delz:totdist;
    subplot(2,1,1); plot(zaxis,M2,'LineWidth',2);
    if phifinal==phiinit
        phiflim=phiinit+0.1;
    else
        phiflim=phifinal;
    end
    set(gca, 'XLim',[0 L]);
    set(gca,'YLim',[sample phiflim]);
    title(sprintf('time = %0.4f sec',delt*m))
    xlabel('Distance (cm)')
    ylabel('\phi')
    set(gca,'fontsize',18);
    subplot(2,1,2); plot(zaxis,C2,'r','LineWidth',2);
    set(gca,'YLim',[0 3*max(cond_lin.C_injProf)]);
    xlabel('Distance (cm)')
    ylabel('Analyte mass')
    set(gca,'fontsize',18);
    Frames(j)=getframe(gcf);
    j=j+1;
    elseif mov==0
    Frames=struct([]);
end
    m=m+1;
end
```

```
Cfinal=Cfinal./(kp+1); %area correction; divide Cfinal by (k at elution+1)
```

C.6. Isothermal simulation

The function model_NKT.m, conditions_lin_isotherm, and chromsim_lin_NK_isotherm incorporates the effect of temperature into simulation using NK model.

model_NKT.m

```
function [model] = model_NKT(kw,B,a,DT,DmTprime,compound)

if exist('compound')

    x={'HP2'; 'HP3'; 'HP4'; 'PB1'; 'PB2'; 'PB3'; 'PB4'};
    lnk0T = [4.60   4.26   4.07   4.62   4.30   4.24   4.30];
    BT  = [2.95   2.67   2.65   2.50   2.64   2.70   2.73];
    a  = [2.42   2.03   1.95   1.96   1.99   2.03   2.07];
    DT = [2559   2878   3260   2890   3271   3774   4323];
    %parameters from S.R. Groskreutz, S.G. Weber/ J.Chromatogr.A 1474
    %(2016) 95-108 Table S2
    DmTprime= [NaN      NaN      NaN   1.09E-5 9.80E-6 9.06E-6 7.04E-6];

    ind=strcmp(x,compound);
if ~ind
    error('Error: compound not found');
else
    %nz=round(L/delz);

    field1='lnk0T';
    %value1(1:nz,1)=kw(ind);
    value1=lnk0T(ind);

    field2='BT';
    value2=BT(ind);

    field3='a';
    value3=a(ind);

    field4='DT';
    value4=DT(ind);

    field5='DmTprime';
    value5=DmTprime(ind);
end

else
field1='kw';
value1=kw;

field2='B';
value2=B;

field3='a';
value3=a;
```

```
field4='DT';
value4=DT;

field5='DmTprime';
value5=DmTprime;
end

model=struct(field1,value1,field2,value2,field3,value3,field4,value4,...
    field5,value5);

end
```

conditions_lin_isotherm.m

```
function [conditions] = conditions_lin_isotherm(delz,Vm,F,L,time,Vinj,...
    inj_exptl,inj_prof,Vaxis,sample,phiinit,delphi,tG,tD,T,Mgrad)

field1='delz'; %cm
value1=delz;

field2='Vm'; %mL
value2=Vm;

field3='F'; %mL/min
value3=F;

field4='tM'; %min
tM=Vm/F;
value4=tM;

field5='L'; %cm
value5=L;

field6='delt'; %sec
delt=delz/(L/tM)*60;
value6=delt;

field7='time'; %min
value7=time;

field8='Vinj'; %uL
value8=Vinj;

field9='slices';
slices=floor(Vinj/1000/Vm*(L/delz));
value9=slices;

field10='sample';
value10=sample;

field11='phiinit';
value11=phiinit;
```

```
field12='delphisam';
delphisam=sample-phiinit;
value12=delphisam;

field13='delphi';
value13=delphi;

field14='tG'; %min
value14=tG;

field15='tD'; %min
value15=tD;

field16='inj_exptl';
value16=inj_exptl;

field17='inj_prof';
value17=inj_prof;

field18='Vaxis';
value18=Vaxis;

field19='Mgrad';
field20='C_injProf';

if exist ('Mgrad');
    value19=Mgrad;
else
tottime=time*60;
nt=round(tottime/delt);
phifinal=phiinit+delphi;
mGradient=ones(1,nt)*phifinal;
tgsteps=round(tG*60/delt);
ntd=tD*60/delt;
slope=delphi/tgsteps;
old_slice_axis=Vaxis/Vm*(L/delz);
scale1=0.00625/60*2.5;
scale2=L/(delz*Vm);
ndelt_spacing=size(Vaxis,1)-1;
new_points=floor(ndelt_spacing*scale1*scale2);
new_slice_axis=[1:new_points];
C_injProf=zeros(1,nt);
for m=1:nt
    if m<=slices
        if inj_exptl==0
        mGradient(1,m)=sample;
        else
        mGradient(1,m)=phiinit;
        end
    elseif m>slices && m<=slices+ntd
        mGradient(1,m)=phiinit;
    elseif m>slices+ntd && m<=tgsteps+slices+ntd
        mGradient(1,m)=slope*(m-(slices+ntd))+phiinit;
        end
```

```
end
    if inj_exptl==1
    inj_prof_new=interp1(old_slice_axis,inj_prof,new_slice_axis);
    inj_prof_new(isnan(inj_prof_new))=0;
    Minj_prof=inj_prof_new*delphisam;
    mGradient(1,1:new_points)=mGradient(1,1:new_points)+Minj_prof;
    Cinj_prof=inj_prof_new/sum(inj_prof_new);
    C_injProf(1,1:new_points)=C_injProf(1,1:new_points)+Cinj_prof;
    else
        inj=1;
        analyte=inj/slices;
        C_injProf(1,1:slices)=analyte;
    end
value19=mGradient;
value20=C_injProf;
end

field21='T'; %K
value21=T;

conditions=struct(field1,value1,field2,value2,field3,value3,...
    field4,value4,field5,value5,field6,value6,field7,value7,...
    field8,value8,field9,value9,field10,value10,field11,value11,...
    field12,value12,field13,value13,field14,value14,field15,value15,...
    field16,value16,field17,value17,field18,value18,field19,value19,...
    field20,value20,field21,value21);
end
```

chromsim_lin_isotherm.m

```
function[Cfinal,Mfinal,kp]=chromsim_lin_NK_isotherm(model_NKT,cond_lin)
lnk0T=model_NKT.lnk0T;
T=cond_lin.T;
DT=model_NKT.DT;
lnkw=-lnk0T+DT/T;
kw=exp(lnkw);
a=model_NKT.a;
BT=model_NKT.BT;
B=(1+DT/T)*BT;
sample=cond_lin.sample;
slices=cond_lin.slices;
phiinit=cond_lin.phiinit;
delphi=cond_lin.delphi;
tottime=cond_lin.time*60; %convert to sec
totdist=cond_lin.L; %unit in cm
u=totdist/cond_lin.tM;
delt=cond_lin.delz/u*60;
D1=1/2;
nz=round(totdist/cond_lin.delz);
nt=round(tottime/delt);
ntd=(cond_lin.tD*60)/delt;
tgsteps=round((cond_lin.tG*60)/delt);
slope=cond_lin.delphi/tgsteps;
phifinal=phiinit+delphi;
C1=zeros(nz,1);
```

```
C2=zeros(nz,1);
pkprime=zeros(nz,1);
kprime=zeros(nz,1);
dM=zeros(nz,1);
dC=zeros(nz,1);
kp=zeros(1,nt);
Mfinal=zeros(1,nt);
Cfinal=zeros(1,nt);
if isscalar(kw)
    kw=kw*ones(nz,1);
end
M1=ones(nz,1)*cond_lin.phiinit;
M1(1,1)=-D1*cond_lin.sample+D1*cond_lin.phiinit+cond_lin.sample;
M1(2,1)=-2*D1*cond_lin.phiinit+D1*cond_lin.sample+D1*cond_lin.phiinit...
    +cond_lin.phiinit;
pkprime(1:nz,1)=kw.*(1+a*M1(1:nz,1)).^2.*exp(-B...
    *M1(1:nz,1)./(1+a*M1(1:nz,1)));
kp(1)=pkprime(nz,1);
D(:,1)=1./(2*(pkprime(:,1)+1).^2);
for m=1:nt
    M2(1,1)=cond_lin.Mgrad(1,m);
    for n=2:nz
        M2(n,1)=M1(n-1,1);
    end
    dM(1)=-D1*M2(1,1)+D1*M2(2,1);
    for n=2:nz-1
        dM(n,1)=-2*D1*M2(n,1)+D1*M2(n-1,1)+D1*M2(n+1,1);
    end
    dM(nz,1)=-2*D1*M2(nz,1)+D1*M2(nz-1,1)+D1*M1(nz,1);
    M2=M2+dM;
    C2(1,1)=cond_lin.C_injProf(1,m);
    kprime(1,1)=kw(1,1)*(1+a*M2(1,1))^2*exp(-B*M2(1,1)/(1+a*M2(1,1)));
    P1(1,1)=pkprime(1,1)/(pkprime(1,1)+1);
    P(1,1)=1/(kprime(1,1)+1);
    D(1,1)=1/(2*(pkprime(1,1)+1)^2);
    C2(1,1)=P1(1,1)*C1(1,1)+C2(1,1);
    for n=2:nz
        kprime(n,1)=kw(n,1)*(1+a*M2(n,1))^2*exp(-B*M2(n,1)/(1+a*M2(n,1)));
        P(n,1)=1/(pkprime(n-1,1)+1);
        P1(n,1)=pkprime(n,1)/(pkprime(n,1)+1);
        D(n,1)=1/(2*(pkprime(n,1)+1)^2);
        C2(n,1)=P1(n,1)*C1(n,1)+P(n,1)*C1(n-1,1);
    end
    dC(1)=-D(1,1)*C2(1,1)+D(2,1)*C2(2,1);
    for n=2:nz-1
        dC(n,1)=-2*D(n,1)*C2(n,1)+D(n-1,1)*C2(n-1,1)+D(n+1,1)*C2(n+1,1);
    end
    dC(nz,1)=-2*D(nz,1)*C2(nz,1)+D(nz-1,1)*C2(nz-1,1)+D(nz,1)*C1(nz,1);
    C2=C2+dC;
    kp(1,m)=kprime(nz,1);
    pkprime=kprime;
    C1=C2;
    M1=M2;
    Cfinal(1,m)=C1(nz,1);
    Mfinal(1,m)=M2(nz,1);
end
Cfinal=Cfinal./(kp+1);
```

C.7. Stationary phase gradient simulation

The function kspg_kw.m allows for setting up of different stationary phase gradient shapes and calculates k_w along the distance of the column before running the simulation.

```
function [kwgrad]=kspg_kw(cond_lin,shape,ratio,kw_stat1,kw_stat2)

% ratio represents the fraction of stat2 (assuming total equals 1)

delz=cond_lin.delz; % distance segment
L=cond_lin.L; % total length of the column
zz=delz:delz:L; % distance vector

switch shape
    case 'linear'
        fstat1=2*ratio*zz/L; %fraction of stationary phase 1
        fstat2=1-fstat1; %fraction of stationary phase 2
        figure; plot(fstat2); hold on; plot(fstat1)
    for n=1:size(zz,2)
        logkwgrad(n,1)=log(kw_stat1*fstat1(1,n)+kw_stat2*fstat2(1,n));
    end
    kwgrad=exp(logkwgrad); %kw vector for linear stationary phase gradient

    case 'step'
        fstat1(1:size(zz,2))=zeros;
        fstat1(1:round(size(zz,2)*ratio))=1;
        fstat2=1-fstat1;
        figure; plot(fstat2); hold on; plot(fstat1)
    for n=1:round(size(zz,2)*ratio)
        logkwgrad(n,1)=log(kw_stat1);
    end
    for n=round(size(zz,2)*ratio)+1:size(zz,2)
        logkwgrad(n,1)=log(kw_stat2);
    end
    kwgrad=exp(logkwgrad); %kw vector for step stationary phase gradient

    case 'exponential'
syms x
coeff=eval(vpasolve(sum(exp(-x*zz))==round(size(zz,2)*ratio),x));
        fstat1=(1-exp(-coeff*zz));
        fstat2=exp(-coeff*zz);
        figure; plot(fstat2); hold on; plot(fstat1)
    for n=1:size(zz,2)
        logkwgrad(n,1)=log(kw_stat1*fstat1(1,n)+kw_stat2*fstat2(1,n));
    end
    kwgrad=exp(logkwgrad); %kw vector for exp stationary phase gradient
    end
    end
```

The functions chromsim_smpg_LSS.m and chromsim_smpg_NK.m are simulation programs for stationary phase gradient. It is possible to simulate both isocratic and mobile phase gradient elution conditions.

chromsim_smpg_LSS.m

```
function[Cfinal,Mfinal,kp,Frames]=chromsim_smpg_LSS(S,cond_lin,kp_spg,...
    movie_tstep)

phiinit=cond_lin.phiinit;
delphi=cond_lin.delphi;
phifinal=phiinit+delphi;
sample=cond_lin.sample;
tottime=cond_lin.time*60;
totdist=cond_lin.L;
delz=cond_lin.delz;
delt=cond_lin.delt;
D1=1/2;
nz=floor(totdist/cond_lin.delz);
nt=floor(tottime/delt);
C1=zeros(nz,1);
C2=zeros(nz,1);
dM=zeros(nz,1);
dC=zeros(nz,1);
kp=zeros(1,nt);
Mfinal=zeros(1,nt);
Cfinal=zeros(1,nt);
M1=ones(nz,1)*phiinit;
M1(1,1)=-D1*sample+D1*phiinit+sample;
M1(2,1)=-2*D1*phiinit+D1*sample+D1*phiinit+phiinit;
pkprime(1:nz,1)=kp_spg.*exp(-S*M1(1:nz,1));
kp(1)=pkprime(nz,1);
D(:,1)=1./(2*(pkprime(:,1)+1).^2);

%establish movie time step
if exist('movie_tstep')
    movie_tstep=floor(movie_tstep);
    mov=1;
figure('units','inches','position',[1 1 8 6]);
frvec=[1:movie_tstep:nt];
j=1;
else
     mov=0;
end

m=1;
while m<=nt %time loop
%call upon established mobile phase gradient profile
M2(1,1)=cond_lin.Mgrad(1,m);
%mobile phase compsition for every distance point with dispersion
    for n=2:nz
        M2(n,1)=M1(n-1,1);
    end
    dM(1)=-D1*M2(1,1)+D1*M2(2,1);
    for n=2:nz-1
        dM(n,1)=-2*D1*M2(n,1)+D1*M2(n-1,1)+D1*M2(n+1,1);
    end
    dM(nz,1)=-2*D1*M2(nz,1)+D1*M2(nz-1,1)+D1*M1(nz,1);
    M2=M2+dM;
    C2(1,1)=cond_lin.C_injProf(1,m);
```

```
    kprime(1,1)=kp_spg(1,1)*exp(-S*M2(1,1));
    P1(1,1)=pkprime(1,1)/(pkprime(1,1)+1);
    P(1,1)=1/(kprime(1,1)+1);
    D(1,1)=1/(2*(pkprime(1,1)+1)^2);
    C2(1,1)=P1(1,1)*C1(1,1)+C2(1,1);
%analyte mass for every distance point with dispersion
    for n=2:nz
        kprime(n,1)=kp_spg(n,1).*exp(-S*M2(n,1));
        P(n,1)=1/(pkprime(n-1,1)+1);
        P1(n,1)=pkprime(n,1)/(pkprime(n,1)+1);
        D(n,1)=1/(2*(pkprime(n,1)+1)^2);
        C2(n,1)=P1(n,1)*C1(n,1)+P(n,1)*C1(n-1,1);
    end
    dC(1)=-D(1,1)*C2(1,1)+D(2,1)*C2(2,1);
    for n=2:nz-1
        dC(n,1)=-2*D(n,1)*C2(n,1)+D(n-1,1)*C2(n-1,1)+D(n+1,1)*C2(n+1,1);
    end
    dC(nz,1)=-2*D(nz,1)*C2(nz,1)+D(nz-1,1)*C2(nz-1,1)+D(nz,1)*C1(nz,1);
    C2=C2+dC;
    %k at elution is kprime at z=L
    kp(1,m)=kprime(nz,1);
    %reset previous time kprime equal to current kprime
    pkprime=kprime;
    %reset previous time analyte mass equal to current analyte mass
    C1=C2;
    %reset previous time mobile phase composition equal to
    %current mobile phase composition
    M1=M2;
    %final chromatogram equals mass at the end of the column
    Cfinal(1,m)=C2(nz,1);
    %final mobile phase profile equals mass at the end of the column
    Mfinal(1,m)=M2(nz,1);
%continue simulation if not returned to baseline
if m==nt
    if Cfinal(1,m)>1e-10
        time=(tottime+5)/60;
        cond_lin=conditions_linn2(delz,Vm,F,L,time,Vloop,fill,...
            inj_exptl,inj_prof,Vaxis,sample,phiinit,delphi,tG,tDm);
        nt=floor(time*60/delt);
        disp('Not long enough simulation time, more time needed.')
    end
end
%get frames for movie
if mov==1 && ismember(m,frvec)
    zaxis=delz:delz:totdist;
    subplot(2,1,1); plot(zaxis,M2,'LineWidth',2);
    if phifinal==phiinit
        phiflim=phiinit+0.1;
    else
        phiflim=phifinal;
    end
    set(gca,'YLim',[phiinit phiflim]);
    title(sprintf('time = %0.2f min',delt*m/60))
    xlabel('Distance (cm)')
    ylabel('\phi')
    set(gca,'fontsize',18);
    subplot(2,1,2); plot(zaxis,C2,'r','LineWidth',2);
```

```
    set(gca,'YLim',[0 2*max(cond_lin.C_injProf)]);
    xlabel('Distance (cm)')
    ylabel('Analyte mass')
    set(gca,'fontsize',18);
    Frames(j)=getframe(gcf);
    j=j+1;
elseif mov==0
    Frames=struct([]);
end
    m=m+1;
end
Cfinal=Cfinal./(kp+1); %area correction; divide Cfinal by (k at elution+1)
```

chromsim_smpg_NK.m

```
function[Cfinal,Mfinal,kp,Frames]=chromsim_smpg_NK(B,a,cond_lin,kp_spg,...
    movie_tstep)

phiinit=cond_lin.phiinit;
delphi=cond_lin.delphi;
phifinal=phiinit+delphi;
sample=cond_lin.sample;
tottime=cond_lin.time*60;
totdist=cond_lin.L;
delz=cond_lin.delz;
delt=cond_lin.delt;
D1=1/2;
nz=floor(totdist/delz);
nt=floor(tottime/delt);
C1=zeros(nz,1);
C2=zeros(nz,1);
dM=zeros(nz,1);
dC=zeros(nz,1);
kp=zeros(1,nt);
Mfinal=zeros(1,nt);
Cfinal=zeros(1,nt);
M1=ones(nz,1)*phiinit;
M1(1,1)=-D1*sample+D1*phiinit+sample;
M1(2,1)=-2*D1*phiinit+D1*sample+D1*phiinit+phiinit;
pkprime(1:nz,1)=kp_spg.*(1+a*M1(1:nz,1)).^2.*exp(-B*M1(1:nz,1)...
    ./(1+a*M1(1:nz,1)));
kp(1)=pkprime(nz,1);
D(:,1)=1./(2*(pkprime(:,1)+1).^2);

%establish movie time step
if exist('movie_tstep')
    movie_tstep=floor(movie_tstep);
    mov=1;
figure('units','inches','position',[1 1 8 6]);
frvec=[1:movie_tstep:nt];
j=1;
else
    mov=0;
end

m=1;
```

```
while m<=nt %establish movie time step
%call upon established mobile phase gradient profile
    M2(1,1)=cond_lin.Mgrad(1,m);
%mobile phase compsition for every distance point with dispersion
    for n=2:nz
        M2(n,1)=M1(n-1,1);
    end
    dM(1)=-D1*M2(1,1)+D1*M2(2,1);
    for n=2:nz-1
        dM(n,1)=-2*D1*M2(n,1)+D1*M2(n-1,1)+D1*M2(n+1,1);
    end
    dM(nz,1)=-2*D1*M2(nz,1)+D1*M2(nz-1,1)+D1*M1(nz,1);
    M2=M2+dM;
    C2(1,1)=cond_lin.C_injProf(1,m);
    kprime(1,1)=kp_spg(1,1)*(1+a*M2(1,1))^2*exp(-B*M2(1,1)/(1+a*M2(1,1)));
    P1(1,1)=pkprime(1,1)/(pkprime(1,1)+1);
    P(1,1)=1/(kprime(1,1)+1);
    D(1,1)=1/(2*(pkprime(1,1)+1)^2);
    C2(1,1)=P1(1,1)*C1(1,1)+C2(1,1);
%analyte mass for every distance point with dispersion
    for n=2:nz
        kprime(n,1)=kp_spg(n,1)*(1+a*M2(n,1))^2*exp(-B*M2(n,1)...
            /(1+a*M2(n,1)));
        P(n,1)=1/(pkprime(n-1,1)+1);
        P1(n,1)=pkprime(n,1)/(pkprime(n,1)+1);
        D(n,1)=1/(2*(pkprime(n,1)+1)^2);
        C2(n,1)=P1(n,1)*C1(n,1)+P(n,1)*C1(n-1,1);
    end
    dC(1)=-D(1,1)*C2(1,1)+D(2,1)*C2(2,1);
    for n=2:nz-1
        dC(n,1)=-2*D(n,1)*C2(n,1)+D(n-1,1)*C2(n-1,1)+D(n+1,1)*C2(n+1,1);
    end
    dC(nz,1)=-2*D(nz,1)*C2(nz,1)+D(nz-1,1)*C2(nz-1,1)+D(nz,1)*C1(nz,1);
    C2=C2+dC;
    %k at elution is kprime at z=L
    kp(1,m)=kprime(nz,1);
    %reset previous time kprime equal to current kprime
    pkprime=kprime;
    %reset previous time analyte mass equal to current analyte mass
    C1=C2;
    %reset previous time mobile phase composition equal to
    %current mobile phase composition
    M1=M2;
    %final chromatogram equals mass at the end of the column
    Cfinal(1,m)=C2(nz,1);
    %final mobile phase profile equals mass at the end of the column
    Mfinal(1,m)=M2(nz,1);

%continue simulation if not back down to baseline
if m==nt
    if Cfinal(1,m)>1e-10
        time=(tottime+5)/60;
        cond_lin=conditions_linn2(delz,Vm,F,L,time,Vloop,fill,...
            inj_exptl,inj_prof,Vaxis,sample,phiinit,delphi,tG,tDm);
        nt=floor(time*60/delt);
        disp('Not long enough simulation time, more time needed.')
    end
```

```
%get frames for movie
if mov==1 && ismember(m,frvec)
    zaxis=delz:delz:totdist;
    subplot(2,1,1); plot(zaxis,M2,'LineWidth',2);
    if phifinal==phiinit
        phiflim=phiinit+0.1;
    else
        phiflim=phifinal;
    end
    set(gca,'YLim',[phiinit phiflim]);
    title(sprintf('time = %0.2f min',delt*m/60))
    xlabel('Distance (cm)')
    ylabel('\phi')
    set(gca,'fontsize',18);
    subplot(2,1,2); plot(zaxis,C2,'r','LineWidth',2);
    set(gca,'YLim',[0 2*max(cond_lin.C_injProf)]);
    xlabel('Distance (cm)')
    ylabel('Analyte mass')
    set(gca,'fontsize',18);
    Frames(j)=getframe(gcf);
    j=j+1;
elseif mov==0
    Frames=struct([]);
end
    m=m+1;
end
Cfinal=Cfinal./(kp+1); %area correction; divide Cfinal by (k at elution+1)
```

C.8. Convolution

The convolution program consists of a set of nested functions. The master convolution code is conv_tot_nk.m, which calls upon the functions conv_sim_nk.m and nkgrad_calc.m. The function conv_sim_nk.m simulates the elution from the first part of the column and the function nkgrad_calc.m calculates the retention time and peak width for the second part of the column.

conv_tot_nk.m

```
function [peak12,L_cf] = conv_tot_nk(model,conditions)
delz=conditions.delz;
Vm=conditions.Vm;
F=conditions.F;
tM=conditions.tM;
L=conditions.L;
Vloop=0;
fill=0;
inj_prof=[];
inj_exptl=0;
Vaxis=conditions.Vaxis;
tDm=conditions.tD-(conditions.Vloop/1000/conditions.F);
time=conditions.time;
delt=conditions.delt/60;
t_axis=delt:delt:time;
phiinit=conditions.phiinit;
delphi=conditions.delphi;
tG=conditions.tG;
```

```
tslices=conditions.slices*delt;
B=model.B;
a=model.a;
kw=model.kw(1,1);
ko=kw*(1+a*phiinit)^2*exp(-B*phiinit/(1+a*phiinit));
[C_convsim,M_convsim,kp_convsim,L_cf]=conv_sim_nk(model,conditions);
if isnan(C_convsim)
    peak12=NaN;
else
Vm_new=Vm*L_cf/L;
tM_new=Vm_new/F;
[area,position,sigma]=moments([1:size(C_convsim,2)],C_convsim);
position_t=t_axis(1,round(position));
if position_t<tDm+tslices
    tD_new=(tDm+tslices)-position_t;
else
    tD_new=0;
end
ko_new=kp_convsim(1,round(position));
phiinit_new=M_convsim(1,round(position));
delphi_new=phiinit+delphi-M_convsim(1,round(position));
tG_new=tG*delphi_new/delphi;
condlin_new=conditions_lin(delz,Vm_new,F,L_cf,time,Vloop,fill,inj_exptl,...
    inj_prof,Vaxis,phiinit_new,phiinit_new,delphi_new,tG_new,tD_new);
[tR_new,sigma_new]=nkgrad_calc(model,condlin_new);
C_convsim_pad(1,1:size(t_axis,2))=zeros;
C_convsim_pad(1,1:size(C_convsim,2))=C_convsim;
uo=delz/delt;
velution=uo./(1+kp_convsim);
t_axis_new=t_axis-position_t;
d_axis_new=t_axis_new*velution(round(position));
phie=(phiinit_new+(1+a*phiinit_new)/B*log(delphi_new*kw*B/tG_new*...
    (tM_new-tD_new/ko_new)*exp(-B*phiinit_new/(1+a*phiinit_new))+1))/...
    (1-a*(1+a*phiinit_new)/B*log(delphi_new*kw*B/tG_new*...
    (tM_new-tD_new/ko_new)*exp(-B*phiinit_new/(1+a*phiinit_new))+1));
Sstar=-(2*a/(1+a*phie)-(B/(1+a*phie)^2));
bstar=tM_new*Sstar*delphi_new/tG_new;
omegao=ko_new/(1+ko_new);
muR=1-(omegao/(1+omegao*bstar));
t_axis_new2=d_axis_new*(tM-tM_new)/((L-L_cf)*muR*(1+bstar*omegao));
t_axis_new2=t_axis_new2+position_t;
C_interp=interp1(t_axis_new2,C_convsim_pad,t_axis,'spline');
sc_f=(t_axis(1,2)-t_axis(1,1))/(t_axis_new2(1,2)-t_axis_new2(1,1));
C_convsim_pad_af=C_interp*sc_f;
peak1=C_convsim_pad_af;
[peak2]=gausspeak(t_axis,tR_new,sigma_new);
peak2=peak2/sum(peak2);
Peak1=fft(peak1);
Peak2=fft(peak2);
Peak12=Peak1.*Peak2;
peak12=ifft(Peak12);
end
end
```

conv_sim_nk.m

```
function [Cfinal,Mfinal,kp,L_cf,conditions] = conv_sim_nk(model,conditions)
```

```
Vm=conditions.Vm;
F=conditions.F;
tM=conditions.tM;
tD=conditions.tD;
tDm=tD-(conditions.Vloop/1000/conditions.F);
time=conditions.time;
phiinit=conditions.phiinit;
slices=conditions.slices;
L=conditions.L;
delz=conditions.delz;
delphi=conditions.delphi;
tG=conditions.tG;
sample=conditions.sample;
B=model.B;
a=model.a;
kw=model.kw;
ko=kw*(1+a*phiinit)^2*exp(-B*phiinit/(1+a*phiinit));
ksam=kw*(1+a*sample)^2*exp(-B*sample/(1+a*sample));
um=L/tM;
va=um/(1+ko);
vsam=um/(1+ksam);
if abs(um-vsam) < 1e-6
    zsam=L;
else
zsam=vsam*slices*delz/(um-vsam);
end
if ko == 0
    tMiso=0;
else
    tMiso=tD/ko;
end
ziso=va*(tD+tMiso);
sigma_col_sam=sqrt((zsam*delz));
sigma_col_iso=sqrt((ziso*delz));
band_width=slices*delz/(1+ksam);
sigma_inj=ko*(ksam+1)/(ksam*(ko+1))*band_width/sqrt(12);
sigma_init_b=sqrt(sigma_col_sam^2+sigma_inj^2+sigma_col_iso^2);
Lsim=zsam+5*sigma_init_b;
if Lsim<0.1*L
    Lsim=0.1*L;
end
L_cf=L-Lsim;
if Lsim>0.9*L
    Cfinal=NaN;
    Mfinal=NaN;
    kp=NaN;
else
Vmsim=Vm*(Lsim/L);
Vloop=conditions.Vloop;
fill=conditions.fill;
inj_exptl=conditions.inj_exptl;
inj_prof=conditions.inj_prof;
Vaxis=conditions.Vaxis;
[conditions]=conditions_lin(delz,Vmsim,F,Lsim,time,Vloop,fill,...
    inj_exptl,inj_prof,Vaxis,sample,phiinit,delphi,tG,tDm);
[tR_approx_1,sigma_approx_1] = nkgrad_calc(model,conditions);
time1=tR_approx_1+5*sigma_approx_1;
```

```
scale1=0.00625/60*2.5;
scale2=Lsim/(delz*Vmsim);
ndelt_spacing=size(Vaxis,1)-1;
new_points=floor(ndelt_spacing*scale1*scale2);
delt=conditions.delt;
if time1<new_points*delt/60
    time1=new_points*delt/60;
elseif time1>conditions.time
    time1=conditions.time;
end
if time1>conditions.time
    time1=conditions.time;
end
[conditions]=conditions_linn2(delz,Vmsim,F,Lsim,time1,Vloop,fill,...
    inj_exptl,inj_prof,Vaxis,sample,phiinit,delphi,tG,tDm);
[Cfinal,Mfinal,kp]=chromsim_lin_NK(model,conditions);
end
```

nkgrad_calc.m

```
function [tR,sigma]=nkgrad_calc(model,conditions)
tM=conditions.tM;
phiinit=conditions.phiinit;
sample=conditions.sample;
slices=conditions.slices;
L=conditions.L;
delz=conditions.delz;
delphi=conditions.delphi;
tG=conditions.tG;
tD=conditions.tD-(conditions.Vloop/1000/conditions.F);
N=L/delz;
B=model.B;
a=model.a;
kw=model.kw(1,1);
ko=kw*(1+a*phiinit)^2*exp(-B*phiinit/(1+a*phiinit));
ksam=kw*(1+a*sample)^2*exp(-B*sample/(1+a*sample));
um=L/tM;
va=um/(1+ko);
vsam=um/(1+ksam);
if abs(um-vsam) < 1e-6
    zsam=L;
else
    zsam=vsam*slices*delz/(2*(um-vsam));
end
if zsam>L
    zsam=L;
end
tMsam=tM*(zsam/L);
tRsam=tMsam*(1+ksam);
tMgrad=tM-tMsam;
phie=(phiinit+(1+a*phiinit)/B*log(delphi*kw*B/tG*(tMgrad-tD/ko)...
    *exp(-B*phiinit/(1+a*phiinit))+1))/(1-a*(1+a*phiinit)/B*log(delphi...
    *kw*B/tG*(tMgrad-tD/ko)*exp(-B*phiinit/(1+a*phiinit))+1));
tgrad=tG*(phie-phiinit)/delphi+tMgrad+tD;
tR=tgrad+tRsam+slices*delz/(2*um);
omega0=ko/(1+ko);
if ko == 0
```

```
    tMiso=0;
else
    tMiso=tD/ko;
end
tMgradonly=tM-tMiso-tMsam;
ziso=va*(tD+tMiso);
zgrad=L-ziso-zsam;
Sstar=-(2*a/(1+a*phie)-(B/(1+a*phie)^2));
ke=kw*(1+a*phie)^2*exp(-B*phie/(1+a*phie));
bstar=tMgradonly*delphi*Sstar/tG;
muR=1-(omega0/(1+omega0*bstar));
G=1/(1+omega0*bstar)*sqrt(1+omega0*bstar+(1/3)*omega0^2*bstar^2);
Ngrad=N*(zgrad/L);
if zgrad==0
    sigmagrad=0;
else
    sigmagrad=G*tMgradonly*(1+ke)*sqrt(delz/zgrad);
end
sigma_col_iso=sqrt((ziso*delz));
sigma_col_sam=sqrt((zsam*delz));
band_width=slices*delz/(1+ksam);
sigma_inj=ko*(ksam+1)/(ksam*(ko+1))*band_width/sqrt(12);
sigmab=sqrt(sigma_col_iso^2+sigma_col_sam^2+sigma_inj^2);
delsigmaiso=tM*sigmab/(L*muR*(1+omega0*bstar));
sigma=sqrt(sigmagrad^2+delsigmaiso^2);
end
```

C.8. Finding retention time and width of a peak

The function fwhm.m returns the peak width at half height. This should be only used if the simulated peak is perfectly Gaussian.

fwhm.m

```
function FWHM=fwhm(x,f)
if nargin<2
    f=x;
    x=[1:length(f)];
end
f1=f-0.5*max(f);
ind=find(f1(1:end-1).*f1(2:end)<=0);
FWHM=x(ind(2))-x(ind(1));
```

The function moments.m is used for asymmetric peaks. It returns peak area, retention time, peak width, and skew.

moments.m

```
function [area,position,sigma,skew]=moments(timeaxis,Cfinal)
% calculate the moments of a peak
area=sum(Cfinal);
pr=Cfinal/area;
position=pr*timeaxis';
sigma=(((timeaxis-position)).^2*pr')^0.5;
skew=(((timeaxis-position)).^3*pr')^(1/3);
end
```

The function fde.m consists of a set of Foley-Dorsey equations [134]. It returns the efficiency of the chromatography system, retention time (peak max), degree of peak asymmetry, and peak width at 10 % height.

fde.m

```
function [tr,width10,A,B,Nsys]=fde(x,f)
[A,l]=max(f);
tr=x(l);
if nargin<2
    f=x;
    x=[1:length(f)];
end
f1=f-0.1*max(f);
ind=find(f1(1:end-1).*f1(2:end)<=0);
width10=x(ind(2))-x(ind(1));
A=tr-x(ind(1));
B=x(ind(2))-tr;
if A<=B
Nsys=41.7*(tr/width10)^2/(B/A+1.25);
else
    Nsys=41.7*(tr/width10)^2/(A/B+1.25);
end
```

APPENDIX D

Simulation program instructions

Table D1: Functions included in the simulation package

Function	Purpose
isotimefit_lss	Extract LSS parameters from isocratic data
gradtimefit_lss	Extract LSS parameters from gradient data
isotimefit_lss_cS	Extract LSS parameters from isocratic data with common S
isotimefit_nk	Extract NK parameters from isocratic data
isotimefit_nk_cBa	Extract NK parameters from isocratic data with common B and a
model_LSS	Select LSS model and set up parameters S and kw
model_NK	Select NK model and set up parameters kw, B, and a
conditions_iso	Establish chromatographic conditions (isocratic)
conditions_lin	Establish chromatographic conditions (gradient)
chromsim_isoLSS	Simulate using LSS parameters (isocratic)
chromsim_isoNK	Simulate using NK parameters (isocratic)
chromsim_lin_LSS	Simulate using LSS parameters (gradient)
chromsim_lin_NK	Simulate using NK parameters (gradient)
kspg_kw	Establish stationary phase gradient
chromsim_smpg_LSS	Simulate stationary phase gradient using LSS parameters
chromsim_smpg_NK	Simulate stationary phase gradient using NK parameters
conv_tot_nk	Master code for convolution
conv_sim_nk	Simulation of C1 (convolution)
nkgrad_calc	Closed form calculation for solvent mismatch condition under mobile phase gradient elution
makevideo	Create .avi movie file from saved frames
Fwhm	Calculate full width at half max
moments	Calculate moments of simulated peak
Fde	Calculate widths using Foley-Dorsey equations

*Additional files included: mat file for experimental injection profiles (exp_inj_prof_new.mat)

D.1. Simulation of mobile phase gradient

STEP 1: Select model for retention factor (*k*) calculation

Linear Solvent Strength (LSS)

$$\ln k = \ln k_w - S\phi$$

Neue-Kuss (NK)

$$k = k_w(1+S_2\phi)^2 \exp\left[\frac{-S_1\phi}{1+S_2\phi}\right]$$

*NOTE: Simulation codes use *B* to represent S_1 and *a* to represent S_2.

LSS input choices:

Manual input: [model] = model_LSS (S, kw);
Preset conditions: [model] = model_LSS([], [],'compound', 'column');

Table D2: Compounds with predetermined LSS parameters

Compound code	Compound name
PE	Phenylephrine
PPA	Phenylpropanolamine
PEA	Phenethylamine
EP	Ephedrine
PSE	Pseudoephedrine
Amp	Amphetamine
MDA	3,4-Methylenedioxy-amphetamine
Mamp	Methamphetamine
Moxy	Methoxyamphetamine
MDMA	3,4-Methylenedioxymethamphetamine

Table D3: Columns tested for LSS parameter extraction

Column code	Column type	Column dimension	Mobile phase
C_{18}	Accucore C_{18} (Thermo Scientific)	100 x 2.1 mm, 3 µm	10 mM potassium phosphate buffer pH 2.5 / Acetonitrile
Phen	Accucore Phenyl-Hexyl (Thermo Scientific)	100 x 2.1 mm, 3 µm	10 mM potassium phosphate buffer pH 2.5 / Acetonitrile

LSS example

Input: [model_PEA_C18] = model_LSS([],[], 'PEA', 'C18');
Output: model_PEA_C18 1x1 struct
S 19.4150
kw 4.7543

NK input choices:

Manual input: [model] = model_NK (kw, B, a, 'compound');
Preset conditions: [model] = model_NK([], [], [],'compound');

Table D4: Compounds with predetermined NK parameters

Compound code	Compound name
AB1	Methylbenzene
AB2	Ethylbenzene
AB3	Propylbenzene
AB4	Butylbenzene
AB5	Pentylbenzene
DiEtF	Diethylformamide
BzAlc	Benzyl alcohol
PB1	Methylparaben
PB3	Propylbaraben
PB4	Butylparaben
AP2	Acetophenone
AP4	Butyrophenone
AP5	Valerophenone

Table D5: Column tested for NK parameter extraction

Column type	Column dimension	Mobile phase
Zorbax SB C_{18} (Agilent Technologies)	50 x 2.1 mm, 3.5 µm (for AB1-AB5) 30 x 2.1 mm, 3.5 µm (rest of the compounds in Table 4)	Water / Acetonitrile

NK example

Input: [model_DiEtF] = model_NK([], [], [],'DiEtF');
Output: model_DiEtF 1x1 struct
kw 22.9198
B 27.3600
a 2.7720

STEP 2: Establish simulation conditions

Command: [conditions] = conditions_lin(delz,Vm,F,L,time,Vloop,fill,...
inj_exptl,inj_prof,Vaxis,sample,phiinit,delphi,tG,tD,Mgrad)

***NOTE:** Mgrad input is only necessary if you have specific mobile phase gradient profile you would like to simulate (i.e., unusual gradient shapes that cannot be calculated from given parameters), so in most cases leave out Mgrad input (see examples below).

Table D6: Inputs for condition structure

Input variable	Official variable	Units	Definition
delz	Δz	Cm	Discrete distance segment (equal to plate height, H)
Vm	V_m	mL	Void volume
F	F	mL/min	Flow rate
L	L	Cm	Total column length
time	time	min	Total run time
Vloop	V_{loop}	µL	Sample loop volume
fill	N/A	N/A	Fractional loop filling
inj_exptl	N/A	N/A	Rectangular injection = 0 Experimental injection = 1
inj_prof	N/A	N/A	Experimental injection profile
Vaxis	N/A	mL	Volume axis
sample	ϕ_{sample}	Unit-less	Sample solvent composition
phiinit	$\phi_{initial}$	Unit-less	Initial mobile phase composition
delphi	$\Delta\varphi$	Unit-less	Equal to $\phi_{final} - \phi_{initial}$ for mobile phase gradient
tG	t_G	Min	Gradient time
tD	t_D	Min	Delay/dwell time
Mgrad	N/A	N/A	Manual input of mobile phase gradient

Table D7: Experimental injection profiles and corresponding injection volumes

Profile No.	Loop size (μL)	Percent fill	Actual injection volume (μL)
1	0.4	200	0.4
2	13.5	25	3.425
3	13.5	50	6.85
4	13.5	75	10.275
5	13.5	100	13.7
6	20	25	5.675
7	20	50	11.35
8	20	75	17.025
9	20	100	22.7
10	40	25	11.375
11	40	50	22.75
12	40	75	34.125
13	40	100	45.5
14	60	25	17.2
15	60	50	34.4
16	60	75	51.6
17	60	100	68.8
18	80	25	20.825
19	80	50	41.65
20	80	75	62.475
21	80	100	83.3

Example inputs:

delz = 0.0025;
Vm = 0.0525;
F = 2.5;
L = 3;
time = 0.3;
phiinit = 0.3;
delphi = 0.35;
tD = 0.027;
tG = 0.25;
sample = 0.3;

Rectangular injection:

Input:
inj_exptl = 0;
Vloop = 40;
fill = 0.25;

```
[conditions_rec] = conditions_lin(delz,Vm,F,L,time,Vloop,fill,. . .
inj_exptl,[],[],sample,phiinit,delphi,tG,tD);
```

Plotting Mgrad and C_injProf:

```
Make time axis
delt = conditions_rec.delt;
time = conditions_rec.time;
timeaxis = delt/60:delt/60:time;

plot(timeaxis,conditions_rec.Mgrad)
plot(timeaxis,conditions_rec.C_injProf)
```

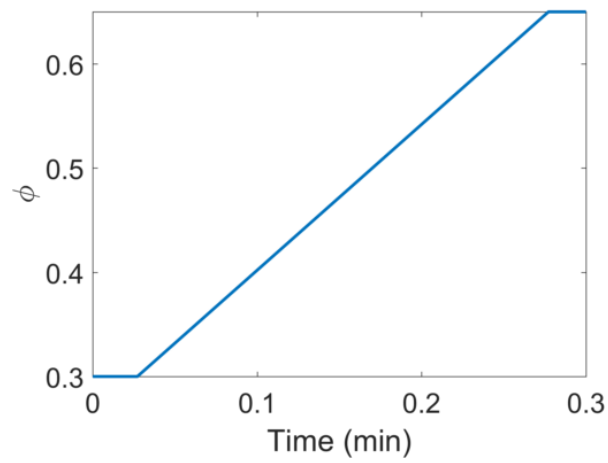

Figure D.1. Rectangular injection – mobile phase gradient profile (Mgrad)

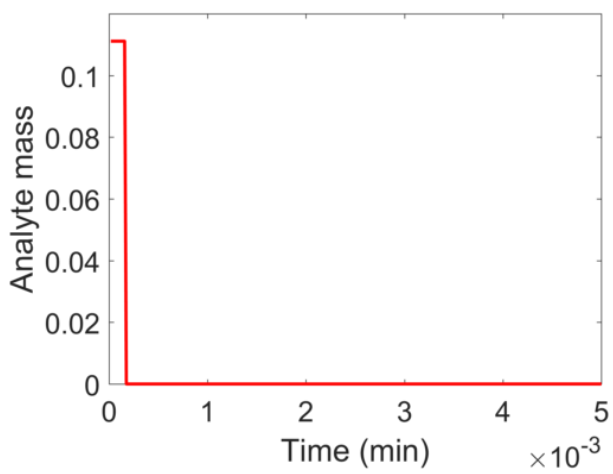

Figure D.2. Rectangular injection – analyte injection profile (C_injProf)

Real/experimental injection:

Input:
inj_exptl = 1;

load('exp_inj_prof_new.mat');

inj_prof_new: experimental injection profiles (see Table 7)
Vaxis: corresponding volume axis for each profile

Example: selecting 10th injection profile (40 µL loop at 25 % fill, see Table 7)
prof_num=10;

```
[conditions_real]=conditions_lin(delz,Vm,F,L,time,Vloop(prof_num,1),fill_all(prof_num,1), . . .
inj_exptl,inj_prof{prof_num,1},Vaxis {prof_num,1},sample,phiinit,delphi,tG,tD);
```

Plotting Mgrad and C_injProf:

Make time axis
delt = conditions_rec.delt;
time = conditions_rec.time;
timeaxis = delt/60:delt/60:time;

plot(timeaxis,conditions_real.Mgrad)
plot(timeaxis,conditions_real.C_injProf)

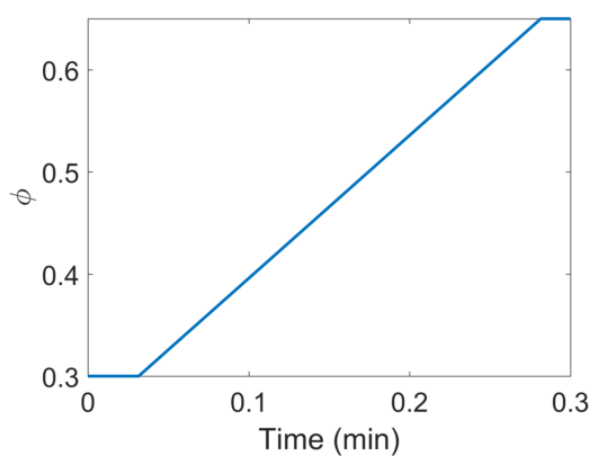

Figure D.3. Real/experimental injection – mobile phase gradient profile (Mgrad)

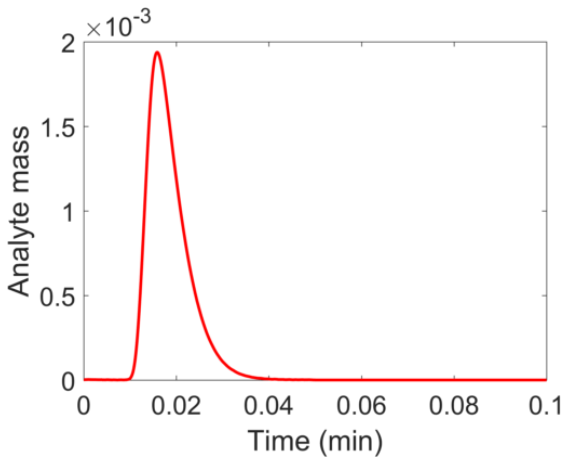

Figure D.4. Real/experimental injection – Analyte injection profile (C_injProf)

STEP 3: Run Simulation

Command:

[Cfinal,Mfinal,kp,time,Frames]=chromsim_lin_LSS(model_LSS,cond_lin,movie_tstep);
or
[Cfinal,Mfinal,kp,time,Frames]=chromsim_lin_NK(model_NK,cond_lin,movie_tstep);

Inputs:

model_LSS or model_NK from STEP1 (model_PEA_C18 or model_DiEtF)
cond_lin from STEP2 (conditions_rec or conditions_real)

Outputs:

Cfinal: simulated chromatogram
Mfinal: mobile phase composition at the end of the column
kp: retention factor of given compound under Mfinal composition
time: simulation time

Movie option

Input movie_tstep sets up how many frames you would get for your movie, it should be an integer.

Example: movie_tstep = 25 means get every 25th frame

If you do not wish to get frames to make movie, then leave out movie_tstep input.

```
[Cfinal,Mfinal,kp,time,Frames] = chromsim_lin_LSS(model_LSS,cond_lin);
or
[Cfinal,Mfinal,kp,time,Frames]=chromsim_lin_NK(model_NK,cond_lin);
```

This should return:
Frames 0x0 struct

Or you could also choose not to return Frames output.

```
[Cfinal,Mfinal,kp,time] = chromsim_lin _LSS(model_LSS,cond_lin);
or
[Cfinal,Mfinal,kp,time]=chromsim_lin _NK(model_NK,cond_lin);
```

Plotting simulated chromatogram:
Plot chromatogram

```
plot(timeaxis,Cfinal);
```

STEP 4: Play movie or create movie file from saved frames (optional)

Option 1: Play movie from saved frames

```
implay(Frames);
```

Option 2: Create .avi movie file from saved frames

```
[video]=makevideo('name' ,Frames);
```

D.2. Simulation of stationary phase gradient

STEP 1: Predefine stationary phase gradient profile

Command: [kprime] = kspg_kw(cond_lin,shape,ratio,kw_stat1,kw_stat2);

Inputs:

cond_lin: separation condition
shape: stationary phase gradient shape (choices are linear, step, or exponential)
kw_stat1 and kw_stat2: extracted k_w values for different stationary phases

Outputs:

kprime: k_w for stationary phase gradient
Stationary phase gradient profile figure

STEP 2: Run Simulation

Command:

[Cfinal,Mfinal,kp,Frames]=chromsim_smpg_LSS(S,cond_lin,kp_spg,movie_tstep);
Or
[Cfinal,Mfinal,kp,Frames]=chromsim_smpg_NK(B,a,cond_lin,kp_spg,movie_tstep);

Inputs:

S, B, and a: common parameters obtained from fitting isocratic retention data from training set using fitting codes isotimefit_cS.m or isotimefit_cBa.m
cond_lin: separation conditions
kp_spg: kprime of stationary phase gradient profile obtained from STEP1
movie_tstep: optional movie time step

Outputs:

Cfinal: simulated chromatogram
Mfinal: mobile phase composition at the end of the column
kp: retention factor of given compound under stationary phase gradient and isocratic or mobile phase composition

D.3. Convolution

The convolution program consists of a set of nested functions. The master convolution code is conv_tot_nk.m, which calls upon the functions conv_sim_nk.m and nkgrad_calc.m. The function conv_sim_nk.m simulates the elution from the first part of the column and the function nkgrad_calc.m calculates the retention time and peak width for the second part of the column.

Operation of the convolution program is simple. It only involves running the master code.

Master code command:

[peak12,L_cf]=conv_tot_nk(model,conditions);

Inputs:

model: options structure from model_LSS.m or model_NK.m
conditions: simulation conditions from conditions_linn2.m

Outputs:

peak12: convoluted peak
L_cf: length of the column for closed form calculationi (C2)

Vita

Lena Na Jeong was born on February 5, 1988 in Monterey Bay, California and is a US citizen. She graduated from Fairfax High School, Fairfax, Virginia in 2006. She received her Bachelor of Science in Chemistry from University of Virginia, Charlottesville, Virginia in 2010. Immediately after graduating, she was employed as a research chemist at PGxHealth Inc. in Charlottesville, Virginia. She attended George Washington University for one school year and completed course work in the forensic science graduate program. She began the part-time master's program at Virginia Commonwealth University in August 2011, and then joined the full-time doctoral program in January 2013. She has been a member of Dr. Sarah Rutan's research group ever since. She is first author on one publication and co-author on two publications. She has presented her research at three scientific meetings.

Publications

L.N. Jeong, D.R. Stoll, P.W. Carr, S.C. Rutan, Simulation of elution profiles in liquid chromatography – IV. Convolution approach to accelerate simulation. *In preparation for submission to J. Chromatogr. A.*

L.N. Jeong, S.G. Forte, S.C. Rutan, Simulation of elution profiles in liquid chromatography – III. Stationary phase gradients. *In preparation for submission to J. Chromatogr. A.*

D.R. Stoll, R.W. Sajulga, B.N. Voigt, E.J. Larson, L.N. Jeong, S.C. Rutan, Simulation of elution profiles in liquid chromatography − II: Investigation of injection volume overload under gradient elution conditions applied to second dimension separations in two-dimensional liquid chromatography, J. Chromatogr. A. (2017). doi:10.1016/j.chroma.2017.07.041.

V.C. Dewoolkar, L.N. Jeong, D.W. Cook, K.M. Ashraf, S.C. Rutan, M.M. Collinson, Amine Gradient Stationary Phases on In-House Built Monolithic Columns for Liquid Chromatography, Anal. Chem. 88 (2016) 5941–5949. doi:10.1021/acs.analchem.6b00895.

L.N. Jeong, R. Sajulga, S.G. Forte, D.R. Stoll, S.C. Rutan, Simulation of elution profiles in liquid chromatography - I: Gradient elution conditions, and with mismatched injection and mobile phase solvents, J. Chromatogr. A. 1457 (2016) 41–49. doi:10.1016/j.chroma.2016.06.016.

Presentations

**indicates poster presentation*

L.N. Jeong, S.G. Forte, S.C. Rutan, Simulations for retention prediction on stationary phase gradients. ACS 254th National Meeting (Washington, DC) August 2017.

*E. Larson, C. Dammann, T. Brau, H. Lhotka, R. Sajulga, L.N. Jeong, S.C. Rutan, P.W. Carr, D.R. Stoll, Numerical simulation of liquid chromatography – Development of a toolkit to enable deeper understanding of nonstandard conditions and advance the state of the art. HPLC 2017 (Prague, Czech Republic) June 2017.

L.N. Jeong, D.R. Stoll, P.W. Carr, S.C. Rutan, Convolution approach to speed up simulation for various conditions of liquid chromatography including volume overload and solvent mismatch. Pittcon (Chicago, IL) March 2017.

*L.N. Jeong, S.G. Forte, R. Sajulga, D.R. Stoll, S.C. Rutan, HPLC Stationary and Mobile Phase Gradient Simulations. Chemometrics in Analytical Chemistry (Richmond, VA) June 2014.